TRITA AVE 2005:17
ISSN 1651-7660
ISBN 91-7283-806-X

DAN BRABIE On the Influence of Rail Vehicle Parameters on the Derailment Process and its Consequences KTH 2005

www.kth.se

On the Influence of Rail Vehicle Parameters on the Derailment Process and its Consequences

DAN BRABIE

KTH Engineering Sciences

Licentiate Thesis in Railway Technology
Stockholm, Sweden 2005



On the Influence of Rail Vehicle Parameters on the Derailment Process and its Consequences

by

Dan Brabie

Licentiate Thesis

TRITA AVE 2005:17
ISSN 1651-7660
ISBN 91-7283-806-X

Postal Address
Royal Institute of Technology
Aeronautical and Vehicle Engineering
Railway Technology
SE-100 44 Stockholm

Visiting address
Teknikringen 8
Stockholm

Telephone
+46 8 790 84 76
Fax
+46 8 790 76 29

E-mail
mabe@kth.se

Contents

Contents i

Preface and acknowledgements iii

Abstract v

1 Introduction 1

1.1 Background information 1
1.2 Previous research 1
1.3 Scope, structure and contribution of this thesis 3

2 Inquiries on incidents and accidents 5

2.1 Introduction to the database 5
2.2 Description of incident and accident events 6
2.2.1 Axle failure on the outside of the wheel 6
2.2.2 Axle failure on the inside of the wheel 9
2.2.3 Broken rails or other track defects 12
2.2.4 Wheel defects 22
2.2.5 Other causes 26
2.3 Empirically based conclusions and discussion 29
2.4 Identification of critical vehicle parameters 32

3 Pre-derailment simulation studies 35

3.1 Introduction 35
3.2 General simulation prerequisites 35
3.3 Axle failure model validation 37
3.3.1 The Tierp incident 38
3.3.2 The Gnesta incident 40
3.3.3 Validation conclusions 41
3.4 Studies on axle failure location in the bogie 42
3.5 Axle failure studies for different combinations of wheelset guidance 44

4 Tentative simulation studies on brake disc position 47

4.1 Introduction 47
4.2 Brake disc basic requirements 47
4.3 Simulation methodology 48
4.4 Simulation results 51

5 Wheel-sleeper dynamic interaction 55

5.1 Introduction 55
5.2 Concrete material model 55
5.3 Tentative model validation 56
5.3.1 Introduction and the validation case 56
5.3.2 FE impact model 57
5.3.3 Simulation methodology 59

5.3.4 Validation results 61
5.3.5 Discussion and conclusions 63
5.4 Impact simulations of an X 2000 trailer car wheel 63
5.4.1 Introduction 63
5.4.2 FE impact model 63
5.4.3 Simulation methodology 65
5.4.4 Results 67
5.4.5 Discussion of results 70

6 Conclusions and future work 73

6.1 Summary of the present work 73
6.2 General conclusions 74
6.3 Future directions of research 75

Appendix A - Database events overview 77

Appendix B - Wheel position at impact with the sleeper 83

Appendix C - Concrete material modelling details 85

Appendix D - Tentative FE model validation results 87

Appendix E - Wheel motion after impact 93

References 97

Symbols and Abbreviations 103

Preface and acknowledgements

The work behind this licentiate thesis has been carried out at the Division of Railway Technology, Department of Aeronautical and Vehicle Engineering at the Royal Institute of Technology (KTH), Stockholm.

The research project was initiated by SJ AB (Swedish Railways) and Interfleet Technology, under the working title "Robust Safety Systems for Trains", triggered by observations of some "successful" derailments with the Swedish high-speed train *X 2000*.

The project was funded by combined efforts of Banverket (National Swedish Rail Administration), Vinnova (Swedish Agency for Innovation Systems) and the Railway Group of KTH (Banverket, Bombardier Transportation, Green Cargo, Interfleet Technology, KTH, SJ AB and SL). The financial and personnel support of the above named companies and organisation is gratefully acknowledged.

Special thanks are passed to the members of the reference and steering group for their support and participation: Christer Ljunggren from SJ AB, Hugo von Bahr from Interfleet Technology, Tohmmy Bustad from Banverket, Tomas Persson from Bombardier Transportation and Stefan Sollander from Järnvägsstyrelsen (Swedish Rail Agency).

I am most grateful to my supervisor, Prof. Evert Andersson, for his guidance, involvement and critical comments along these years, as well as for his comprehensive review of the manuscript.

All my colleagues at the Railway Division deserve special thanks, in particular Prof. Mats Berg for the critical review of the manuscript.

Likewise, I wish to thank Dr. Anders Ansell at the Division of Concrete Structures at KTH for fruitful discussions as well as for the partial manuscript review.

In addition, I wish to express my thanks to Dr. Johan Bäckman for allowing me to access the database and Mr. Ingemar Persson for all the help received with the simulation software, and especially for the implemented tailor-made routines in the simulation package GENSYS.

Finally, my dear family deserves a big hug for their endurance with my, at times, irregular working hours.

Stockholm, May 2005

Dan Brabie

Abstract

This thesis aims at systematically studying the possibilities of minimising devastating consequences of high-speed derailments by appropriate measures and features in the train design, including the running gear. The course of events immediately after derailments is studied with respect to whether the train stays upright and close to the track centre line or deviates laterally with probably serious consequences. There is a belief in the railway community that some trains can better cope with derailment then others, although this superiority is apparently hard to quantify.

Firstly, an empirical database has been established containing as much relevant information as possible of past incidents and accidents occurred at higher speeds due to mechanical failure close to the interface between the running gear and the track, as well as other causes that ultimately brought the train into a derailed condition. Although never two derailments are the same, certain patterns appeared to crystallise after analysing the course of events immediately after the failure based on the descriptions available in each incident or accident report. Ultimately, this led to that several critical vehicle parameters could be distinguished as capable to influence the outcome of a derailment.

Secondly, two of the critical vehicle features found in the first stage have been subject to detailed analysis by means of multi-body system (*MBS*) simulations. The first phase of the computer simulation program focused on studying the tendency of a wheelset to derail as a result of an axle journal failure on the outside of the wheel. The pre-derailment computer simulation model has been validated with good results for two authentic Swedish events of axle journal failure.

Thereafter, one of the newly found critical vehicle feature, the wheelset mechanical restrictions relative to the bogie frame, have been extensively studied on an *X 2000* power unit and trailer car model. The results show that a vertical mechanical restriction of the wheelset relative to the bogie frame of approximately 50 to 60 mm is capable of keeping the wheelsets on the rails after an axle journal failure, for the studied conditions.

An axle mounted brake disc constitutes the second critical vehicle feature that has the potential to favourably influence the sequence of events in cases of wheel flange climbing. A minimal range of geometrical parameters for which the rail would safely fill the gap between the brake disc and the wheel has been calculated.

The third and last part of the thesis establishes the prerequisites necessary in order to study the remaining of the critical vehicle parameters found in the first part, which requires complete *MBS* simulations of derailed vehicles rolling on track structures, i.e. concrete sleepers. To accomplish this task, hysteresis data for the force as function of concrete material indentation, are aimed to be acquired by means of finite element (*FE)* simulations. Therefore, the intended *FE* model of wheel-concrete sleeper impact is subjected to a tentative validation procedure. A good agreement is observed when comparing the *FE* model results with an authentic accident in terms of concrete sleeper indentation. Furthermore, preliminary results in terms of a wheelset tendency to rebound after concrete sleeper impact are presented.

Keywords: train, railway, rail vehicle, accident, incident, derailment, bogie design, simulation, wheel, sleeper, impact.

1 Introduction

1.1 Background information

The railway system is worldwide recognized as a safe mean of transportation. However accidents and incidents continue to occur. Due to the complexity of the railway, with many parties involved, the misfortunes are apparently difficult to eliminate completely, regardless of the amount of money input in the system. Bearing in mind the constantly increasing speeds of the trains, a further increased safety in railway operations is desired.

The railway industry is generally focused on minimizing the probability of an undesired event by implementing safety measures -"barriers"-, preferably on several levels. These "barriers" are not always sufficient when dealing with mechanical fractures close to the wheel-rail interface or with causes out of the manufacturer's or operator's control.

Failures on mechanical parts guiding the wheelsets on rails are highly dangerous phenomena, causing a high probability of derailment. Also various obstacles on the track may cause a derailment. Although the probability is small, it will someday occur. Due to the nature of the train-track system, there is a major risk of serious consequences, but it does not necessarily mean that a serious accident is bound to happen. Only in case the train leaves the rails and the track bed, resulting in turnover or collision with other objects, a serious situation arises. In this circumstance, it would be possible to influence the course of events by introducing another set of last "barriers", which would ultimately limit the vehicle deviation from the track centre line. Design of the running gear is believed to be a critical issue in this context.

There is a belief within the railway community that some types of train designs can cope better with derailments, hereby having an incorporated, robust, "last barrier". One such example may be the articulated train units (*TGV*, *Eurostar* etc. with two carbodies resting on the same bogie) which have empirically shown to be safe at high-speed derailments. In the same manner the Swedish train operator *SJ* and Interfleet Technology Sweden describe some current Swedish trains (*X 2000*, *X 10*) as having favourable properties in this respect. In a number of incidents the trains have behaved very well, in the sense that the trains have stayed upright on - or sufficiently close to - the track bed after, for example, an axle failure.

1.2 Previous research

The research and development disclosed in this area of railway safety is rather scarce. Especially the disproportion between the amount of papers written on crash safety on one side, and train stability after a derailment on the other side, is striking. There is, to the author's knowledge, no research results published that systematically analyses the relationships between the seriousness of an event when a vehicle leaves the rails and the respective train design, in particular the design of the running gear.

The oldest references found in the field of post-derailment assessment date back to 1972 [52] [51], where the equations of motions for tank wagons (three degrees of freedom for each car in the horizontal plane) are coupled with a simplified system of constraints. The motion of each derailed vehicle is governed by a horizontal ground friction vector, inversely directed to the velocity vector, and the couplers, which are not allowed to fail. Several dependencies are sought such as the influence of ground friction coefficient, number of cars in the train, train speed, coupler moment etc. The model is validated with good results in terms of the number of derailed cars for an authentic case, chosen to best match the two-dimensional assumption. The results follow a pattern according to accepted mechanical principles. In this context, one finding is interesting to mention: a mixed consist of vehicles, two loaded followed by one empty, leads to a substantial increase of the lateral deflection from the track centre line.

In an attempt to improve the safety of freight wagons, a computer program was developed to predict different catastrophic scenarios related to tank wagon accidents [6] [7] (liquid spill, fire effects, explosions etc.). One of the sub-models in the program considers the derailment mechanics, which allows motion with four degrees of freedom per vehicle as well as coupler separation. Roll is, however, only included in the equations of motion for uncoupled vehicles. Derailment is initiated at a pre-defined vehicle in the train consist. All the following vehicles are considered as derailed, implying that Coulomb friction forces act in reverse direction to the velocity vector at the two bogie locations of the vehicles. This program is not reported to be validated, but an example of a hypothetical derailment prediction is presented.

In paper [16] the main focus is train impact on adjacent structures. A mathematical model describes the vehicle's motion after derailment. As in the previous work, once a derailment state is postulated, a simplistic approach to the wheel-ground interface is implemented. The two-dimensional equations of motion in the horizontal plane are then solved iteratively using the principle of virtual work. A parametric study is presented, thus involving the speed of the train at the instant of derailment, the friction coefficients and the so-called derailment angle. The authors conclude that the lateral train velocity component is highly affected by the wheel-ground friction coefficient. Meanwhile, the friction coefficients are reported to have a negligible effect on the longitudinal velocity component.

The possibility of applying three-dimensional multi-body system (*MBS*) simulations, instead of finite element (*FE*) simulations in crash analysis is studied in paper [17]. The model accounts for six degrees of freedom for each relevant rigid-body part of the vehicle. Although the main focus is the possibility to determine the gross motion of trains after a crash impact, the authors announce that derailment dynamics is also incorporated for crash scenarios. However, little is revealed regarding the wheel-ground contact. In order to study the possibility of derailment, a side crash simulation involving the Korean High Speed Train (*KHST*) is performed. The lateral displacements of the overridden cars await, however, experimental validation.

1.3 Scope, structure and contribution of this thesis

The scope of this thesis is to systematically analyse various train features and design parameters in order to minimise the risk of catastrophic consequences related to high-speed derailments. In this context "high-speed" is considered to be speeds above 70 km/h.

The database including all the collected incidents and accidents relevant for the scope of this thesis, are presented in Chapter 2, subdivided into five categories based on the initial cause of derailment. A general discussion follows, as well as a list of potential critical vehicle parameters.

Chapter 3 focuses on the possibility of preventing derailments after an axle failure on the outside of the wheel, at the journal. Two validation cases of the intended pre-derailment computer model are presented. Additionally, a parameter study is performed on the wheelset mechanical restriction relative to the bogie frame and its influence on the tendency of derailment in curves.

In Chapter 4, a tentative study is presented on the geometrical requirements of an axle-mounted brake disc to act as a substitute guidance mechanism.

Chapter 5 focuses on means to obtain a better understanding of impact phenomena between a rail vehicle wheel and concrete sleepers through a finite element approach. A tentative validation of the proposed computer model is presented.

This thesis is believed as being a pioneering work in the area of railway safety aiming at reducing the lack of knowledge on derailment dynamics and its consequences, in particular the influence of the vehicle features and the design parameters.

This thesis makes the following contributions to the field of railway safety and also to simulations methodology in itself:

- A compilation of accidents and incidents is presented on which basis several vehicle features and train design parameters are identified as being able to limit the consequences associated with train derailments at higher speeds.
- A comprehensive vehicle model is developed and successfully validated with two authentic events in terms of the pre-derailment sequence of events after axle journal failures.
- Presents and analyses in detail one method to limit flange climbing derailments caused by axle journal failures by inserting mechanical restrictions between the wheelset and the bogie frame.
- Presents a sensitivity analysis of the wheelset guidance stiffness and its effect on the derailment tendency after an axle journal failure.
- Indicates an alternative guidance mechanism in case of wheel climbing derailments by allowing the brake disc to engage with the rail, thus stopping a possible lateral displacement. The thesis also studies the lateral geometrical requirements of an axle-mounted brake disc for a safe engagement with the high rail in curves, as a result of wheel flange climbing derailments.

- A finite element (*FE*) model is developed for studying the impact phenomena between a rail vehicle wheel and concrete sleepers. In particular, the proposed *FE* model will be used for obtaining hysteresis data for the force as function of concrete material indentation for further development of the multi-body simulation technique.
- The *FE* model is tentatively validated with good results based on one authentic accident event.
- *FE* simulations are performed on the initial rebound, as a rail vehicle wheel impacts concrete sleepers.

2 Inquiries on incidents and accidents

2.1 Introduction to the database

The task of collecting detailed qualitative and quantitative information regarding railway vehicles accidents and incidents across country borders is not trivial. This state of affairs has also been pointed out by the European Transport Safety Council, who mandates the European member states to set up an *EU* accident and incident database [15].

One obvious impediment, besides language barriers, is the tendency of some authorities and railway companies not to make such information public. Unless direct contact is established with key representatives of such organisations, one is left to rely on brief general observations from newspapers or internet web sites. Other difficulties appear as the degree of detailed information seems to be proportional to the amount of deceased and injured people; thus, many incident reports are lacking relevant detailed data. Generally, the quality of information varies largely among the incident and accident reports. One common feature shared by most of the reports is, naturally, a focus to reveal the root cause of the problem. Doing so, many of them neglect to mention basic factual information, for example on which side of the track did the wheelset derail or the type and location of encountered switches in the track. This unintentionally obstructs any future post-accident analysis of the vehicle's dynamic behaviour within and after a derailment. Further, it is sometimes hard to obtain detailed vehicle data.

Fortunately the Swedish organisations SJ *AB*, Banverket, Bombardier Transportation, the Swedish Railway Agency (former Railway Inspectorate) and Interfleet Technology Sweden have provided a quite open access to relevant data for the purpose of this research project. Therefore, a considerable amount of relevant detailed information has been collected from Swedish cases. In most other cases a more brief and general information is available, with a few exceptions.

As a basis for this research project, a previously developed database [9] containing Swedish incidents and accidents was used. This database was originally set up from different sources. As a first step in this project, the original database was condensed according to the following criteria: (i) passenger trains with a speed above 70 km/h and (ii) with the primary cause of derailment being axle or wheel failure, track defects or objects on track.

Successively more cases have been included in the database. In April 2005 a total number of 33 relevant incidents and accidents are included.

Based on available reports, many of them including relevant photos, the course of events has been studied immediately after the failure, paying special attention to the lateral deviation from the track, thus causing train buckling, train turn over, collisions with heavy obstructions or similar events. The first intention in setting up such a database was to accumulate as much information as possible in order to relate post-derailment dynamics with various types of train design. In some cases the collected empirical data enables partial conclusions to be drawn directly, but most of the cases would require further studies, e.g. full computer simulations.

A summary of factual information relevant for the studied topic, divided into their primary cause, is presented for each event in the section to follow. In some cases, the sequence of events is the author's interpretation, based on the collected factual information. Each description is preceded by an event ID number, in order to simplify any cross-reference identification along the current report.

The number of deceased or injured passengers or crew members has been deliberately left outside each accident description. In the present study, the outcome of a derailment is considered "safe" or "successful" as long as *no part of the train is deflected laterally as to leave the track bed or collide with heavy obstacles or to turn over*, although material damage or minor passenger injuries may also occur in such cases Along this thesis the following definitions will be used for describing the events, according to [9]:

- incident - a non-intended event with no harmful consequences
- accident - a non-intended event with harmful consequences

Unless otherwise stated, all positioning descriptions are related to the intended direction of travel of the train. All measures are in common standard European units (m, km/h etc.) and have sometimes been approximately converted from 'inches', 'miles', 'miles per hour' or similar.

Finally, an attempt to draw general conclusions and to find the common features is presented at the end of this chapter. This is followed by a general discussion.

2.2 Description of incident and accident events

The narrative description of each event in the database is divided into five categories based on the initial derailment cause. These are: (1) axle failure on the outside of the wheel; (2) axle failure on the inside of the wheel, i.e. between the wheels; (3) broken rail or other track defects; (4) wheel defects and (5) other causes, i.e. derailments that could not be placed directly in any of the other categories but having relevance to the studied topic.

2.2.1 Axle failure on the outside of the wheel

(**Event ID 1**)

On the 8th of September 2001 at 4 km north of *Tierp*, Sweden, an axle journal failure affected the *X 2000* rear end power unit on the outside of the trailing wheelset of the leading bogie, on the left-hand in the direction of travel [44]. A general photo of this type of train is shown in Figure 2-1.

Just as the vehicle entered the circular part of a right-hand curve of radius R = 1805 m, the leading axle derailed towards the right (i.e, above the lower rail) at a speed of 200 km/h and with a lateral track plane acceleration a_y *of* approximately 1 m/s^2 (cant deficiency of about 150 mm). The affected trailing wheelset remained however on or above the rails, presumably with the left unloaded wheel bouncing vertically on the

railhead until the train stopped. Meanwhile the train passes a right-hand trailing switch which sustained extensive damage, according to the report. The train unit stopped approximately 5600 metres further on from the point of derailment with the left wheel uplifted about 20-30 mm above the rail, see Figure 2-2.

Figure 2-3 shows the left-hand wheel of the derailed leading wheelset together with its bogie frame. It is worth noticing a slight guiding effect provided by the lowered bogie frame in its contact with the high rail. Furthermore, the contact between the low-reaching bogie frame and rail head seems to diminish the negative effect of the unloaded wheel, hereby stopping a further vertical displacement of the bogie. This event will be subject to extensive computer simulations presented in Section 3.3 in order to analyse and possibly explain the quite unexpected behaviour of *the leading wheelset derailing towards the low (inner) rail in the curve* as a result of an axle failure on the trailing axle above the high (outer) rail.



Figure 2-1 Exterior photo of an X 2000 train composed of:
- one power unit
- four or five trailer passenger cars
- one driving trailer car.



Figure 2-2 Detailed picture of the left-hand wheel of the trailing wheelset, *as a result of a axle journal failure at 200 km/h on this axle. The derailed leading wheelset is seen in the background.*

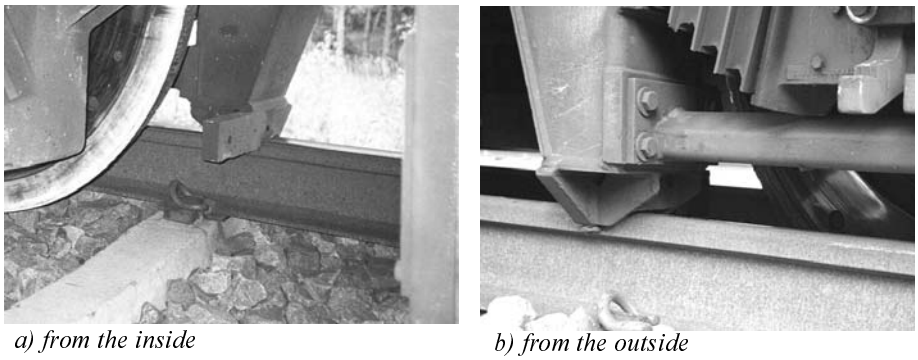

a) from the inside *b) from the outside*

Figure 2-3 Detailed photo of the left-hand wheel on the derailed leading wheelset and the low-reaching bogie, *seen from different positions.*

(Event ID 2)

On the 10th of September 2001, another axle failure at the same location in the train as in Tierp, occurred on the *X 2000* power unit on the Stockholm-Gothenburg main line in the neighbourhood of *Gnesta*, Sweden [43]. Since the power unit was now located at the front end, the affected axle is now located in the trailing bogie in the direction of travel, as the leading wheelset on right-hand wheel. The train entered an S-curve at a speed of 180 km/h, initially to the right then to the left, both with a radius of R = 998 m leading to a lateral track plane acceleration a_y of approximately 1.6 m/s^2 (cant deficiency 245 mm). A hot-box detector warned the driver, who immediately applied the emergency brakes as the train was just entering the circular part of the second (left-hand) curve. No wheel derailed as a result of the failure but, as in Tierp, the wheel on the side where the axle failed was hanging about 20-30 mm above the rail as the train came to a safe stop, see Figure 2-4. This case is also extensively studied further on in this work by means of computer simulations, in an attempt to find out why the leading outer wheel did not derail and under what circumstances the wheelsets would have derailed.

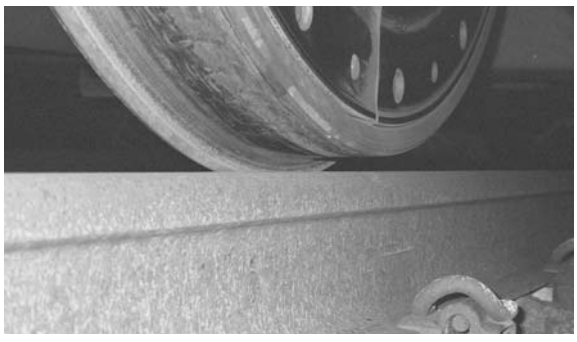

Figure 2-4 Detailed picture of the right-hand wheel of the third wheelset in Gnesta, *as a result of an axle journal failure above this wheel at 180 km/h.*

(Event ID 3)

The *X 2000* power unit was even earlier involved in an axle journal failure, on the 29th of June 1998 on the main line section *Kumla-Hallsberg* [45]. The incident occurred on the fourth axle in the direction of travel, at the right-hand wheel at a speed of 140 km/h, with the power unit located at the leading end. The train was brought to a stop by a hot-box detector alarm, passing a number of switches. However, all the wheels remained in contact with the rails and consequently no derailment occurred.

2.2.2 Axle failure on the inside of the wheel

(Event ID 4)

On the 18th of February 2001 at *Lindekullen*, Sweden, the fourth car of an *X 2000* train derailed with the leading wheelset, as a result of an axle failure at the right-hand brake disc at a speed of 140 km/h [42]. The driver applied full service braking and stopped in 1800 m. Along this distance the train passed through a left-hand curve at a lateral track plane acceleration of $a_y \approx 1.6$ m/s^2, as well as three switches at the above mentioned speed. At the first left-hand trailing switch, the right-hand diverging rail was severally bent by the bogie frame, see Figure 2-5. At the next trailing switch, also seen in Figure 2-5, the bogie frame broke through a section of the left-hand diverging rail. The damage on the next following facing switch was not documented.

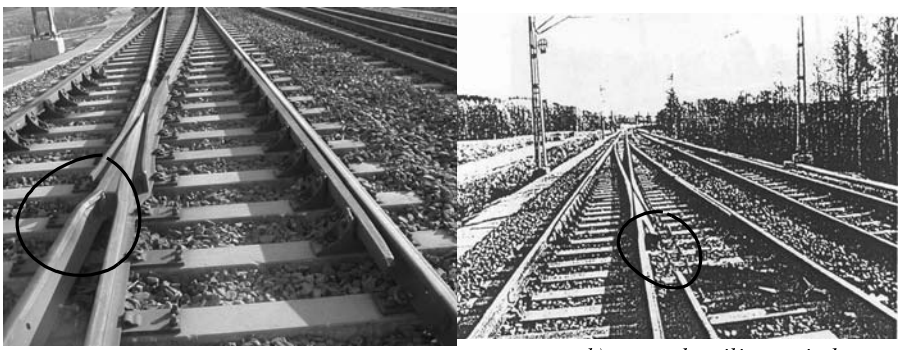

a) first trailing switch *b) second trailing switch*

Figure 2-5 Damage by the running gear to the first and second encountered trailing switch at Lindekullen.

However, the train remained aligned on the track bed as the low-reaching parts of the bogie frame forced the car to follow the track centre line by vertically sinking down and capturing both rails from the outside. This mechanism is outlined in the schematic of Figure 2-6. The favourable function of the low-reaching bogie frame passing in a derailed condition through curves can easily be understood. When it comes to passing switches in the same condition, the sequence of event might not be as easily anticipated. Nevertheless, analysis of the damage inflicted to the first and second switch reveals the

ability of this particular bogie frame type to literally brake through the diverging rails of the switches, without any large lateral deviation. This favourable behaviour, from a safety point of view, can also be attributed to the low-reaching bogie frame in combination with its superior strength, see Figure 2-7 showing the right side, forward section of the derailed bogie, with an almost intact frame.

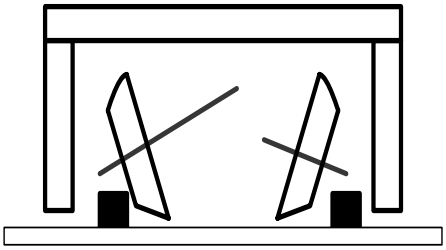

Figure 2-6 Scheme showing the favourable effects of the "low-reaching" bogie frame involved at Lindekullen.



Figure 2-7 Photo of the forward section of the leading bogie, including the failed axle at Lindekullen.

(Event ID 5)

On the 30th of May 1997 at *Slätte*, Sweden, another case of axle failure on the inside of the wheel occurred with an *X 2000* train [45]. The train was travelling at a speed of 190 km/h, when the right-hand leading axle on the leading driving trailer failed and as a result, the right-hand wheel on this axle derailed. However, the wheel on the left-hand of the same axle maintained rail contact. Although the driving trailer was positioned as the first unit in the train, it did not deviate laterally when passing through a left-hand facing switch, and further on, a slight left-hand curve with a radius $R = 2578$ m.

Unfortunately, no photo documentation could be found from this interesting event. The report mentions, however, that the bogie continued its forward motion after the failure

skidding with the guard-rail on the right-hand rail. A guard-rail is a metal beam connected with each side of the low-reaching bogie frame, located only at the front and rear end of the train. An *X 2000* driving trailer guard-rail of identical design as in the Slätte case can be seen in Figure 2-8.

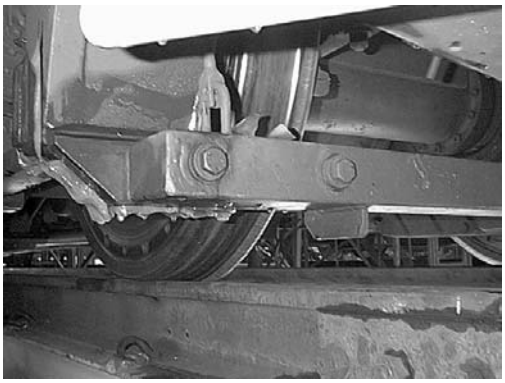

Figure 2-8 Photo of an X 2000 driving trailer guard-rail.

(Event ID 6)

On the 16th of March 1992, a leading axle failed at the gear-box side on the second car of an *X 10* commuter train in the north of Stockholm, Sweden, between *Märsta* and *Rosersberg* stations [37]. The train had a speed of 90 km/h at the time of derailment. The report does not clarify how, where, and under what conditions the derailment occurred. However, based on the author's own inquiries with an on-site inspector at the time of the incident, the following observation can be made: the derailed wheelset started eventually to deviate laterally towards the other parallel track at a facing switch. At a switch, the front end of the second car stopped to diverge and regained the intended forward path.

The *X 10* bogie shares similarities with the bogies of *X 2000* in terms of a low-reaching bogie frame design, as well as vehicle inter-connections that allow small lateral relative movements of the carbody ends. These facts may have played a role for the successful cause of events, although it can not be proved at this stage.

(Event ID 7)

On the 3rd of September 1997, a *VIA Rail* passenger train consisting of two front end *F40PH-2D* diesel-electric locomotives, followed by 19 cars, derailed at *Bigger*, Canada, when travelling at a speed of 107 km/h [48]. As a result of an axle failure between the wheel and the gear-box, the leading wheelset of the second locomotive could no longer maintain gauge and the right-hand wheel dropped on the inside of the rail. The unit travelled for about 1.6 km, until the derailed wheel ran into a guard rail of a trailing switch. The train finally stopped 180 m further on with both locomotives derailed and overturned as well as 13 cars resting at various positions, see Figure 2-9.

It is the author's opinion that the train buckled as a result of the sudden retardation (107 to 0 km/h in 8 s) producing large compressive forces in the train. This caused large unstable lateral displacement that is clearly seen in the aerial view.



Figure 2-9 Aerial photograph of the scattered VIA Rail locomotives and cars.

(Event ID 8)

On the 5th of March 1984, the *Amtrak* Silver Star train on route from Washington D.C. to Miami, Florida, derailed due to an axle failure near *Kittrell*, North Carolina, USA [31]. The train consisted of three *F40-PH* diesel-electric locomotives pulling 18 cars at a speed of 126 km/h. An overheated traction motor support bearing on the left-hand of the leading wheelset of the third locomotive led to the derailment of both wheels on the inside of the rails. A trailing switch located 450 m further from the initial derailment switch, linking the main line with a left-hand diverging sidings track, caused the general derailment of all subsequent cars from the third locomotive. The first 10 cars ended up at a substantial lateral deflection from the main track, and three of them jack-knifed. Furthermore, the second car in the train was completely decoupled from the rest of train.

2.2.3 Broken rails or other track defects

(Event ID 9)

The night train on the main line up track Malmö-Stockholm, Sweden, consisting of one front end *Rc* locomotive and 13 passenger cars, derailed on the 23rd of January 1992, at *Sävsjö* station, Sweden [39]. The train had a speed of 110 km/h at the time of derailment.

The following hypothesis regarding the sequence of events is being put forward in the incident report:

- A previously known crack on the right-hand rail developed to a full rail gap of 0.9 m under the leading bogie of the 10th car. A combination of factors, i.e. the train speed, the vertical resistance imposed by the car couplings etc. is believed to have prevented the following wheels from falling off the top of the rail level into the gap. However, the wheels of the rearmost bogie did fall in the gap and impacted the right-hand rail from the outside. This impact led to another 3.25 m piece of rail to break.

The train was stopped safely within 800 m from the point of derailment, on a tangent track section. However, the derailed trailing bogie of the rear end car ended up fouling the down main track. Luckily, the train scheduled on the down track was two minutes late and could be stopped in time.

The report does not make any attempt to explain as to why the bogie deviated so much laterally. Additionally, no information regarding the presence of switches could be found throughout the report. It is the author's hypothesis that in the course of events followed by the wheel's impact with the outside of the right-hand rail, the derailed bogie gained a certain yaw angle towards the other track in combination with a lateral rebound after impact with the rails. This could be the explanation why, in the absence of switches, the bogie could have diverted laterally.

(Event ID 10)

On the 14th of January 1986 a trainset consisting of one front end *Rc* locomotive followed by 10 cars and one rear end *Rc* locomotive, derailed on the main track *Upplands Väsby - Antuna*, Sweden [38]. As the train was travelling at a speed of 125 km/h, a rail failure initiated the derailment of the trailing bogie of the eighth car and the leading bogie of the ninth car, which deviated substantially towards the up main track. As the train stopped, 1800 metres from the point of derailment, a commuter train passed on the up main track and a minor collision occurred with the rear view mirrors of the commuter train. The final position of the derailed trailing bogie on the eighth car is shown in Figure 2-10, which is otherwise of the same bogie type as in the Sävsjö incident (Event ID 9). This type of bogie has no means of retaining any lateral deviation by means of a low-reaching bogie frame or brake discs engaging with the rail.



Figure 2-10 The derailed leading bogie of the eighth car in the Upplands Väsby - Antuna incident.

(Event ID 11)

On the 6th of July 1997, one front end *Rc* locomotive followed by seven cars derailed as a result of a track buckle on the single track section of the main line Stockholm-Malmö, at *Tystberga*, Sweden [46]. The buckle developed under the train, which was travelling at a speed of 110 km/h, and led to the derailment of the trailer bogie on the sixth car and both bogies on the seventh car, which also was the rear end vehicle in the train. Figure 2-

11 shows the end of the train, in the direction of travel, with its rear bogie approximately 1 m to the left.

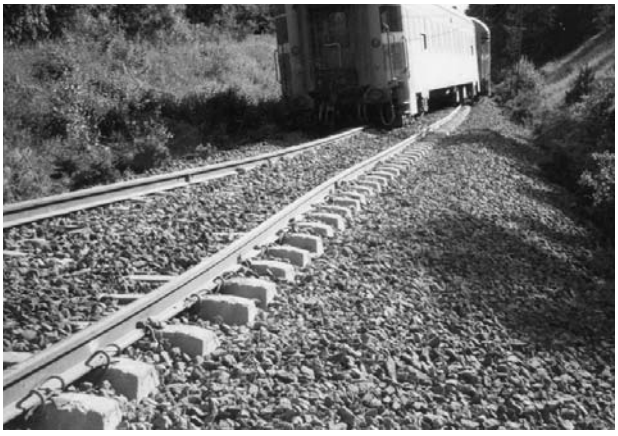

Figure 2-11 ***The rear end car with the trailer bogie at a substantial lateral deflection*** *(photo: Håkan Hansen).*

It is the author's opinion that such a displacement could have caused the car to overturn if it would not have been for the relatively flat ballast shoulder as well as a possible stabilizing effect from the preceding sixth car. Impact marks on the sleepers on the right-hand of the right rail, suggest that at least one of the wheelsets also derailed to the right of the track. The train was stopped in approximately 370 m from the point of derailment, as shown in Figure 2-12.



Figure 2-12 ***The track buckle and also the point of derailment at Tystberga*** *(photo: Håkan Hansen).*

(Event ID 12)

On the 18th of July 1994, a crane lorry, exceeding its maximum height limit, shifted a viaduct and its track laterally when passing under the West Coast Main Line, near *Varberg*, Sweden [40]. A few minutes later, the train from Malmö to Gothenburgh, consisting of one front end *Rc* locomotive and 12 cars passed by at a speed of 100 km/h. The locomotive, the subsequent five cars and the leading bogie of the sixth car derailed with all wheelsets and stopped after 120 m in the following configuration: all locomotive wheelsets ended up to the right of the right-hand rail, the first and second car straight across the track, the third and fourth car with all wheelsets to the right of the right-hand rail, the fifth car with bogies straight across the track and the sixth car with the leading bogie wheelsets to the right of the right-hand rail. Post-accident measurements showed a track misalignment of 0.6 m on the side where the train entered the viaduct and 0.14 m on the opposite side of the viaduct. However, part of the rail shift might be a result of the derailment.

(Event ID 13)

On the 31st of October 2001, an *SNCF TGV* train derailed at a speed of 130 km/h on the Paris to Hendaye main track at *Saubusse*, France, as a result of a rail section fracturing beneath the train [18]. The rear power unit overturned and the remaining 10 articulated cars derailed but remained upright at a minimal lateral distance from the rails, see Figure 2-13. No information could be found regarding the front end power unit.

The absence of further information makes impossible to draw any conclusion regarding this accident. However, it is interesting to note that apparently, the only overturned vehicle, the power unit, is also the one two conventional bogies.



a) **b)**

Figure 2-13 ***a) The rear end of the articulated rack of cars*** *(seen opposite to the direction of travel);*
b) The overturned rear end power unit, with the upright standing articulated cars partly hidden *(seen in the direction of travel)*.

(Event ID 14)

On the 21st of December 1993, an *SNCF TGV* train derailed at a speed of 294 km/h at *Haute Picardie*, France [3]. A trench under the track bed from World War One developed into a large sink-hole, seven metres long and four metres wide, see Figure 2-14. The unsupported track section caused a derailment of the last four rear cars and the rear end power unit. However, the unit stopped safely in approximately 2300 metres. No other information could be obtained regarding this incident.



Figure 2-14 The suspended high-speed track, after the passage of a TGV trainset at 294 km/h. *(photo: Jean-Marie Hervio / Le Parisien Libéré.)*

(Event ID 15)

On the 17th of October 2000, an *IC225* train derailed south of *Hatfield* station on the down line London - Leeds, UK [21]. Just as the train was starting to negotiate a right-hand curve of radius R = 1462 m at a speed of 180 km/h, the left-hand outer rail fractured for a distance of approximately 35 metres due to rolling contact fatigue. From the fourth car on all subsequent wheelsets became derailed, and some of the bogies detached from the carbody underframe. The seventh, eighth and ninth car overturned, in the author's opinion probably as a result of wheelsets impacting with rails of the down slow line in, probably in combination with the outer wheels sinking down in the ballast bed.

Schematic and aerial photo are presented in Figure 2-15. Furthermore, the ninth car was completely detached from the rest of the train as the coupler element failed. The type of bogies equipped on the *Mark 4* coaches, had apparently no "last barrier" to cope with the loss of lateral guidance. For this particular sequence of events, a bogie frame with the ability to capture the low rail from the outside would have, probably, changed the tragic outcome of the derailment.

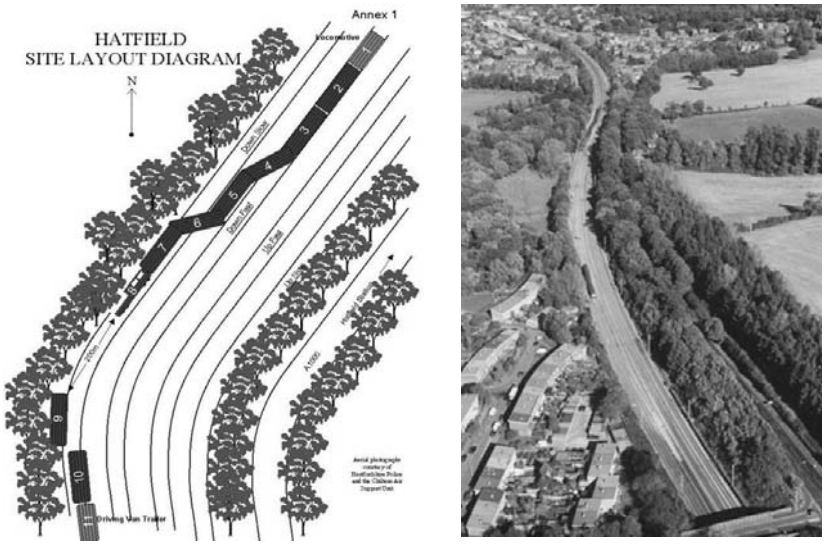

a) vehicle location after derailment *b) derailment site aerial photo*

Figure 2-15 The accident at Hatfield.

(Event ID 16)

A similar type of accident as the Hatfield case (ID 15) occurred on the 12th of November 1983 on the route Texarkana to Dallas, near *Woodlawn*, Texas, USA [30]. The train consisted of two *F40-PH* diesel-electric locomotives pulling nine double-decker Superliner cars, travelling at a speed of 115 km/h. Just as 15 m were left of the circular part of a left-hand curve of radius R = 1247 m, a 10 m rail section on the outer (high) rail started to fracture. According to the report, the fracturing occurred most probably underneath the second car, as the two front end locomotives and the subsequent car did not derail, unlike the rest of the cars. Furthermore, the rearmost three cars overturned, while the fourth from the rear end tilted towards the right (outwards relative to the curve) at an angle of 30° .

(Event ID 17)

On the 10th of May 2002, a class *365 EMU* consisting of four cars, derailed at *Potters Bar* station at a speed of 153 km/h, on the route London to King's Lynn, UK [22]. As the train was negotiating a facing switch, the front strecher bar fractured, leading to a movement of the switch blade as the last three bogies of the train were passing through. The trailing bogie of the third car and the leading bogie of the forth car derailed to the left but continued the forward motion through the switch. However, the trailing bogie of the fourth car became rerailed, with its wheels properly engaged for the left diverging route towards the down slow line. The schematic of the site area with the position of the cars is presented in Figure 2-16. Based on the sequences of events concluded by *HSE* for

this particular event, it is the author's opinion that little could have been achieved by any "last barrier" in the bogies.

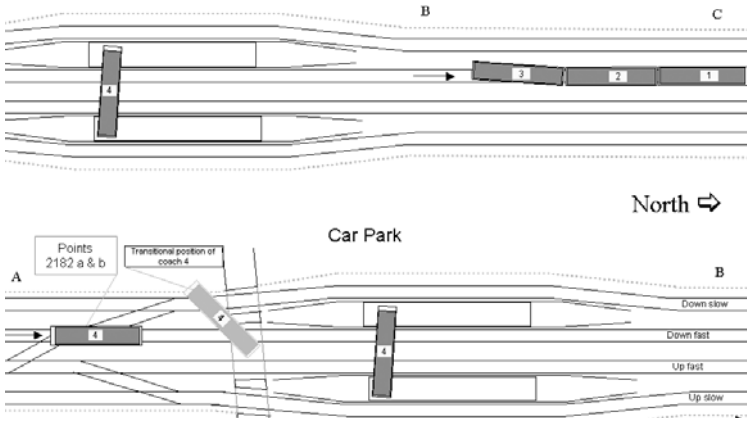

Figure 2-16 Diagram showing the position of the cars at Potters Bar.

(Event ID 18)

On the 29th of July 2002, the *Amtrak* Capitol Limited from Chicago to Washington D.C., USA, consisting of two *P42DC* locomotives pulling 13 Superliner double-decker cars, derailed at *Kensington* due to a track buckle [26]. An initial service brake was applied from a speed of 96 km/h, at a distance of 350 m from the misalignment, estimated by the driver to about 0.45 m to the right. The locomotives remained in contact with the rails, but 11 cars derailed and four of them overturned, see Figure 2-17. Just after the derailment, the train entered into emergency braking as one of the car separated from the others. The accident site was on tangent track and no switches are mentioned in the report.



Figure 2-17 Some derailed and overturned vehicles at the Kensington accident.

(Event ID 19)

On the 17th of March 2001, an *Amtrak* California Zephyr, consisting of two locomotives and 16 Superliner double-decker cars, derailed near *Nodaway*, Iowa, USA [25]. The cause of the accident was attributed to a broken rail which developed as the train was travelling at a speed of 80 km/h. All but the five rearmost cars derailed, and so also the front end locomotives which decoupled from the rest of the train. The aerial photo of the accident site in Figure 2-18 shows the typical dangerous, zig-zag formation [24], with cars overturned and large lateral deviation from the track.

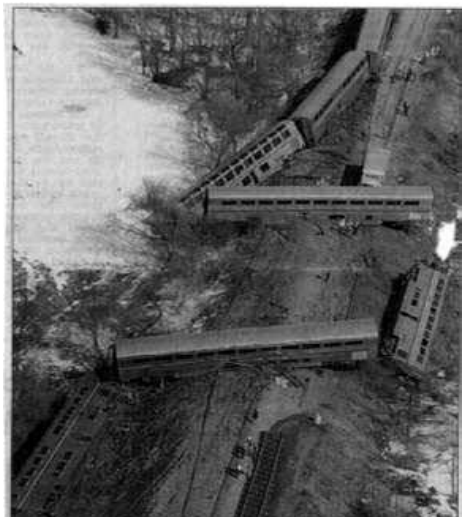

Figure 2-18 Aerial photograph at the Nodaway accident, with scattered carriages down the embankment.

Moreover, the substructure formation consists of embankment with high slopes, which could have had an aggravating factor on the consequences. No further information could be found regarding the track geometry.

(Event ID 20)

On the 18th of April 2002, an *Amtrak Autotrain*, consisting of two locomotives, 16 Superliner double-decker cars and 24 *Autorack* cars derailed due to a track buckle condition near *Jackonville*, Florida, USA [27]. As the train was negotiating the circular section of a left-hand curve of R = 3500 m at a speed of 90 km/h, the driver observed a misalignment ahead of about 0.25 m with both rails parallel towards the outside of the curve. The train was immediately put into emergency braking and stopped approximately 380 m from the point of derailment. The leading locomotives and the succeeding two cars remained on the rails. All the other cars up the 18th, derailed and were found either on their side or leaned at various angles. Although cars 18 to 23 (all autorack cars) did not pass the initial point of derailment, they derailed in a less dangerous, saw-tooth [24] mode remaining however upright and close to the track. The post-accident disposition of the vehicles can be seen in an aerial photo of the accident site in Figure 2-19. The *NTSB* accident report concluded that one aggravating factor in

contributing to the dangerous zig-zag or "accordion" formation of some of the derailed cars was a seven second delay in the brake application between the front and the rear end of the train.



Figure 2-19 Aerial photograph of overturned vehicles and the "accordion" formation at Jackonville.

(Event ID 21)

A track buckle condition near *Batavia*, Iowa, on the 23rd of April 1990 was also the cause of derailment for the *Amtrak* California Zephyr train on route from Oakland, California to Chicago, Illinois, USA [29]. The train consisted of three front end diesel-electric locomotives, *F40PH*, and 16 Superliner double-decker cars, travelling at a speed of 120 km/h. All the rearmost eight cars derailed as a the track started to buckled under the train. The S-shaped misalignment was estimated by on-site officials to have a magnitude of almost 0.5 m maximum lateral diplacement over a 9 m length of track. All the derailed cars remained coupled, the first one upright and the rest leaned at various angles, two of them as much as 60° towards the opposite track. The rearmost derailed car stopped after approximately 250 m from the point of derailment and 60 m ahead of a right-hand trailing switch.

(Event ID 22)

On the 5th of August 1988, the *Amtrak* Empire Builder train on route from Chicago, Illinois to Seattle, Washington derailed as a result of a track buckle near *Saco*, Montana, USA [33]. The train consisted of two *F40-PH* diesel-electric locomotives and 12 Superliner double-decker cars, travelling at a speed of 126 km/h when the engineers observed an S-shaped lateral misalignment. The train entered the damaged area, of unknown magnitude, at a slightly lower speed of 112 km/h and derailed. Both locomotives and the following car remained, however, on the rails. The second and third

car derailed and remained upright, but uncoupled from the subsequent five cars which overturned, see Figure 2-20. The ninth car tilted at an angle of 45 degrees, while the three rearmost cars remained upright. The track from the point of derailment to full stop was tangent with no switches.



Figure 2-20 Overturned cars at Saco *(photo: Richard C. Logan)*.

(**Event ID 23**)

On the 9th of August 1997, the *Amtrak* Southwest Chief train derailed on the east bound track near *Kingman*, Arizona, USA [28]. The train consisted of four locomotives, 10 Superliner double-decker cars and six material handling cars (*MHC*) travelling at a speed of 145 km/h when crossing an unsupported bridge section. Heavy flooding in this areas had resulted in erosion of the foundation supporting the 11 m bridge. The train was brought to a stop just as the rearmost passenger car crossed the bridge. The first two locomotives did not derail but uncoupled from each other and the rest of the train. The third and fourth locomotives derailed and uncoupled, but remained aligned with the track bed. All the other cars that passed the bridge derailed but remained upright, however some at large lateral deviation from the track centre line.

(**Event ID 24**)

On the 24th of November 2002, a First Great Western intercity train derailed at *West Ealing*, on the up main Swansea - Paddington line, UK [19]. The train consisted of eight *Mark 3* cars and two power units, one at each end when travelling at a speed of 200 km/h. The left-hand leading wheel of the leading bogie of the fifth car ran over a piece of a broken fishplate originating from the attachment between the crossing of a facing switch with the main line. Both wheelsets of the leading bogie derailed towards the down main line. However the train came to a stop safely, upright and in-line, after travelling a distance of 2200 m from the point of derailment, see Figure 2-21.



Figure 2-21 Photograph of the derailed bogie at West Ealing.

The report points out that there is evidence of a 17 m length of rail, placed in between the main lines and just after the switch, had been disturbed, indicating that the derailed wheel landed on or very close to it. Whether this sequence of events prevented the bogie to deviate even further towards the other line seems to be questionable, according to the author. However, as the train came to a stop, no switches and only tangent track was encountered. The possible effect of brake discs in this case can not be assessed since no information could be achieved regarding the path of the derailed wheels.

This particular incident is very interesting and a more detailed analysis should be undertaken once more detailed information is made available.

2.2.4 Wheel defects

(Event ID 25)

On the 16th of July 1998, a Great North Eastern Railway operated *IC225* train derailed with one car on the main down track Kings Cross to Edinburgh at *Sandy*, UK [34]. The rearmost passenger car, in front of the driving van trailer, left the rails with all its wheels as the train was travelling at 200 km/h and stopped within 1200 m from the point of derailment, upright and in-line.

The derailment started in a left-hand curve of R = 1851 m and was caused by the detachment of half of the rim of the left-hand wheel belonging to the trailing wheelset of the leading bogie. Based on the author's own inquiries, the derailed wheels were initially rolling to the right of the track but after encountering a trailing switch to the up fast line, and a facing switch to the down slow line, the rolling of the wheels diverted to the left of the track. No information could be obtained regarding the location of the switches along the track, which could help to establish the speed at which they were passed successfully.

Once again, as in the West Ealing incident (ID 24), more information should be collected, as for example the bogie design, which would possibly establish the cause of such a favourable behaviour.

(Event ID 26)

On the 14th of December 1992, a *TGV* train on the high-speed line Annecy to Paris derailed as passing the station Mâchon-Loché at a speed of 270 km/h [47]. One bogie derailed, assumed to be caused by a flat wheel. However, the train came to a stop safely. Unfortunately, no other information could be retrieved for this event.

(Event ID 27)

On the 3rd of June 1998, the Wilhelm Conrad Röntgen *ICE1* train derailed when travelling at a speed of 200 km/h on the line from München to Hamburg at *Eschede*, Germany [12][13]. Due to an unfortunate combination of events, the derailment finally led to impact with a reinforced concrete bridge which collapsed over the train.

The primary cause of this major accident was attributed to the failure of the leading right-hand rim of a resilient rubber cushioned wheel of the trailer bogie in the first passenger car after the power unit. The train continued for approximately 5.5 km on a tangent track segment with no switches, with the failed wheel disc rolling on the rails and with the wheel rim caught and hanging in the bogie. At a distance of 300 m ahead of the bridge, partly seen in Figure 2-22, parts of the disc of the failed wheel impacted a check rail of a trailing switch so that an 8 m length of rail was pulled up from the track and penetrated the floor of the first passenger car.



Figure 2-22 Aerial view of the entrapped cars in the collapsed bridge at Eschede.

At the same time, the leading wheelset of the trailing bogie derailed to the right and continued forward destroying the rod of a facing switch located just 100 m from the bridge. The leading bogie of the second car deviated through the switch towards the slow line towards the right and derailed. From this switch on, the trailing bogie of the second car and both bogies of third and fourth car derailed in a similar manner.

As the longitudinal train forces increased, a separation occurred between the third and fourth car which increased the lateral deviation of the already derailed cars. The bridge collapsed over the train, once the third car impacted the supporting pillar causing the catastrophic entrapment of the rest of the train.

(**Event ID 28**)

On the 24th of August 1980, a train consisting of one *Rc* locomotive and 13 cars derailed due to a loose wheel rim at a speed of 120 km/h on the main line Uppsala to Stockholm at *Upplands Väsby*, Sweden [41]. How and when this wheel on the right-hand of the leading wheelset in the trailing bogie of the sixth car reached this catastrophic condition is unknown. Certain is, however, the point of derailment, located at the tip of the crossing of a facing switch, seen in the photograph in Figure 2-23.



Figure 2-23 ***The point of derailment,*** *at the crossing marked with 1, at the Upplands Väsby accident. Wheelset derails as soon as the guard-rail, marked with 2 ends.*

As the wheelset could not maintain the prescribed gauge, the flange of the wheel ran into the tip of a facing switch crossing, marked with 1 in Figure 2-23 and started rolling with the flange on the right-hand railhead. As soon as the check rail ended, marked with 2 in Figure 2-23, the leading wheelset derailed towards the right and started rolling at a

significant yaw angle towards the opposite up main line. After 15 m from the point of derailment and as the leading wheelset deviated laterally approximately 0.6 m, the trailing wheelset of the same bogie became also derailed, as the marks on the twin block concrete sleepers indicate, see Figure 2-24. After 115 m from the point of derailment, the derailed bogie encountered on its right-hand, the left-hand diverging rail of a facing switch connecting the two main lines, see Figure 2-25.



Figure 2-24 ***The point of derailment of the trailing wheelset,*** *where the arrows mark the first contact with the sleeper.*



Figure 2-25 ***The trailing switch which detached the derailed bogie,*** *located 115 m from the point of derailment.*

The bogie is now guided towards the left together with the front end of the car behind. The fifth car decouples from the sixth car as the trailing bogie of the sixth car impacted the above mentioned switch. At the same time this bogie is detached from the sixth car and is overrun by the subsequent car, number seven. This impact led to the overturning of the seventh car, which ended up in the ditch on the left-hand together with the eighth car.

The reason why the derailed bogie started such an extensive lateral deviation from the track is not fully understood. This certainly aggravated the impact with the diverging rail of the switch which led to the catastrophic detachment of the bogie, becoming an imminent obstacle for the subsequent car.

2.2.5 Other causes

(Event ID 29)

On the 5th of June 2000, an *Eurostar* train, consisting of 10 articulated passenger cars and one power unit at each end, travelling on the main line Paris-London derailed at a speed of 300 km/h near the town of *Croisilles*, France [47]. This, up to date likely the world's highest speed derailment, was caused by the failure of a reaction link in the trailing bogie of the front end power unit leading to parts of the transmission assembly to impact the track. Three bogies in the whole train derailed, namely the trailing bogie of the front end power unit, the leading bogie of the leading passenger car and the leading bogie of the rear end power unit, all of them having conventional non-articulated bogie arrangement. However, the train was stopped safely at a distance of 1500 m from the initial derailment, with minimal lateral deviation, see Figure 2-26.

No information could be found on the type of track the train rolled on in the derailed condition. At this point and based on rather sparse information, no feasible explanation can be found as to why the only derailed bogies were the ones linked with a non-articulated design.

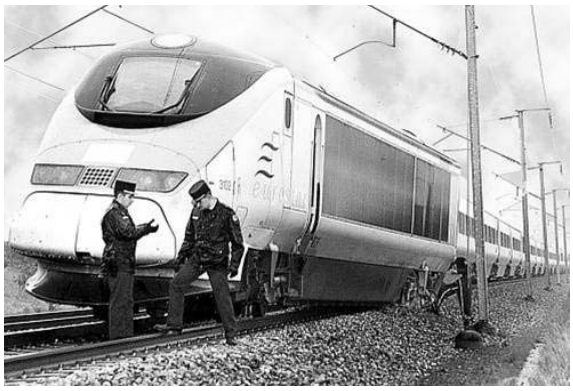

Figure 2-26 The front end Eurostar power unit with the derailed trailing bogie.

(Event ID 30)

On the 28th of February 2001, a Great North Eastern Railway train on the main up line from Newcastle to London collided with a trailer of a Land Rover car, accidentally blocking the track at *Great Heck*, near Shelby, UK [20]. The *IC225* train consisted of a driving van trailer (*DVT*) at the front end, eight *Mark 4* passenger cars and a *Class 91* locomotive at the rear end, travelling at a speed of 200 km/h. The impact of the *DVT* with the car trailer led to the derailment of the leading bogie in the train towards the right, with the left-hand wheels running close to the track centre line and parallel to the rails. The two wheelsets ran in such a manner for a tangent track distance of 450 m until they became engaged with a closure rail of a trailing switch coming from the nearby left-hand sidings, see Figure 2-27.

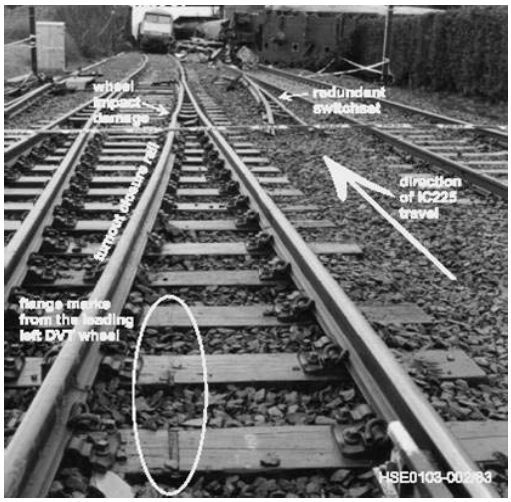

Figure 2-27 The trailing switch at the Great Heck accident.

The impact, at a speed of approximately 140 km/h, caused the leading bogie to became airborne for 23 m and landed on the ballast area further laterally deviated towards the opposite track. On the opposite down line track a freight train, carrying 1000 tonnes of coal, was approaching and the catastrophic collision of the two trains was inevitable.

(Event ID 31)

On the 25th of August 2003, a *VT610* trainset, travelling at a reduced speed of 70 km/h due to track maintenance, derailed on the line *Nürnberg* - *Weiden*, Germany [14]. Both wheelsets of the leading bogie left the rails towards the left side, just ahead of a right-hand curve of R = 590 m with cant D = 130 mm. Available evidence suggests that the brake discs on the axle close to the derailed wheels engaged with the high rail and stopped a further lateral deviation down the steep embankment, see photographs of the curve in Figure 2-28 and of the vehicle in Figure 2-29. The exact root cause of the derailment is not identified.



Figure 2-28 The curve in which the brake disc of the VT610 power unit encountered the high rail.

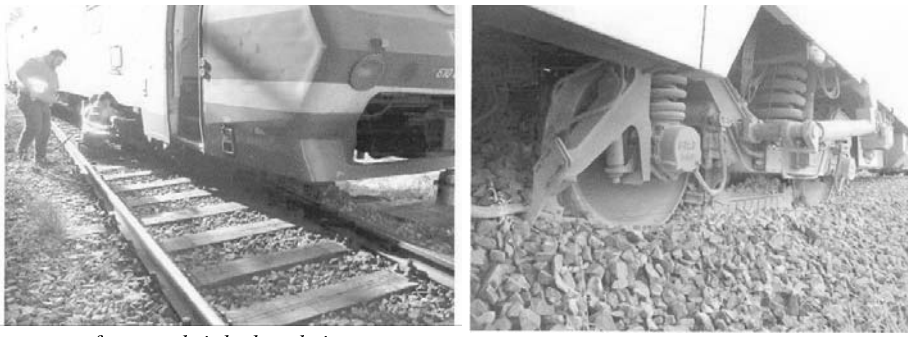

front end right-hand view *left-hand view of the leading bogie*

Figure 2-29 Detailed photos of the VT610 power unit involved at the Nürnberg-Weiden incident.

(Event ID 32)

On the 6th of November 2004, a First Great Western *HST* trainset, travelling at a speed of 160 km/h from London to Plymouth on the down line, collided with a stationary car at a level crossing near *Ufton Nervet*, UK [23]. The train consisted of two diesel power units with eight *Mark 3* passenger cars in between. Preliminary evidence suggests that the impact with the road vehicle resulted in the derailment of the leading wheelset of the train, which continued as such on a tangent track section. A facing switch, located 91 m from the point of derailment, was encountered, which probably lead to the catastrophic derailment of all vehicles.

The consequences of the switch is best observed in Figure 2-30. More factual information is required in order to attempt an understanding of how the wheelsets behaved when encountering different parts of the points.



Figure 2-30 Aerial view of the aftermath in the Ufton level crossing impact and the subequent derailment *(photo from BBC News)***.**

(Event ID 33)

On the 26th of May 1981, an *Amtrak* train, consisting of one front end *F40PH* diesel-electric locomotive and nine cars, derailed on the route Jacksonville - Miami at *Lochloosa*, Florida, USA [32]. The direct cause of the derailment was attributed to an improperly positioned right-hand facing switch to allow a proper straight forward passage, as the train was passing at a speed of 120 km/h. The locomotive started to derail as the flange of the right-hand wheel of the leading wheelset was running on the right-hand switch blade. All but the rearmost bogie in the train derailed to the right of the tangent track. The vehicles remained coupled and in an upright position. However, some cars deviated substantially from the main track, ending up over both rails of the right-hand sidings track.

2.3 Empirically based conclusions and discussion

The most difficult part of any empirical study is seeing through various accidental circumstances in order to draw the right general conclusions. In the present study, the situation is not made easier as there is no standardised way of presenting the factual information between different accident and incident reports, hereby most accidents and, especially incidents lack sufficient detailed information. It is also worth pointing out that the number of incidents in the database collected outside Swedish sources is rather limited. A feasible explanation could be that mostly major events, involving injuries or loss of human life, are made public to some extent.

An attempt is made to pinpoint some obvious common features as well as highlight areas which would require further studies. For this task, all the described events have been inserted into tables in Appendix A on page 77, in order to obtain a better overview of the

conditions in combination with the sequence of events. The tables highlight important information from the point of view of the current study and it should be conceived as a complement to the more extensive narrative descriptions in Section 2.2.

A limited number of events from the database will be subject to more extensive analysis in the current study. At these stage, these events are primary chosen from categories that involved mechanical failure affecting the wheel-rail interface, as for example, axle failures on the outside of the wheel.

In the present database, only three entries appear under the above mentioned category, all involving the Swedish high-speed train *X 2000.* Moreover, in two of them (ID 2 and 3), there was no derailment at all in spite of axle journal failure; the wheels remained on or slightly above the rails. *Restrictions of the wheelset's vertical movement in relation to the bogie frame is believed to be a positive factor* for this "successful" outcome.

Once a wheelset is rolling in a derailed condition, three minimum conditions should be met for achieving a safe outcome regardless of other train design parameters:

- tangent track
- no switches
- a minimal initial bogie yaw angle relative to the track centre line.

In the studied cases, see Appendix A or Section 2.2, at least six of them exist (ID 18, 19, 22, 23, 24, 33) where the first two conditions are met. However, in three of these events, the bogies deviated so much laterally as to cause overturned vehicles. Once a wheel loses the vertical support imposed by the sleepers and starts to roll on the weak support of the ballast shoulder or the gravel, there is an imminent danger of overturning. One factor that could account for the lateral deviation might be related to the properties of the yaw resistance between the bogie and the carbody or the wheelset guidance between the wheelset and the bogie frame.

Other means to restrain the running gear to leave the "safe" sleeper area is by implementing some kind of a mechanical device on the bogie frame or the wheelsets having the ability *to engage with the rails laterally and establish a substitute guidance mechanism.*

The database includes several incidents involving the Swedish high-speed train *X 2000* which have shown a positive behaviour after several axle failures. One interesting design feature in this train, is the robust low-reaching bogie frame shown in Figure 2-31 representing the bogies of the passenger cars and power unit respectively.

Axle failure that resulted in derailments has occurred on *X 2000* on three different occasions, one event (ID 1) on the outside of the wheel at the axle journal and two events (ID 4, 5) on the inside of the wheel. The train speed range was from 140 to 200 km/h and in all cases the vehicles passed potentially aggravating track features, such as curves or switches. Moreover, in two cases the vehicles ran through curves with a comparatively large lateral track plane acceleration of approximately 1 and 1.6 m/s^2 (150 and 245 mm of cant deficiency respectively). The train remained aligned on the track bed in all cases and for at least two of them the favourable behaviour can be attributed to the low-reaching bogie frame design.

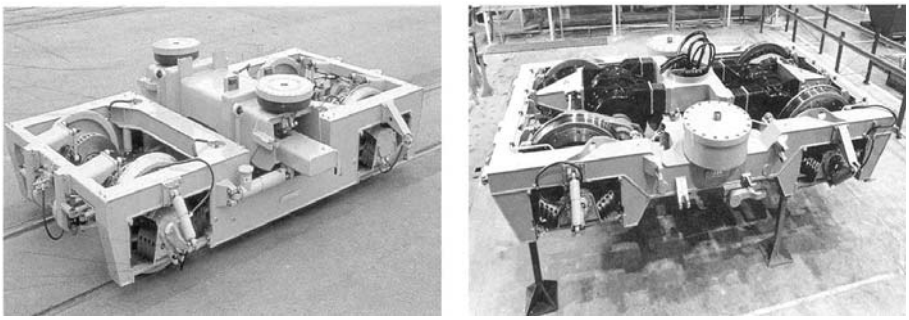

a) passenger car bogie *b) power unit bogie*

Figure 2-31 X 2000 bogies belonging to:
a) the passenger car
b) the power unit

The trains with an articulated bogie design, *TGV* and *Eurostar* (ID 14, 26, 29) showed a similar positive behaviour as the *X 2000* trains by maintaining stability and remaining on the track bed after derailments, even at speeds ranging from 270 to 300 km/h. In another case (ID 13), a rail failure managed to overturn the non-articulated power unit at a speed of 130 km/h. The author's inquiries [5][11][35] together with the media coverage of the involved events indicate a solid belief in the safety of the articulated train design, although no studies are apparently said to be available.

The difficulties to obtain detailed information on the *TGV* and *Eurostar* incidents (e.g. the existence of switches or curves as well as vehicle data) contribute to the inability to arrive at a conclusion based on observations only. Also, the reasons for the favorable outcome of the articulated cars could at least partly be others than the articulated design itself, for example the height of centre of gravity, the connections between carbody ends or other factors related to the running gear design. However, *studies on the effect of articulated bogie architecture in combination with the height of centre of gravity on derailment consequences are here identified as a key goal of future research.*

More generally and mainly outside the issue of articulated designs, studies of the height of centre of gravity in combination with properties of couplers and other carbody interconnections are another priority research area. Primarily, this is to a large extent emerging from observations on the poor behaviour of many Superliner double-decker cars in the USA, being apparently more predisposed than other cars to divert laterally and to overturn.

Switches are track features with the devastating potential of turning a somehow controlled forward motion of a derailed wheelset into a catastrophe. Typical examples would be Bigger (ID 7), Great Heck (ID 30), Upplands Väsby (ID 28) and Ufton (ID 32), where the derailed wheelset(s) rolled uneventfully on sleepers for distances of 1600, 450, 115, 91 m respectively, until the running gear engaged with the switch(es).

Apart from the *X 2000* events discussed above, one more case exists where the derailed bogies on the rearmost car, managed to cope successfully with switches, namely at

Sandy (ID 25) with an *IC225* train. This is the same type of train as in the Great Heck event (ID 30) where the derailment occurred on the leading bogie with disastrous effects. However, the two cases are not directly comparable, since a derailment on the leading wheelsets of a train is probably the worst possible location when dealing with switches.

One possible way to minimise further lateral displacements after derailments is by making use of brake discs of sufficient diameter and strength, located on the axle between the wheels. There is only one case in the database where available evidence undoubtedly leads to this conclusion, namely the *VT610* derailment on the line Nürnberg - Weiden, Germany (ID 30). However, a brake disc would only have a positive effect if certain geometrical criteria are fulfilled, based on the dynamic effects generated as the brake disc fall down towards the closest rail and - later on - when the wheelset impacts the sleepers and possibly rebounds up again. Moreover, a brake disc would not be beneficial for events similar to Hatfield (ID 14) or Woodlawn (ID 15) where the outer rail failed in the curve. In those cases, a low-reaching bogie frame, to capture the remaining intact inner rail from the outside as the wheelsets start to deviate laterally outwards in the curve, would have the possibility to change the sequence of events. However, the wheels would possibly rebound on the sleepers to some extent, thus making the course of events to a more dynamically complicated issue.

2.4 Identification of critical vehicle parameters

After studying the accidents and incidents collected in the first step of the present study, the following vehicle characteristics have been identified to have a potential to positively influence the outcome of a derailment, or to prevent a derailment to occur:

1) Wheelset mechanical restriction relative to the bogie frame and to the carbody, see Figure 2-32, area a).

2) Low-reaching brake disc (i.e. a comparatively large disc radius), see Figure 2-32, area b).

3) Low-reaching bogie frame design, see Figure 2-32, area c).

4) Adequate strength of running gear steering parts, for example to cope with track switches.

Other train design features would also influence the outcome of a derailment, such as:

5) Suspension system.

6) Bogie frame mechanical restriction relative to the carbody, including gaps in the suspension as well as the yaw resistance.

7) Carbody inter-connections, i.e. couplers, dampers and possibly other means.

8) Height of centre of gravity.

9) Articulated train architecture, i.e. bogies connected to an articulated joint between the carbody ends.

The current report will assess the influence of the first two features as well as establishing the methodology for further studies of the remaining design parameters.

The list of critical vehicle parameters is by no means definite or complete. Further parameter would be added, while others disregarded, based on conclusions drawn from an interactive process where *MBS* computer simulations will be compared with empirical observations from the database.

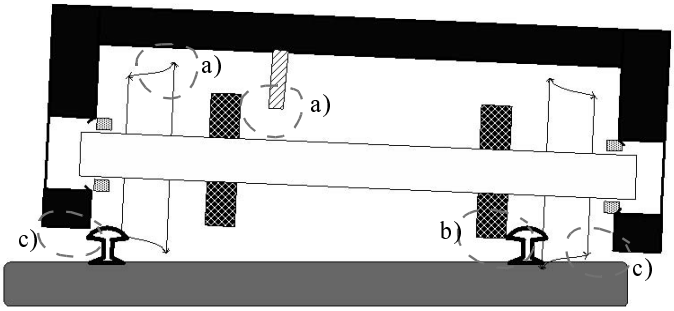

Figure 2-32 ***Sketch over various substitute guidance mechanisms in case of a derailment:***

a) wheelset vertical mechanical restriction relative to the bogie frame or to the carbody,
b) low-reaching brake disc,
c) low-reaching bogie.

3 Pre-derailment simulation studies

3.1 Introduction

The present chapter deals specifically with axle journal failure, i.e. on the outside of the wheel, and methods to minimise the consequences up to the instant that any of the wheelsets leaves the rails. Although, not being the most common cause of derailments in the collected database, see Section 2.2 or Appendix A, such failure would generally be considered as a severe-consequence event. However, axle failure of such kind has affected the Swedish high-speed train *X 2000* on several occasions with limited consequences. Consequently, time-domain simulation studies of axle journal failure emerged as the starting point of evaluating the robustness of the involved vehicles.

To the best of the author's knowledge, this type of simulations has not been accomplished elsewhere. Therefore, two validation simulations are also performed and included in the current chapter.

3.2 General simulation prerequisites

The multi-body system (*MBS*) rail vehicle analysis tool GENSYS [36] is here being used in all time-domain simulations. One vehicle is considered only, i.e. there are no coupled vehicles in a train. Each vehicle is consisting of one carbody, two bogie frames and four wheelsets. All parts are modelled as rigid bodies with six degrees of freedom each, three translations and three rotations.

The primary suspension, i.e. the suspension between wheelsets and bogie frame, is modelled by linear springs in parallel with linear and non-linear dampers acting in all three translational directions. Furthermore, the maximal vertical and longitudinal play, as parts of the axle and bogie frame come into contact, are taken into consideration and implemented as springs with piecewise linear stiffnesses with no effect unless certain limits are reached. Exceeding these limits, adequately stiff metallic contacts are considered. Some mechanical restrictions are described in more detail in the section to follow.

The secondary suspension, i.e. the suspension between bogie frame and carbody, consists of non-linear springs acting in all three translational directions in parallel with non-linear viscous lateral dampers. Furthermore, each bogie includes a roll bar to produce a linear roll stiffness between bogie and carbody, as well as two yaw dampers modelled as non-linear viscous dampers, the latter acting primarily in a longitudinal direction between bogie and carbody. The model also includes lateral bumpstops modelled as picewise linear stiffness. Vertical 'semi-flexible' stops are introduced between the four corners of the bogie frames and the carbody. For large bogie pitch and roll angles, these stops prevent the bogie frame to perforate the carbody floor. Additionally, the bogie yaw angle is restricted by a 'semi-flexible' stop implemented in the yaw damper elements.

It is worth mentioning, that these 'semi-flexible' restrictions are redundant under normal operating conditions. However, under extreme conditions, corresponding to pre- and post-derailment sequence of events, the stops may play an important role.

The track flexibility model is based on the concept of a so-called "moving track piece" which follows under each wheelset and incorporates four distinct rigid bodies: rails, track piece and 'ground' see Figure 3-1. The 'ground' is however fixed.

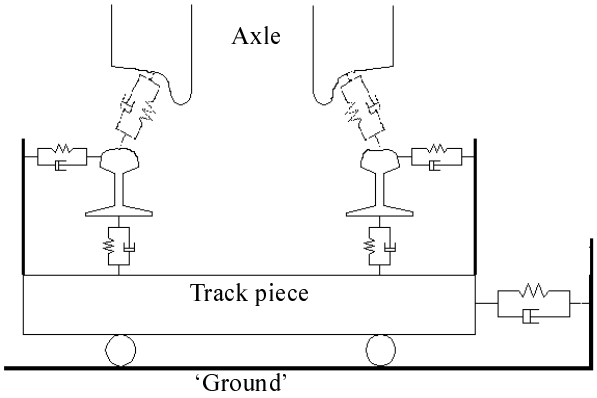

Figure 3-1 'Ground' - track - wheelset model used for MBS simulations **[36].**

Thus, each rail is connected laterally with the track by linear springs in series with linear dampers. In the same manner, the track piece is connected laterally with the 'ground'. In the vertical direction, the rails are connected with the track piece by linear springs in series with linear dampers.

The wheel-rail interaction model includes creep forces calculated with Kalker's *FASTSIM* algorithm. The contact stiffness between wheel and rail is described as a linearized Hertizan stiffness (around its nominal state) and a linear viscous damper. The wheel-rail friction coefficient is chosen arbitrarily.

All simulations use *UIC/ORE S1002* wheel profiles running on *UIC 60* rails according to Swedish standards, i.e. inclined at 1:30, with a 1435 mm gauge.

Furthermore, all time-domain analyses are performed with the second order Runge-Kutta integration method.

The actual axle journal failure is simulated by removing the longitudinal and vertical primary suspension elements at the involved axle side at a specified location. In the lateral direction, the stiffnesses is maintained as long as the axle is pushed towards the journal. A derailment is said to happen as long as the wheel flange climbs on the opposite half of the rail head surface, i.e. on the non-gauging side of any rail.

3.3 Axle failure model validation

The *MBS* computer simulations scheme started with the aim to re-create and, at the same time, analyse the actual sequence of events caused by the axle journal failures on the outside of the wheels, as it occurred on two high-speed *X 2000* power units in Tierp and Gnesta, Sweden, earlier presented in Section 2.2.

For both cases, the following unknown conditional parameters are considered and subjected to sensitivity analysis:

- The exact location of axle failure along the track; several possibilities are studied.
- The coefficient of wheel-rail friction; tested values are 0.30, 0.45 and 0.60.
- The interaction between the broken side of the axle and the bogie frame (approximately implemented as a linear longitudinal and vertical viscous damper acting only when the axle is pushed in laterally towards the bogie frame; tested damping coefficient values are 0 and 10 kNm/s.

The implemented track curvature and geometrical irregularities describe the actual conditions at the incident sites of Tierp and Gnesta, measured with Banverket's measurement vehicle *STRIX*, at 80 and 73 days, respectively, prior to the incident's date.

The tendency of derailment as a result of the wheelset's mechanical restriction relative to the bogie frame is also included in the current validation series of simulations. For this purpose, two additional parameters are taken into consideration: (i) the vertical and (ii) the longitudinal mechanical restriction between the wheelset and the bogie frame as mentioned in the previous section, sketched in Figure 3-2. For an *X 2000* powered bogie, they represent the maximum play movements of the axle relative to the tube drive system, and are for both directions approximately 50-60 mm. The restrictions are modelled as described in the previous section, i.e. spring elements with zero stiffness up to certain deflections, presented in Table 3-1, and thereafter a high stiffness value corresponding to the structural stiffness of an eventual metallic contact. In the vehicle computer model, these restrictions are located at a distance of ±0 .52 m on both sides of the wheelset centre line.

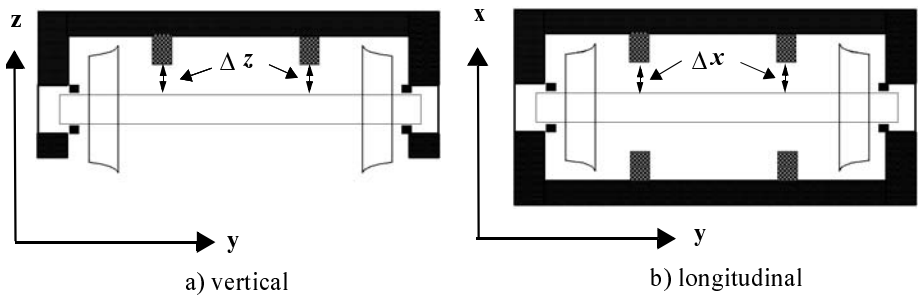

Figure 3-2 Wheelset mechanical restrictions (maximum play) relative its bogie frame. *a) The vertical (Δz) and b) longitudinal (Δx).*

Table 3-1 The tested values for the maximum allowed longitudinal and vertical play between the axle and the bogie frame for two incident conditions.

	Tierp	Gnesta
Longitudinal play Δx (mm)	40, 50, 60	40, 50, 60
Vertical play Δz (mm)	50, 60, 70, 80, 90, 100, 110	50, 60, 70, 80, 90, 100, 110, 120, 130

3.3.1 The Tierp incident

The factual incident information for the Tierp case (ID 1) was introduced in Section 2.2. In this context the following elements are of interest:

- An *X 2000* train was running at a speed of 200 km/h with the power unit as the rear-most vehicle while negotiating a right-hand curve having a radius R = 1805 m and a track cant of 110 mm. The circular curve section is preceded by a transition curve with a length of 110 m.
- A journal failure on the left (high) side of the second axle in the *X 2000* power unit led to a derailment of the leading axle directed inward in the curve, i.e. on the diagonally located low wheel.

The input track geometry for all Tierp simulation case studies is shown in Figure 3-3. The first damaged sleeper was located at 11 m from start of the circular curve section, which suggests a plausible initial axle failure location to be on the transition curve section or just before. In this case, three possible alternative axle failure locations are investigated: 20 m before start of the transition curve, i.e. on tangent track, alternatively 5 and 45 m from start of the transition curve. Along with the other unknown parameters and the values in Table 3-1, this series of computer simulations included 378 different runs.

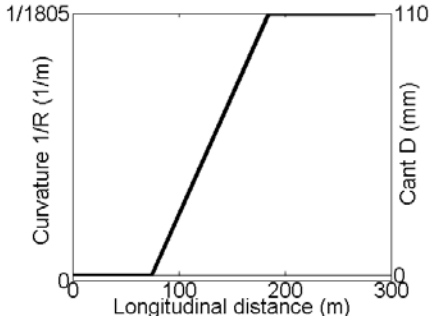

Figure 3-3 Curvature and cant data for the Tierp case simulations.

The computer simulations clearly show that for certain combinations of parameters, the leading wheelset of the vehicle derails towards the low (inner) rail in the curve as a result

of an axle failure on the trailing wheelset above the high (outer) rail. Furthermore, the simulations successfully predict that the leading axle leaves the rails within a few metres from entrance of the circular curve section, climbing over the low rail, in accordance with observations from damaged sleepers from the authentic case.

The explanation for this behaviour is not obvious. As a result of the failure, the vertical force on the trailing high (outer) wheel is diminished, thus the creep forces on this wheel are lost, hereby allowing the trailing wheelset to be laterally displaced towards the high rail of the curve. The high wheel flange on the trailing wheelset is occasionally running above the high rail. The new occasional large yaw angle steers the leading wheelset towards the low rail, thus leading to a derailment due to flange climb on its low wheel. The vertical force of the low wheel is now also greatly diminished, because it is diagonally located with respect to the axle failure. This is a credible description of the cause of events, based on observations from simulations and the authentic incident case.

The parameters having the strongest and most distinct effect on the wheelset's tendency to derail seems to be:

(i) the vertical restriction between the axle and the bogie frame, and

(ii) the coefficient of wheel-rail friction.

Furthermore, it has been found that the damping value, representing the friction between the broken side of the axle and the bogie frame, together with the axle failure location parameter only affects the derailment process marginally.

The series of simulations concerning the Tierp case is summarised in a so-called derailment map in Figure 3-4, presented as functions of the maximal vertical and longitudinal axle-bogie frame restrictions.

.

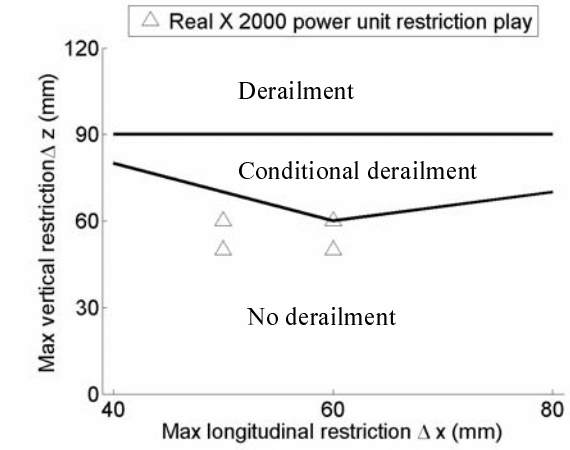

Figure 3-4 Derailment map for different combinations of mechanical restrictions of the wheelset and conditional parameters for the Tierp case.

The simulated line delimiting the two areas "No derailment" with "Conditional derailment" tangents the lowest possible combination of mechanical restrictions between the axle and the bogie frame that would result in the derailment of the leading wheelset. In the "Conditional derailment" area, the wheelset behaviour is strongly influenced by the unknown conditional parameters described above. Exceeding the vertical restriction value of 90 mm, leads always to derailment regardless of the tested conditional parameters. The figure marks also the area of real maximal longitudinal and vertical restriction observed on the *X 2000* power unit. A correspondence with the simulation results is observed in this respect as well, as the lower limit of the conditional derailment area tangents these points.

3.3.2 The Gnesta incident

Detailed incident information regarding the Gnesta case (ID 2) can be found in Section 2.2. The following elements are of interest:

- An *X 2000* train was running at a speed of 180 km/h with the power unit at the front end of the train, while the train negotiated an S-shaped set of curves, see Figure 3-5 for curvature and cant data of the track section of interest.
- A axle journal failure occurred on leading axle journal right side (low in the first curve, high in the second curve) side of the trailing bogie (exact the same location in the vehicle as in the Tierp case, but this time the *X 2000* power unit was at the leading end).

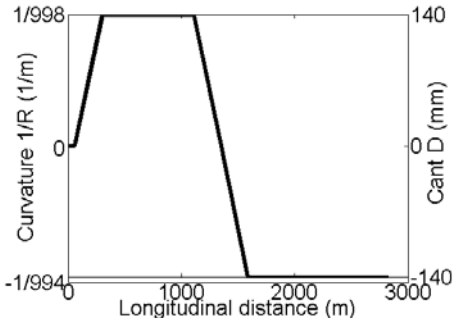

Figure 3-5 Curvature and cant data for the Gnesta case simulations.

Since no actual derailment occurred, the exact location of the axle journal failure along the track is not possible to determine. However, the incident report indicates that full braking was automatically applied by the *ATC* system at approximately 137 m from start of the second circular curve section. It can therefore be assumed that at least from that location and further on, the journal side detached completely from the rest of the axle. Four different possible axle failure locations have been included in the list of unknown parameters, along with three coefficients of friction and two damping values for the failed axle surfaces interaction. Combined with the vertical and longitudinal wheelset-

bogie frame restriction parameters, see Table 3-1, the Gnesta case amounted to 578 different simulation runs.

The simulation results are presented in Figure 3-6, as a derailment map. Although the "Conditional derailment" area includes larger vertical restriction values than for Tierp, see Figure 3-4, the map follows a similar pattern. It is clear that certain combinations of values of the conditional parameters together with the mechanical restrictions between the axle and the bogie frame would lead to the derailment of the third axle. Depending on the (exact) location of the axle failure along the track, the derailment would occur either in the right- or left-hand curve. Just as in Tierp, the minimal restriction values for which conditional derailment occur tangent the area which includes the real restrictions on the *X 2000* power unit.

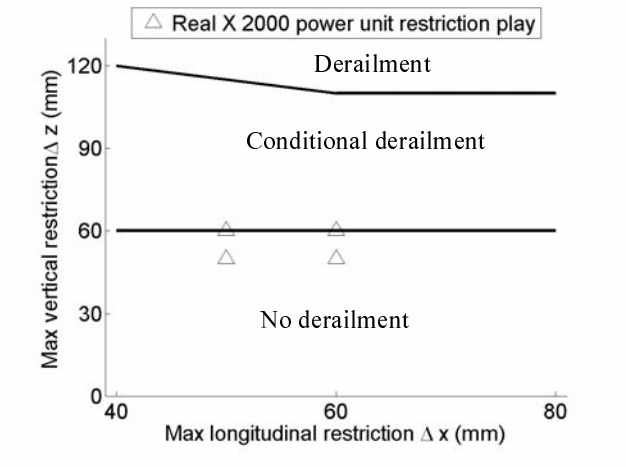

Figure 3-6 Derailment map for different combinations of mechanical restrictions of the axle and conditional parameters for the Gnesta case.

3.3.3 Validation conclusions

In an attempt to compare the vehicle behaviour, especially the derailment tendency of two authentic cases of axle journal failure with the *MBS* generated simulation results, the following can be concluded:

- **i.** For one case (Tierp), a good compliance with reality is obtained in terms of the location of derailing wheelset, its derailing direction, as well as location along the track under certain conditional premises and with the maximal vertical and longitudinal restriction play that tangent the real restriction found on the power unit.
- **ii.** For the other case (Gnesta) no derailment occurs, as in reality, under certain conditional premises and with the maximal vertical and longitudinal restriction play that tangent the real restriction found on the power unit

iii. The maximum vertical wheelset-bogie frame restrictions play a critical role in the derailment tendency as a result of an axle journal failure.

3.4 Studies on axle failure location in the bogie

In order to obtain a better understanding of derailment caused by axle failures outside the wheels, in particular in curves, a parameter analysis is performed for alternative axle failure location in either the power bogies or in the trailer bogies. It is assumed that a failure occurs on either of the four axle journals of the leading bogie on an *X 2000* power unit and on a trailer car.

The following conditional parameters are considered in this part of the study:

- Coefficient of wheel-rail friction; tested values are 0.30, 0.45 and 0.60.
- The interaction between the broken side of the axle and bogie frame (approximately implemented as a linear longitudinal and vertical viscous damper acting only when the axle is pushed in laterally towards the bogie frame); tested damping coefficient values are 0 and 10 kNm/s.

As observed in the previous *MBS* simulations, the maximal vertical restriction values between the wheelset and the bogie frame play an important role for the derailment tendency. In the current study the tested values for the maximal vertical play include the range from 50 to 180 mm, at an interval of 10 mm, while the longitudinal one is held constant at 60 mm. It is worth mentioning that these mechanical restrictions are not found at all on an actual *X 2000* trailer car. In reality, the first restriction that a failed trailer car axle would encounter, is established as the wheel flange contacts vertically to the carbody underframe. A total of 312 simulation runs for each vehicle type were performed.

The track chosen for this series of simulations has the same design geometry, shown in Figure 3-3, and irregularity data as for the Tierp case described in the previous section. A axle journal failure is simulated by removing the longitudinal and vertical primary suspension elements on the respective axle side as the train reaches a certain switch located 45 m from the start of the transition curve. The train speed is held constant at 200 km/h for all simulations, which leads to a lateral track plane acceleration of $a_y = 1$ m/s^2.

The behaviour of the bogie in terms of whether it derails or not, as a function of the vertical mechanical restriction wheelset-bogie frame, is summarised in Figure 3-7 and Figure 3-8 for an *X 2000* power unit and trailer car, respectively. The horizontal axis indicates the wheel location on which the axle journal failure was simulated in relationship to its position in the vehicle and in the curve. As mentioned earlier, a derailment is considered as soon as any wheel flange in the bogie climbs over the opposite half of the rail head surface, i.e over the non-gauging side of the rail.

The bogie seems to be most sensible for an axle failure at the leading wheelset outside the low (inner) wheel. On the other side, the least sensitive place for a failure appears to be, quite unexpectedly, on the high wheel of the leading axle. The bogie frame drops

towards the axle in the failure corner, thus preventing the corresponding wheel to climb over the rail. Another interesting observation is that the trailer car bogie allows larger vertical mechanical restrictions as an average before derailment, in comparison to the power bogie. One pertinent explanation would be the fact that the bearings are closer to the wheels, thus a smaller bending moment is produced on the axle side opposite to the failed one.

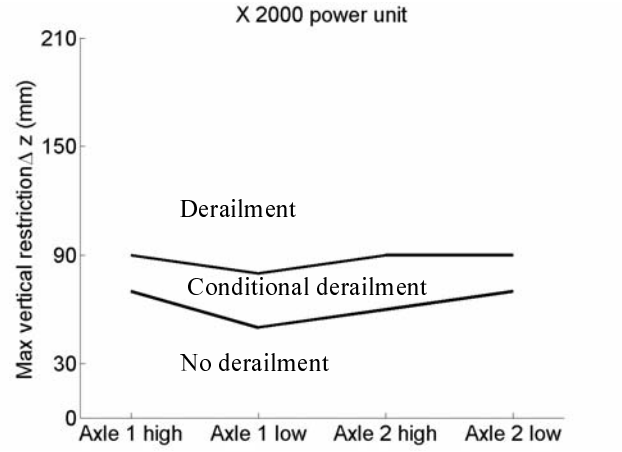

Figure 3-7 Derailment map for different axle failure locations as function of maximal vertical restriction value.
X 2000 power unit bogie, longitudinal restriction fixed at 60 mm.

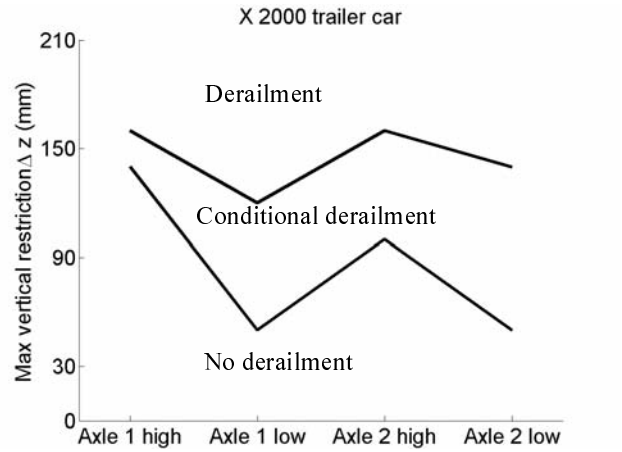

Figure 3-8 Derailment map for different axle failure locations as function of maximal vertical restriction value.
X 2000 trailer car bogie, longitudinal restriction fixed at 60 mm.

3.5 Axle failure studies for different combinations of wheelset guidance.

The effect of an axle journal failure has so far been studied with the relatively flexible wheelset guidance that the *X 2000* vehicles are equipped with. The intention is this section is to study how a stiffer axle guidance would influence the derailment tendency in a curve.

The combinations of different wheelset guidance stiffnesses (lateral and longitudinal) implemented and tested in the *X 2000* power unit model are presented in Table 3-2.

Table 3-2 Formulated wheelset guidance parameters (lateral and longitudinal).

	Flexible	Semi-flexible	Stiff
Lateral stiffness axle journal - bogie frame, each side (kN/m)	600	2000	10000
Longitudinal stiffness axle journal - bogie frame, each side (kN/m)	4000	8000	30000

The track used for this set of simulations is the same as the one in the previous studies; see Figure 3-3 for curvature and cant information.

Similar conditional parameters as in the previous sections are included in this study:

- Coefficient of wheel-rail friction; tested values are 0.30, 0.45 and 0.60.
- The interaction between the broken side of the axle and bogie frame (approximately implemented as a linear longitudinal and vertical viscous damper acting only when the axle is pushed in laterally towards the bogie frame); tested damping coefficient values are 0 and 10 kNm/s.

In order to obtain a wider statistical confidence, two more conditional parameters have been included in the simulations:

- Unshifted track irregularities as in the Tierp case, and shifted *5* metres forward relative to the actual measured track geometry.
- Two different positions for the axle journal failure along the track, 20 and 120 m from start of the transition curve.

The tested vertical and longitudinal maximum mechanical restrictions wheelset-bogie frame coincide with the ones used for Tierp validation case, see Table 3-1. A total of 504 simulation runs were performed.

The results are presented in Figure 3-9 as a derailment map for different wheels in the bogie (as their location in the curve) affected by the axle journal failure as function of the wheelset guidance stiffness (lateral and longitudinal) and the vertical mechanical restrictions.

For constant conditional parameters, the wheelset is slightly prone to derail as the stiffness in the wheelset guidance increases.

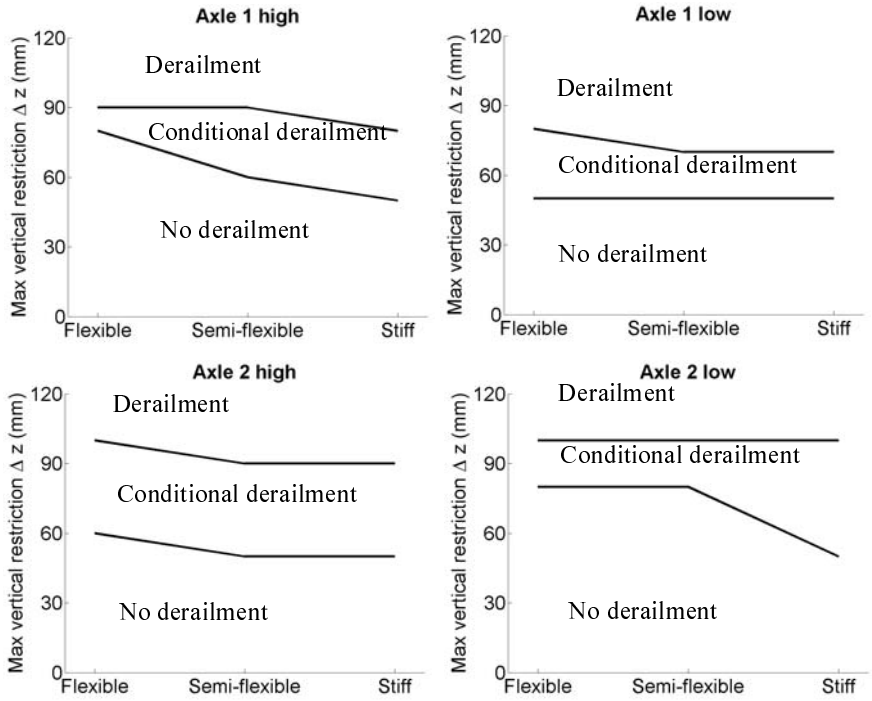

Figure 3-9 ***Derailment maps for different vertical mechanical restrictions and wheelset guidance stiffnesses*** *for different wheels in the vehicle relative their position in the curve.*
X 2000 power unit, longitudinal restriction fixed at 60 mm.

4 Tentative simulation studies on brake disc position

4.1 Introduction

As mentioned in Section 2.4, a low-reaching brake disc has been identified as a vehicle parameter with the potential to positively influence the course of events in cases of wheel flange climbing conditions. This can be achieved by the simple principle of allowing the rail to fill the lateral gap formed by the brake disc and the wheel, hereby guiding and stabilising the derailed wheelset. This has been observed in one case, the incident on Nürnberg - Weiden line in Germany (ID 31).

4.2 Brake disc basic requirements

Assuming that the rail and the brake disc provide a sufficient lateral strength and neglecting at this stage any possible interaction with track switches, the following basic criteria should be fulfilled according to Figure 4-1:

$$r_{bd} + h_r > r_w + h_f + f_z \tag{4-1}$$

$$b_{w\text{-}bd} > b_r + f_y \tag{4-2}$$

where, (see Figure 4-1)

r_{bd}	brake disc radius
h_r	vertical distance from top of the rail to sleeper upper surface
r_w	nominal wheel radius
$r_w - r_{bd} = h_{w\text{-}bd}$	radius difference between wheel and brake disc
h_f	wheel flange height
$b_{w\text{-}bd}$	minimal lateral gap between wheel and brake disc
b_r	rail width
f_z, f_y	vertical and lateral margin parameters.

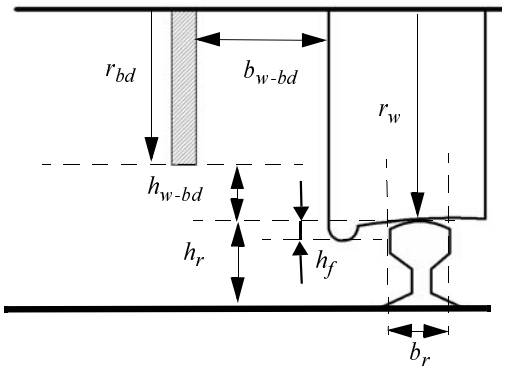

Figure 4-1 The nomenclature used for analysing the geometrical position of an axle mounted brake disc.

4.3 Simulation methodology

The possibility of the brake disc to prevent the wheelset from moving laterally towards the outer side of the curve will be assessed, as the vehicle runs through sections of curves. In particular, the lateral margin required to stop a wheelset equipped with an axle mounted brake disc from further lateral deviation will be studied under the assumption that the wheelset would not rebound after impact with the sleepers.

It is expected that the geometrical parameters, dictated as the wheelset is exposed to maximum lateral track plane acceleration (maximum cant deficiency), would also pertain to any other case of wheel flange climbing condition at lower lateral track plane accelerations.

The *MBS* software GENSYS with an *X 2000* tilting trailer car vehicle model will be used again in all subsequent simulations. The essential track and vehicle models have been introduced in Section 3.2.

As discussed in Section 2.4, the trailer car bogies are equipped with a low-reaching frame. Those are not modelled here due to a risk of interference with the scope of the current section.

Simulations are run in two different curves with radii R = 300 and 1200 m respectively, see Figure 4-2. In both cases the track cant (superelevation) in the circular section is constant, D = 150 mm. In Sweden, the permissible lateral track plane acceleration for the *X 2000* type of vehicle is a_y = 1.6 m/s^2. In order to maintain the maximum permissible lateral track plane acceleration in the circular section, the vehicle speeds for the above-mentioned curves are set to V = 100 and 200 km/h, respectively.

At this stage, the wheel is assumed not to rebound as impact with the sleeper terminates. This aspect is studied further on in Section 5.4. Furthermore, the brake disc is modelled as a non-rotating rigid body. The rotational effects in the contact with the rail, i.e.

creepforces, are therefore not considered. The rail profile (*UIC60*) is modelled as a rectangle of width b_r = 72 mm and height $h_r \approx 158$ mm, see Figure 4-3.

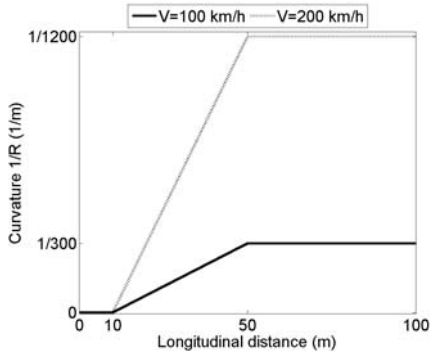

Figure 4-2 Track curvature with the respective vehicle speed used in the brake disc geometrical position simulations.
Cant D = 150 mm in the circular curve for both curvature cases.

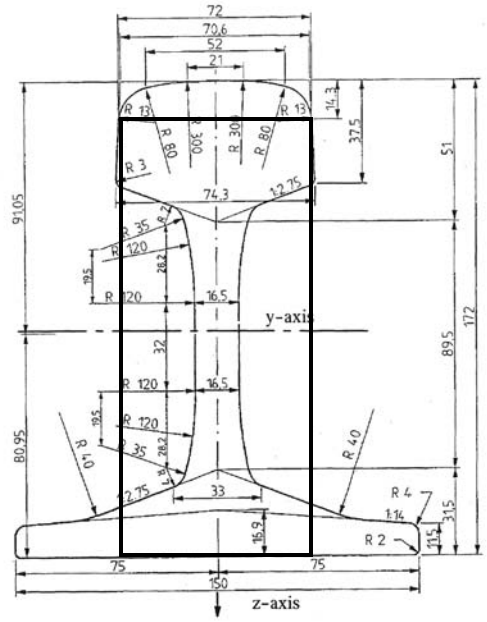

Figure 4-3 The simulated rail profile for the tentative brake disc studies - thicker lines forming a rectangle - overlaid on the real unworn UIC 60 rail profile used.

The maximum height of the real rail is 172 mm up to the rail head. However, the considered rail width and height correspond to a location where the almost vertical surfaces of the rail head turn into radii of 13 mm, at approximately 14 mm below the top of the rail. For reasons of possible vertical rail wear and safety margins as well as shortcomings imposed by a non-rotating disc, the curved surface of the rail is therefore omitted and neglected.

The following scenario is considered, sketched in Figure 4-4: an axle journal failure is imposed on the trailing wheelset, left side (inner side in the curve) of the leading bogie just as the vehicle enters the circular curve section. This leads to a derailment of the leading wheelset as the outer (high) wheel is unloaded and the flange therefore climbs over the rail. Thus, the geometrical parameters of the brake disc closest to the high rail on the leading wheelset will be studied.

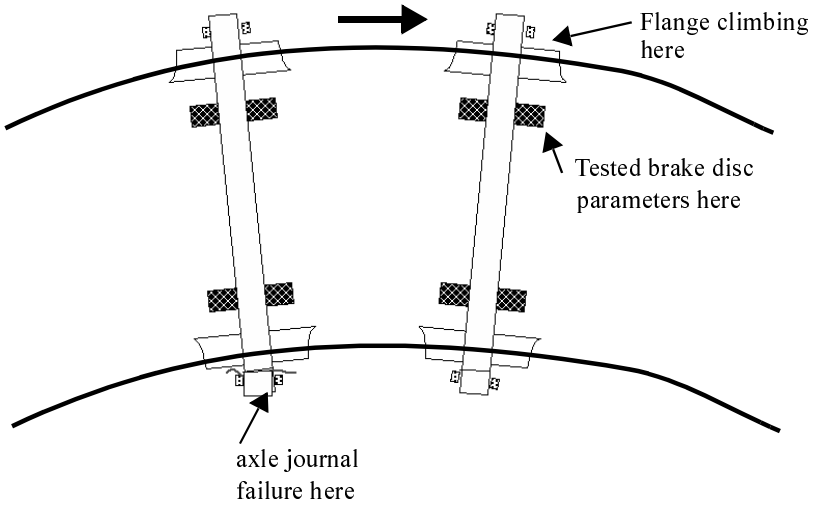

Figure 4-4 Sketch over leading and trailing wheelsets of the leading bogie of an X 2000 trailer car involved in the proposed scenario for testing various geometrical brake disc parameters.

Once the leading wheelset leaves the rails and in combination with a suspension unloading on the outer side, the wheelset starts to move vertically with a certain roll angle, the latter due to the flange climbing over the high rail. This implies that the inner wheel may reach the sleeper surface level before a verdict can be given whether the studied brake disc engages successfully or not with the rail, i.e. whether the brake disc really prevents the wheelset from moving further outside the high rail. Therefore, the contact between the low wheel and concrete sleeper has to be taken into consideration, although no complete model has yet been developed. In this respect, a simplified approach is considered, based on a linear spring of stiffness 60 MN/m and linear damper with damping coefficient 300 kNs/m, inserted in the wheel-sleeper contact.

Furthermore, the lowest point of a wheel can drop up to a certain maximal distance under the sleeper surface level before sleeper impact takes place, because there is a certain

space between two sleepers. Based on Equations (B-1) to (B-5) from Appendix B, the maximum vertical wheel position at impact, h_z can be 18 mm and 33 mm for the considered train speeds of 200 and 100 km/h, respectively.

With respect to the wheel-sleeper interaction, two courses of events will be considered:

- *High Contact:* the wheel interacts with the sleepers at the same instant as the wheel's lowest point reaches the sleeper's surface level, that is at h_z = 0 mm for both tested train speeds.
- *Low Contact*: the wheel interacts with the sleepers at the same instant as the wheel's lowest point reaches an h_z value of 33 and 18 mm for the two tested train speeds 100 and 200 km/h, respectively.

Together with the two different track curvatures described above, four sets of simulations are run.

4.4 Simulation results

The simulation results are presented in Figure 4-5 for both tested track curvatures with their respective different course of events *Low Contact* and *High Contact*, as minimal allowed lateral gap $b_{w\text{-}bd}$ wheel to brake disc, and vertical distance $h_{w\text{-}bd}$ brake disc to rail head. The brake disc successfully manages to stop any lateral diplacement of the wheelset for all vertical and lateral play parameter combinations on and to the right of each respective line. *The minimal lateral brake disc to wheel play should not be smaller than 0.130 m in order for the brake disc to provide the intended guidance mechanism.*

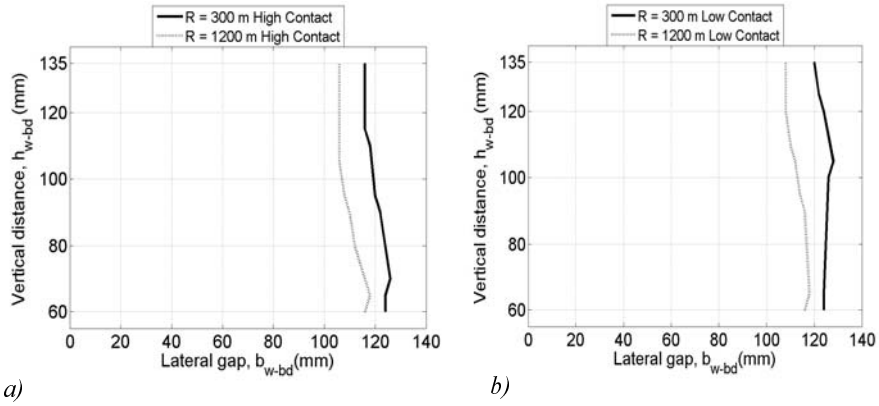

a) *b)*

Figure 4-5 Minimum allowed lateral gap $b_{w\text{-}bd}$ for different brake disc to rail head distances $h_{w\text{-}bd}$.
a) R = 300 and 1200 m for High Contact
b) R = 300 and 1200 m for Low Contact

Since the current simulation model is not in the position to asses the vertical distance $h_{w\text{-}bd}$, the simulations were deliberately stopped as the radius difference between wheel and brake disc reached 135 mm.

For the same track curvature, the geometrical parameters are slightly underestimated for most of the geometrical parameter combinations once the low (inner) wheel is assumed to fall in between the sleepers, i.e *Low Contact*. This phenomenon is sketched in Figure 4-6. Once a contact is established, earlier for *High Contact*, the contact force leads to a wheelset roll angle decrease, which changes the vertical, $v_{bd\text{-}z}$ to lateral $v_{bd\text{-}y}$, brake disc velocity ratio. Ultimately, this allows a safe engagement with the rail even at higher nominal vertical play values.

A larger difference between the radii of wheel and brake disc tends to allow a smaller lateral play for all cases, although this might appear as a contradiction. A large brake disc radius (small radius difference) in combination with smaller lateral play has the potential to contact the rail surface prior to the opposite wheel reaches the sleeper surface level. Once this condition is reached, the brake disc continues to skid on the high rail surface towards the outer side of the curve. On the other hand, a smaller brake disc radius allows the opposite wheel to contact the sleepers, prior to reaching the rail head top level. In such a case, the lateral play is enlarged as discussed above according to Figure 4-6.

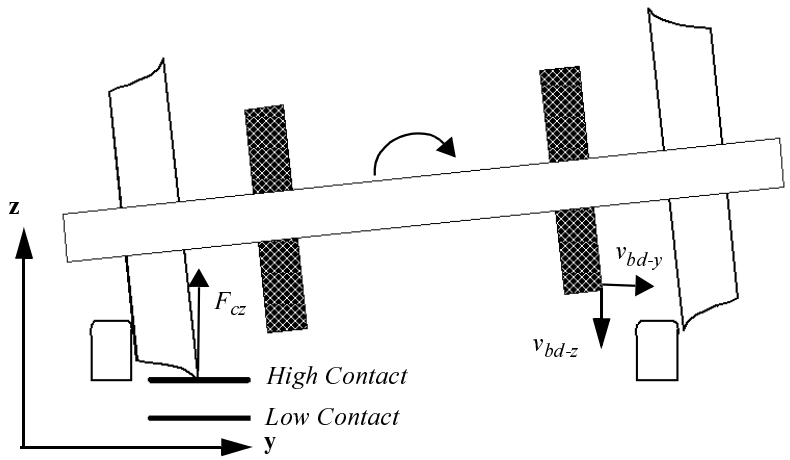

Figure 4-6 Sketch over the leading wheelset, just about to impact the sleeper's surface with the inner (low) side wheel.
Two sequence of events are considered:
- the wheel's lowest point falls on the sleeper surface - High Contact
- the wheel's lowest point falls in between the sleepers - Low Contact.

Regarding the effect of the track curvature, it appears as though the smaller curve, R = 300 m, dictates the geometrical parameters necessary for a successful contact with the high rail. This is most probably related to the fact that in small-radius curves, the yaw angle between the carbody and the bogie is larger then in large-radius curves. Furthermore, the stiffness of the yaw resistance is relatively high for the *X 2000* trailer cars. Hereby, the additional yaw moment on the bogie for small-radius curves is

sufficient to alter the lateral velocity of the brake disc, while its vertical component remains relatively unchanged.

Finally, the inter-dependency between the lateral f_y and vertical f_z margin parameters is plotted in Figure 4-7, based on the most stringent set of brake disc geometrical parameters obtained from the four simulation sets.

The values on the line should be interpreted as *the lowest combination of marginal parameters that would allow a safe engagement with the high rail* for flange climbing derailments. *All combination of values to the right of the line would also stop a possible lateral diplacement* towards the high rail.

For the simulated cases, it seems as the vertical margin parameter has a limited dependency with the lateral margin parameter.

Once again, the margin parameter values presented here, are calculated under the assumption the wheel does not rebound from the sleeper surface at impact. A tentative approach to the dynamic effects of an *X 2000* trailer car wheel impacting concrete sleepers is presented in Section 5.4.

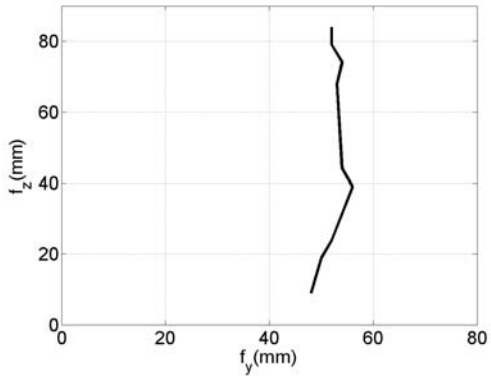

Figure 4-7 The relationship between vertical (f_z) and lateral (f_y) margin parameters *for an axle mounted disc brake in order to successfully stop the lateral deviation due to flange climbing derailments.*
All combination on and to the right of the line have this stopping effect.

5 Wheel-sleeper dynamic interaction

5.1 Introduction

In order to simulate a train in a derailed condition, a thorough understanding of the impact phenomenon wheel-sleepers in the post-derailment phase is required.

Experiments involving railway wheelsets impacting a concrete sleeper target at high speeds (100-200 km/h) would require a costly experimental set-up and a hazardous experiment. Even under the assumption that such experiments could be performed under laboratory conditions, the benefit of the results might be questionable. Therefore simulations with a proper model is used.

Due to the complicated three-dimensional shape of a railway wheel in combination with its two-dimensional principal movement, a finite element (*FE*) assessment was primarily chosen at this stage, instead of a purely analytical solution. The general-purpose explicit dynamics *FE* program ANSYS [1], with incorporated LS-DYNA [49] processor, widely used for impact simulations, is implemented in the current study.

For all simulations, a local response of the sleeper under impact will be assumed, hereby only a limited sleeper volume is modelled.

Two different sets of simulations are run. Firstly, the simulations will verify some sleeper indentations observed in a Swedish accident. This case will be used as a first validation of the model and the *FE* simulation technique. Thereafter, the kinetic energy loss and dynamics of an *X 2000* trailer car wheel impacting concrete sleepers will be studied.

These simulations represent the first step towards a more general analysis in order to predict the behaviour of derailed wheelsets, i.e. the vertical rebound as well as the tendency to diverge laterally as a function of various parameters.

5.2 Concrete material model

The LS-DYNA preprocessor offers a multitude of constitutive models to represent geomaterials, many relying on complex parameters that would necessitate complicated laboratory tests. However one material model, Model 16 (*Pseudo Tensor*) Mode II C [8], can be used with limited material characterisation data, which makes it a first choice for preliminary concrete impact studies. At this stage no concrete experimental data is made available, thus the above mentioned material model is used with the option of internally generated parameters. The material model is further described in Appendix C.

The following parameters need to be specified:

- the unconfined compressive strength (normally found by laboratory testing of the axial stress for which a test specimen fails)
- density

- shear modulus
- Poisson's ratio.

Based on density and compressive strength values, the volumetric strain response of the material (equations of state) is generically calculated, assuming an independent relationship with the shear failure surface. The material tensile strength is also internally generated on the basis of the compressive strength. Furthermore, the concrete material model incorporates damage scaling (stiffness degradation due to microcracking) and takes into account strain-rate effects (strength enhancement due to dynamic loading).

The sleeper reinforcement is not taken into account in the current model. This simplification is justified, as long as the transient wheel indentation depth into the sleeper material does not reach a certain critical value. For the studied cases, this value is less than the reinforcement depth.

Sleepers are under a state of lateral compressive stress due to the pretensioned reinforcement. This is, however, approximately taken into account by applying an uniformly distributed positive pressure on one of the edges along the sleeper's lateral axis.

5.3 Tentative model validation

5.3.1 Introduction and the validation case

The most cost-effective and admittedly reliable method to obtain impact data is by studying authentic derailments, under the premises that certain vital information can be acquired, such as:

- an assurance that the indentation depth originates from one wheel only impacting the sleeper in question,
- geometrical data on the impacting wheel,
- longitudinal wheel velocity ($\approx$ train speed) at the time of impact,
- inertial properties of the mass above the wheel,
- sleeper type and geometrical data,
- approximate vertical stiffness and damping of the structure under the sleeper,
- sleeper indentation depth.

It becomes clear that, in order to validate the *FE* computer model based on real accidents or incidents, first-hand information would be required since such data can seldomly be found in the accident reports.

However, one case could be found in the database set up in the first stage of the current research work, which to a large extent fulfils the requirements listed above: the accident at Upplands Väsby, Sweden in 1980 (ID 28) which is thoroughly described in Section 2.2.4 on page 22. Particularly one photograph, see Figure 2-24 on page 25, reveals essential track and wheelset behaviour information which complements the

written accident report. The photograph is taken over a track section where the trailing axle in the bogie initially impacts the sleepers. The only source of information regarding the concrete indentation of the right-hand wheel impact damage is by zooming in the right-hand of Figure 2-24, see Figure 5-1. The following (approximate) estimation is made regarding the indentation depth on the sleeper edge closest to the camera for the first three damaged sleepers:

- Sleeper 1: 15 - 25 mm depth
- Sleeper 2: 15 - 25 mm depth
- Sleeper 3: 3 - 10 mm depth.

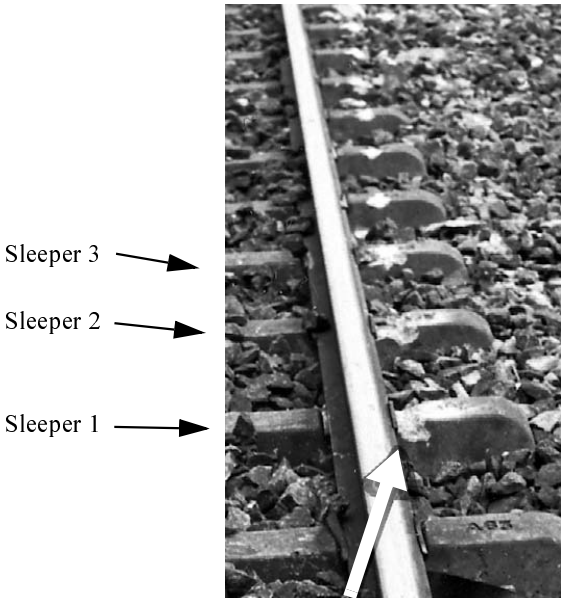

***Figure 5-1 Zoomed-in concrete sleeper damage details in the Upplands Väsby accident** (ID 28).*

5.3.2 *FE* impact model

The tentative *FE* wheel-sleepers impact simulation model has the following features described in the top-down order, sketched in Figure 5-2:

- **Carbody + bogie**: Represented by a lumped mass with two degrees of freedom (vertical and longitudinal translation) nominally located and concentrated in the wheel´s radial centre and suspended to the axle by a stiffness representing the primary suspension. The arbitrary equivalent mass that carbody and bogie together impose on the primary suspension is m_{cb} = 6200 kg. The secondary suspension is neglected.

- **Primary suspension**: The primary suspension is modelled with two springs of arbitrary linear stiffness, linking the lumped mass with the wheel's radial centre and acting in a vertical (z) and longitudinal (x) direction.
- **Wheel**: a sixth (60°) of an unworn *UIC S1002* wheel profile of radius R = 0.44 m, modelled as a rigid body with 2 degrees of freedom, vertical (z) and longitudinal (x) translation. The inertial properties correspond to 1/2 the mass of a wheelset, m_{wheel} = 750 kg.
- **Sleeper**: Since only the local response is considered, a representative upper part section of the twin block sleeper is modelled (a trapezium-shaped area extended in the lateral direction, see Figure 5-3). This volume is meshed with solid 8-node elements with dimensions 8.8 x 9.3 x 5.0 mm. The sleeper section rests on a rigid plate. The nodes of one of the edges (area spanning z-x coordinates) are restricted not to translate in the lateral (y) direction. Furthermore, the nodes on the lower bottom edge (area spanning the x-y coordinates) are restricted not to translate in the longitudinal (x) direction in order to capture the resistance imposed by rail fasteners and ballast against longitudinal motion. The concrete material model is implemented according to Section 5.2 and Appendix C.
- **Rigid plate**: Meshed with 8-node rigid body elements constrained to translate in the vertical (z) direction only. Other translational and rotational degrees of freedom are removed.
- **Sleeper-ground connection**: The sleepers' vertical connection with the underlying ballast bed is incorporated through a linear spring and damper in parallel, linking the rigid plate with the ground.
- **Ground:** Modelled by one node with all degrees of freedom constrained to zero.

In order to compensate for the shortcomings imposed by the removed rotational degree of freedom on the wheel, a null friction coefficient is applied in the wheel-sleeper contact. This limits the study to impacts prior to any applied braking on the wheels, which is consistent to the initial derailment course of events in the Upplands Väsby case.

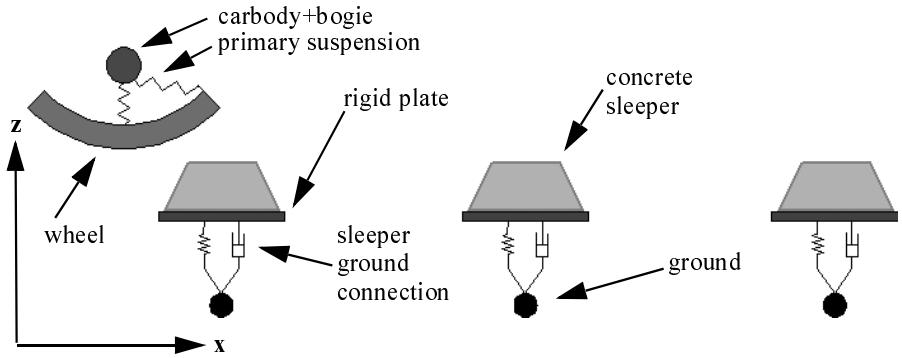

Figure 5-2 General sketch over the model implemented in the Upplands Väsby validation FE simulations, *longitudinal-vertical (x-z) section.*

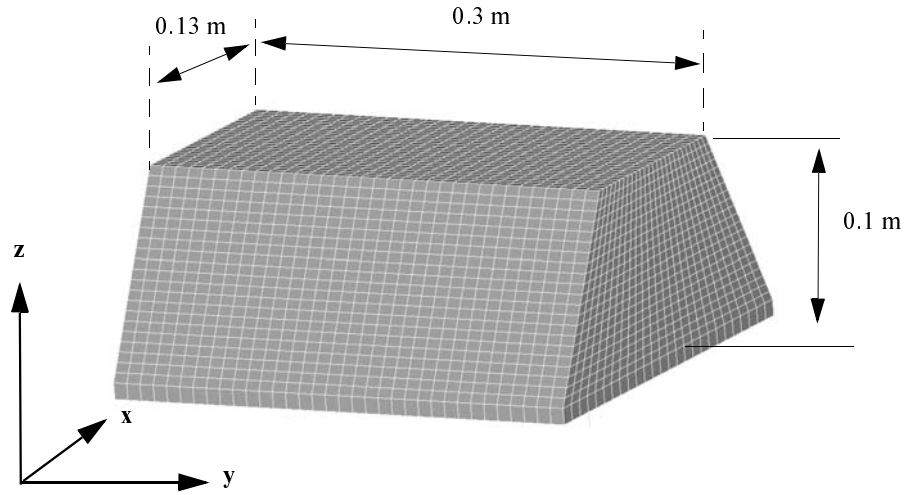

Figure 5-3 3D Ansys/LS-Dyna capture of the meshed sleeper volume with its principal geometrical dimensions.

5.3.3 Simulation methodology

As mentioned in the introductory part, the Upplands Väsby accident report provided sufficient information for a tentative attempt of validating the authentic dynamic behaviour of the wheel-sleeper impact with *FE* simulations. This can be achieved by allowing the wheel to translate over three subsequent sleepers with initial conditions that resemble the authentic case as close as possible. Thereafter, the results obtained from the *FE* simulations in terms of wheel's indentation in the sleepers are processed and compared with values deduced from Figure 5-1. In this respect, two initial condition values are critical, shown in Figure 5-4, and they can not be derived empirically afterwards:

- v_{wz}: the vertical wheel velocity at impact
- h_z: the vertical position of wheel's lowest point F relative the sleeper upper surface at impact.

A closer look at Figure 2-24 on page 25, reveals some further indications for an appropriate assessment of the above-mentioned parameters: the sleeper that precedes the first damaged sleeper by the right-hand wheel, has slight impact marks on its left side and none on the right-hand. This phenomenon could have the following explanation: as the trailing wheelset becomes laterally displaced towards the right, the left-hand wheel falls towards the sleeper from a shorter vertical distance, as opposed to the right-hand wheel, which has an additional approximately 28 mm of height, i.e the climbed flange height (here assumed to be nominal with no wheel wear). A special *MBS* simulation with vehicle parameters consistent with the Upplands Väsby case has been performed, indicating a vertical wheel velocity of 2.6 m/s and a close to zero vertical force in the primary suspension, just as the flange reaches the upper surface of the sleepers.

Moreover, the simulation predicts a vertical position difference of approximately 10 mm between the wheels at the instant when the left side wheel reaches the sleeper surface level. These findings facilitates a fairly good predication of the two critical parameters, namely, the vertical wheel position at the instant of impact, h_z, together with its corresponding vertical wheel velocity, v_{wz}.

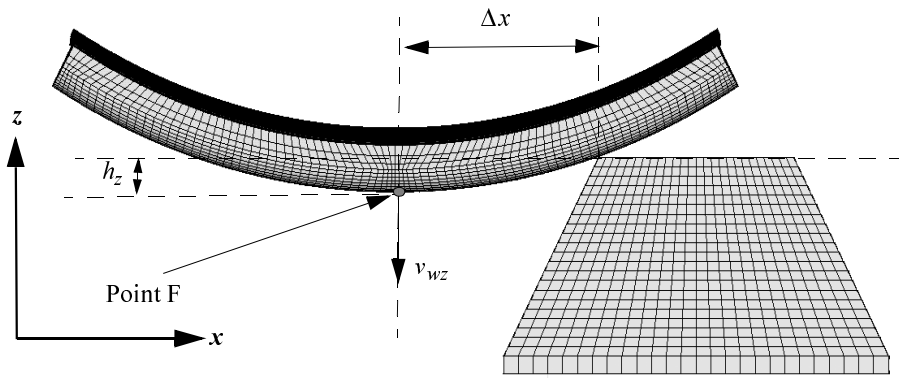

Figure 5-4 Sketch over primary initial wheel - sleeper geometrical impact conditions.

Let's consider the initial geometrical conditions equivalent to the case presented in Figure B-1 in Appendix B and the *MBS* predictions mentioned on the previous page: the wheel is located initially at z_{iF} = -10 mm, that is above the surface of sleeper A on its way to impact sleeper B. Furthermore, consider the upper edge right-hand of sleeper A (in Figure B-1 in Appendix B), as the initial longitudinal location, x_{iF} = 0. The aim is to find the value of h_z, see Figure 5-4, at impact for actual initial conditions. At the instant of impact with sleeper B, Equation (B-3) in Appendix B can be equalled with h_z as this value will be coincident with the vertical position z_F of point F.

For the Upplands Väsby case, the following parameters are valid: v_{wx} = 33.3 m/s (120 km/h), z_{iF} = -10 mm, d = 0.88 m (20 mm radial wear is assumed), h_f = 0.028 m, x_{si} = 0.65 m and x_{sl} = 0.13 m. Assuming the vertical wheel velocity to be v_{wz} = 2.6 m/s and acceleration a_{wz} = 10 m/s^2, as obtained from *MBS* simulations, introducing Equation (B-3) and (B-4) into (B-5) from Appendix B and solving for h_z leads to an initial vertical position h_z of the wheel's lowest point relative to the sleepers upper surface at impact of 18.6 mm. At the same time, it is known that the wheel on the left side of the wheelset touched the sleeper. This might have resulted in a slightly higher vertical velocity v_{wz} of the right-hand wheel then the one calculated from *MBS* simulations. For example, an initial speed increase as much as 0.4 m/s from the nominal value would result in an h_z at impact of 22 mm, for the case where the wheel is located 10 mm above the surface of sleeper A. Due to the uncertainty of the initial state, the following initial vertical velocities and positions of the wheel are included in the *FE* validation simulations: v_{wz} = 2.2, 2.6, 3.0 m/s and h_z = 20, 25, 30 mm.

However, the most likely combination is judged to be around v_{wz} = 2.6 m/s and h_z = 20 mm.

Regarding the involved concrete sleepers, the photograph in Figure 2-24 reveals 1963 as the manufacturing year. Long term data of concrete specimens stored outdoors [50], indicate a compressive strength increase f'_c of 30 to 40% relative the corresponding 28-day strength. The concrete in question is designed for a 60 MPa unconfined compressive strength at 28 days. Therefore, an appropriate value for f'_c at the time of the accident is assumed to be 80 MPa. For the purpose of comparison the 28-day compressive strength is also included in the simulation sets.

Furthermore, no data could be found regarding the vertical sleeper-subgrade dynamic parameters. Swedish measurements [2] for a vertical static load of 60 kN on twin block concrete sleepers on a non-frozen track indicate a vertical stiffness value of approximately 150 MN per rail. However, dynamic excitation tends to increase the static value up to 80% [4]. Assuming the vertical stiffness value per rail to be distributed on two to three sleepers, a standard track has been approximated, see Table 5-1. Due to a high degree of uncertainty, the *standard* track parameters are being lowered by 50% and increased by 100%, denominated, *soft* and *stiff* respectively.

Table 5-1 Formulated vertical track (sleeper-subgrade) parameters per sleeper.

	Soft	*Standard*	*Stiff*
Stiffness (MN/m)	50	100	200
Damping (kNs/m)	150	300	600

5.3.4 Validation results

As mentioned in the introductory part of the current section, the only measure of validation at this stage lies in the authentic photograph from the Upplands Väsby accident, taken in the direction of travel of the foremost damaged sleepers. Accordingly, the permanent damage induced by the wheels motion over three subsequent sleepers is evaluated for each sleeper and denominated *indentation* with the following definition:

- the average permanent vertical displacement of three nodes per sleeper relative their location prior to wheel contact (the undeformed sleeper).

The evaluation nodes are located at 0, 25 and 50 mm from the front edge, forming a line located laterally on a coordinate coincident with the lowest point on the wheel profile, i.e. on the outer edge of the flange.

The complete set of simulation results is presented in Appendix D, in terms of permanent indentation in the three subsequent concrete sleepers as a function of the tested vertical wheel velocity and position at impact, v_{wz} and h_z, respectively. The results are grouped by the sleeper's concrete compressive strength and track property parameters. A negative indentation depth value corresponds to the minimal distance at which the wheel passes above the sleeper's upper surface at the instant point F, see Figure 5-5, longitudinally located at the front edge of the sleeper.

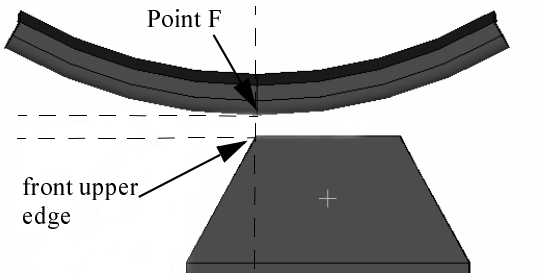

Figure 5-5 Explanation of a negative indentation depth value.

The results strengthen the importance of the initial vertical wheel position at impact as being the most critical parameter regarding the imposed damage on sleepers, followed by the concrete compressive strength. The track stiffness appears to have a marginal effect on the first sleeper indentation, however its influence is increased as the wheel reaches the subsequent sleepers. Furthermore, the sensitivity analysis concerning the vertical wheel velocity, v_{wz}, performed in the interval 2.2 - 3.0 m/s, positions this parameter as having the least effect on the indentation depth. Undoubtedly, the widest span of indentation depth is found as the third sleeper is reached, from an indentation of 9 mm all the way to a wheel translating above the sleeper surface at a distance of 16 mm.

Finally, the parameters found as most plausible to apply in the Upplands Väsby validation simulations are: a vertical wheel position at impact of h_z = 20 mm, a vertical wheel velocity v_{wz} = 2.6 m/s and a concrete compressive strength f'_c = 80 MPa. Based on the above-mentioned input parameters, Figure 5-6 presents the indentation depth (positive values) for the three subsequent sleepers. The values should be compared with Figure 5-1 for validation purposes.

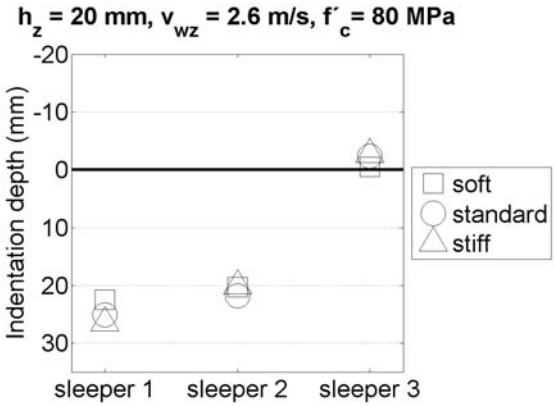

Figure 5-6 Concrete indentation depth results as function of track parameters; *corresponds to simulation parameters judged as most plausible for the Upplands Väsby accident.*

Firstly, it appears clear that the values obtained from the *FE* analysis are within the correct order of magnitude for all cases, see Appendix D. Moreover, the results are within the estimated range for two cases with an initial vertical wheel position of h_z = 20 mm for both *soft* and *standard* track properties. Regarding the third sleeper, the implemented computer model tends to overestimate the ability of the wheel to rebound after impact. The discrepancy between the relatively simple wheel and suspension model and a wheelset in a complete complex vehicle - impacting concrete sleepers - seems to become more pronounced as several continuous impact sequences are simulated.

5.3.5 Discussion and conclusions

It would be desirable to have more than one authentic cases for validation, also with more exactly determined sleeper indentation data than have been possible to collect in the above described case. Although the validated case was quite successful, the validation process should continue as soon as more authentic cases are made available.

Nevertheless, the wheel-sleeper impact model and simulation technique are shown to be a useful tool for further studies of wheelsets rolling on sleepers after a derailment. The hysteresis loops - i.e. the relations between impact force, sleeper indentation and wheel lateral and vertical velocity - could and should be used in more complete *MBS* post-derailment simulations.

5.4 Impact simulations of an X 2000 trailer car wheel

5.4.1 Introduction

As discussed in Section 2.4, the axle mounted brake discs could have favourable effects in some type of derailment, as long as certain criteria are fulfilled. In Section 4, the lateral criteria have been analysed for a derailment due to an assumed axle journal failure for an *X 2000* trailer car. In this section, the vertical motion of an *X 2000* trailer car wheel impacting concrete sleepers is studied, in preparation for a more comprehensive investigation with *MBS* simulations.

5.4.2 FE impact model

The FE model is sketched in Figure 5-7, and its principal parts consist of:

- **Carbody**: Represented by a lumped mass with two degrees of freedom (vertical and longitudinal translation) with inertial properties corresponding to one eighth of the *X 2000* trailer carbody mass.
- **Secondary suspension**: Represented by two springs of arbitrary linear stiffness acting in a vertical (z) and longitudinal (x) direction. The springs link the two lumped carbody and bogie masses.

- **Bogie**: Represented by a lumped mass with two degrees of freedom (vertical and longitudinal translation) with inertial properties corresponding to one fourth of the *X 2000* trailer bogie mass.
- **Primary suspension**: Represented by two spring of arbitrary linear stiffness acting in a vertical (z) and longitudinal (x) direction. The springs link the two lumped carbody and bogie masses.
- **Wheel**: A sixth (60°) of an unworn *UIC S1002* wheel profile of diameter 0.88 m, (unworn wheel) modelled as a rigid body with two degrees of freedom, vertical (z) and longitudinal (x) translation. The inertial properties correspond to 1/2 the mass of an *X 2000* trailer car wheelset. The wheel-sleeper contact algorithm includes a zero friction coefficient.
- **Sleeper**: Since only the local response and impact close to the rail fastening is considered, a simplified upper part section of an *A9P* concrete sleeper (Abetong, Sweden) is modelled as a trapezium-shaped area extended in the lateral direction, see Figure 5-8. This volume is meshed with solid 8-node elements with dimensions of 7.8 x 9.6 x 5.8 mm. The sleeper section rests on a rigid plate. The nodes of one of the edges (area spanning z-x coordinates) are restricted not to translate in the lateral (y) direction. Furthermore, the nodes on the lower bottom edge (area spanning the x-y coordinates) are restricted not to translate in the longitudinal (x) direction in order to capture the resistance imposed by rail fastners and ballast against longitudinal motion. Concrete material model is according to Section 5.2 and Appendix C.
- **Rigid plate**: Meshed with 8-node rigid body elements constrained to translate in the vertical (z) direction only. Other translational and rotational degrees of freedom are removed.
- **Sleeper-ground connection**: The sleepers' vertical connection with the underlying ballast bed, is incorporated through a linear spring and damper in parallel, linking the rigid plate with the ground.
- **Ground:** Modelled by one node with all degrees of freedom constrained to zero.

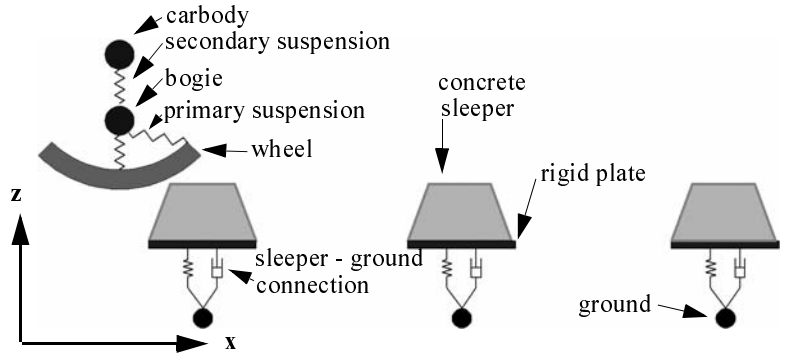

Figure 5-7 General sketch over the model implemented in the X 2000 trailer car wheel impact FE simulations, *shown in a vertical-longitudinal section.*

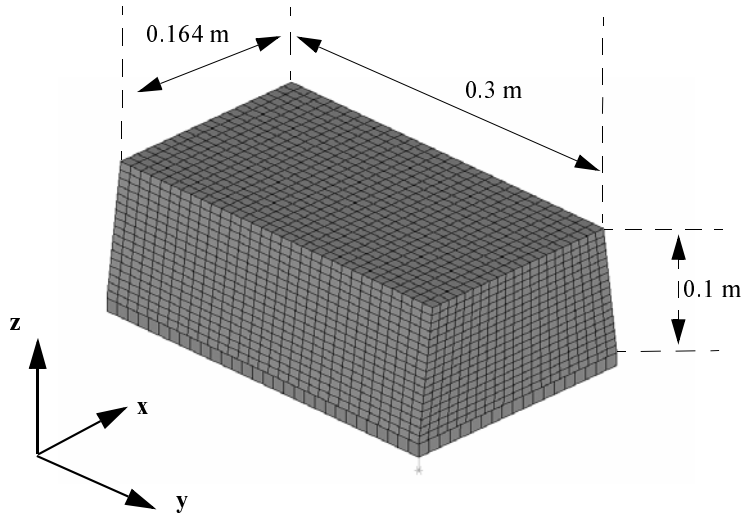

Figure 5-8 3D Ansys/LS-Dyna capture of the meshed sleeper volume section in the X 2000 trailer car wheel impact FE simulations with its principal geometrical dimensions.

5.4.3 Simulation methodology

At a first sight, it is expected that the risk of vertical rebound of a rail vehicle wheel impacting a sleeper surface to be highest in the initial contact phase, as the vertical wheel velocity prior to impact reaches its largest value. Therefore, the maximum possible vertical wheel velocity is an important input variable. Specially performed *MBS* simulations of an *X 2000* trailer car wheel derailing from an *UIC60* rail, indicate a vertical wheel velocity at the sleeper surface level of v_{wz} = 2.8 m/s. Furthermore, *MBS* simulations furnish data regarding the vertical forces developed by the primary and secondary suspension prior to the wheel reaches the sleeper surface level. These are transferred in the *FE* model as an initial offset in each respective stiffness element at time zero.

The vertical wheel position h_z at impact is sought for the vertical wheel velocity, v_{wz}. For this task, the equations from Appendix B are applied.

Consider the case sketched in Figure B-1 in Appendix B with an initial vertical longitudinal wheel position above sleeper A of $z_{iF} = x_{iF} = 0$. For a train speed of 200 km/h and other initial state variables obtained from *MBS* simulations inserted into Equation (B-1) to (B-5), give an initial vertical wheel position at impact of $h_z \approx 18$ mm. Based on a similar approach, a train speed of 120 km/h would result in an initial vertical wheel position at impact of $h_z \approx 29$ mm. The immediate question arising is how these two critical parameters, h_z and $V = v_{wx}$, mutually affect the vertical wheel velocity at the end of the concrete sleeper impact.

Based on the law of impulse and assuming that force in the primary suspension is small compared to the contact ones, the following proportionality is valid:

$$\Delta v_{wz} \sim \int_{\Delta t} F_{cz} dt \qquad (5\text{-}1)$$

where,

F_{cz} vertical component of the contact force exerted on the wheel during impact,

Δv_{wz} change of vertical wheel velocity during impact,

Δt total impact time.

A lower longitudinal wheel velocity implies a larger contact time, resulting in a larger vertical wheel velocity change for the same h_z and consequently the same angle β, see Figure 5-9. However, a larger longitudinal wheel velocity is expected to increase the vertical component F_{cz} of the impact force F_{cn}. Meanwhile, a higher longitudinal wheel velocity contributes with a diminished initial vertical wheel position h_z at impact.

Consequently, it appear necessary to test a lower train speed as well, as the maximum permissible train speed is not automatically associated with the highest risk of undesired wheel rebound.

Furthermore, two different concrete compressive strength values for the sleepers will be tested: at 28 days and after approximately 20 years (concrete stored outdoors according to [50]), thus f'_c = 60 and 80 MPa respectively. Furthermore, three different types of track parameters, *soft*, *standard* and *stiff* will be included in some simulation sets. The track parameters are set according to Table 5-1.

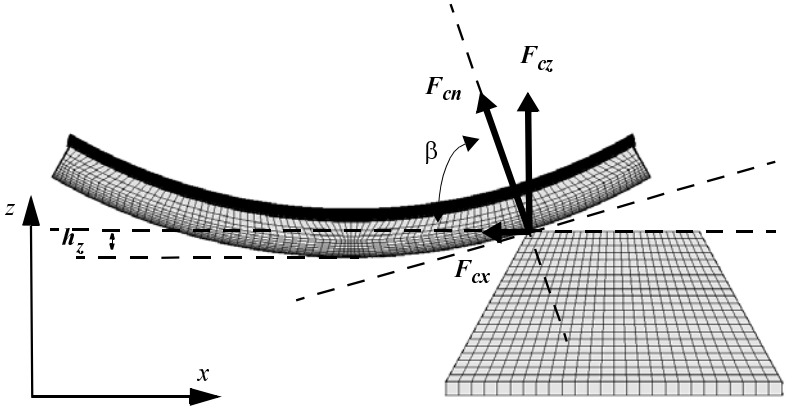

Figure 5-9 Sketch over the longitudinal (F_{cx}), normal (F_{cn}) and vertical (F_{cz}) force vector imposed by the sleeper on the wheel at the instant of impact.

5.4.4 Results

The absolute vertical position of the wheel's lowest point (Point F in Figure B-1 from Appendix B) relative to the initial sleeper surface together with its vertical velocity were registered along three subsequent sleepers. The simulation was terminated as the wheel's lowest point reached the longitudinal distance consistent with the end of the third sleeper upper surface level.

The *FE* simulation scheme for assessing the vertical rebound of an *X 2000* trailer car is divided in three simulation sets, which are combinations of various initial state conditions and track parameters.

For each simulation set a "worst case" is presented, as the absolute vertical position and velocity of the wheels's lowest point with respect to its longitudinal position. In this context, a "worst case" is the scenario corresponding to the highest recorded values of vertical motion during the wheel's longitudinal position. The complete set of results for all simulation sets is presented in Appendix E.

Simulation set 1

- train speed, longitudinal wheel velocity: V = 200 km/h; v_{wx} = 55.56 m/s
- vertical wheel velocity: v_{wz} = 2.8 m/s
- vertical wheel position at impact, h_z = 10 and 18 mm
- sleeper concrete compressive strength: f'_c= 60 and 80 MPa
- track design parameters: *soft*, *standard* and *stiff*

The results for the first simulation set are presented in Figure E-1 and Figure E-2 in Appendix E, for h_z = 10 and 18 mm respectively. In no case the wheel is rebound as to move longitudinally above the sleeper surface along the three subsequent sleepers. As expected, the closest distance from the wheel's lowest point to the sleeper surface is obtained for a lower initial vertical wheel position (large h_z = 18 mm), aged concrete f'_c = 80 MPa and a *stiff* track. The highest vertical velocity is obtained for the same state conditions as above. The results consistent to the "worst-case" of simulation set 1 are presented in Figure 5-10, for the vertical position and velocity of the lowest point of the wheel. Although the wheel's lowest point is found below the sleeper surface level, there appears to be an uprising direction as the end of the third sleeper is reached.

In next simulation set, a sensitivity analysis of the initial vertical wheel velocity is performed, while maintaining the nominal values of the vertical carbody and bogie velocities, as obtained from the special *MBS* simulations. For comparison reasons, an even lower vertical wheel velocity than the nominal value of v_{wz} = 2.8 m/s will be tested. Furthermore, a constant initial vertical wheel position h_z of 18 mm is set. Based on the results obtained from the simulation set 1, where a stronger concrete always showed a higher risk of rebound, only one concrete compressive strength is considered, f'_c = 80 MPa.

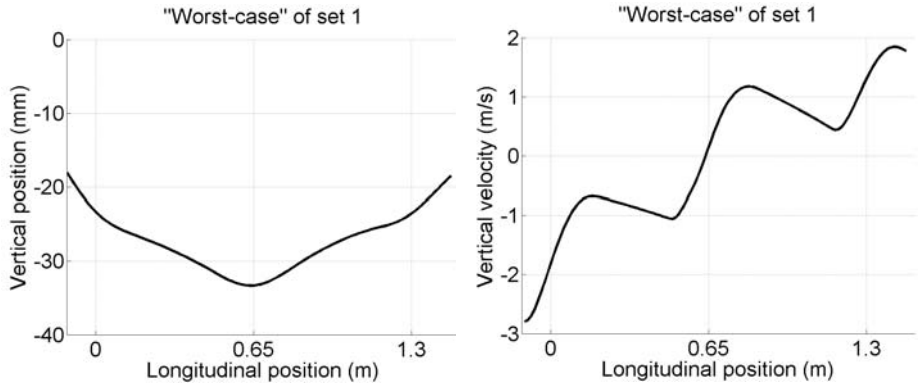

Figure 5-10 ***The absolute vertical position*** *(left-hand)* ***and velocity*** *(right-hand)* ***along three subsequent sleepers*** *of the wheel's lowest point relative to the sleepers surface (0 level).*
"Worst-case" of simulation set 1.
v_{wz} = 2.8 m/s, v_{wx} = V = 55.56 m/s (200 km/h),
h_z = 18 mm,
f'_c = 80 MPa,
stiff track.

Simulation set 2:

- train speed, longitudinal wheel velocity: V = 200 km/h; v_{wx} = 55.56 m/s.
- vertical wheel velocity, v_{wz} = 0.5, 1.5, 3.0 and 3.5 m/s
- initial vertical wheel velocity: h_z = 18 mm
- sleeper concrete compressive strength: f'_c= 80 MPa
- track parameters: *soft*, *standard* and *stiff*

Figure E-3 in Appendix E presents the results for the three track parameters in combination with the four tested vertical wheel velocity at impact, v_{wz}. Out of the four initial vertical wheel velocities the lowest one v_{wz} = 0.5 m/s contributes, apparently, to a more rapid wheel ascend towards the sleeper surface level. The vertical contact force due to the wheel's longitudinal motion is constant in all cases for the first impacted sleeper. Therefore, a lower initial vertical wheel velocity, implies a higher total vertical contact force on the wheel for the first sleeper. This can be observed in Figure 5-11 which presents the "worst case" for simulation set 2 obtained at an initial vertical wheel velocity of v_{wz} = 0.5 m/s and *stiff* track. The other extreme, v_{wz} = 3.5 m/s is also plotted in the same graph for comparison reasons.

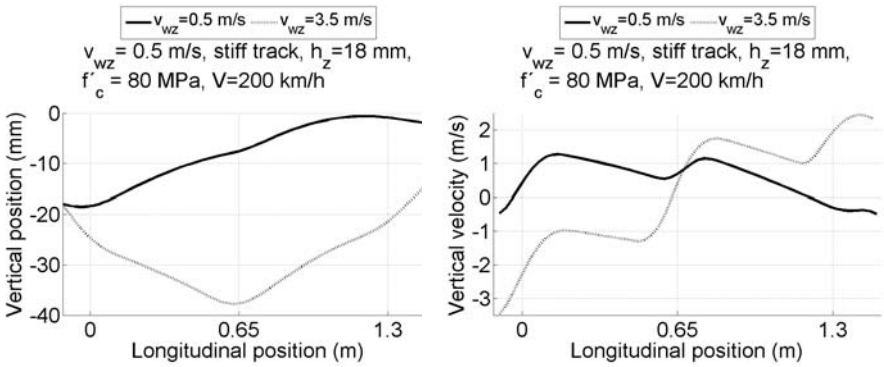

Figure 5-11 ***The absolute vertical position*** *(left-hand)* ***and velocity*** *(right-hand)* ***along three subsequent sleepers*** *of the wheel's lowest point relative to the sleeper surface.*
"Worst-case" of simulation set 2.
v_{wz} = 0.5 m/s, v_{wx} = V = 55.56 m/s (200 km/h),
h_z = 18 mm,
f'_c = 80 MPa,
stiff track.

The absolute vertical wheel position just tangents the sleeper surface level prior to impacting the third sleeper for the case of low vertical wheel velocity. The vertical wheel position corresponding to a higher vertical wheel velocity is at a considerable distance below the sleepers surface level. However, the vertical velocity graph gives reasons to consider *the case of higher vertical wheel velocity a more alarming condition*; as the contact with the third sleeper is terminated, the vertical wheel velocity is considerably higher as to lift the wheel upwards.

In next simulation set, a lower longitudinal wheel speed, v_{wx} = 120 km/h is tested. Based on the previous discussion and results, only an aged concrete sleeper is considered, f'_c = 80 MPa. Furthermore, the soft track parameter is omitted as all the results so far have indicated that a stiffer track is corresponds to a higher risk of wheel rebound. The initial vertical wheel position, h_z will be varied for *standard* and *stiff* track parameters. The following combinations of initial conditions and track design parameters are included:

Simulation set 3:

- train speed, longitudinal wheel velocity: V = 120 km/h; v_{wx} = 33.33 m/s
- vertical wheel position at impact, h_z = 18, 25 and 30 mm
- sleeper concrete compressive strength: f'_c = 80 MPa
- track design parameters: *standard* and *stiff*

Figure 5-12 presents "the worst case" from the third simulation set which occurs, as expected, at the lowest initial wheel vertical position, h_z=30 mm. From all the simulations performed in this section, this is also the case where the vertical wheel

position comes next closest to the sleeper surface level, after the lowest initial vertical wheel velocity from simulation set 2. However, as in all the previous cases, the wheel proceeds longitudinally below the sleeper surface.

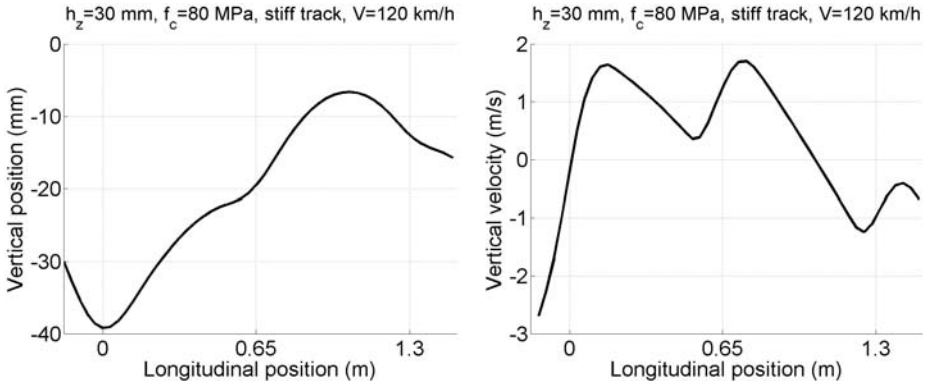

Figure 5-12 ***The absolute vertical position*** *(left-hand)* ***and velocity*** *(right-hand)* ***along three subsequent sleepers*** *of the wheel's lowest point relative to the sleeper surface.*
"Worst-case" of simulations set 3:
v_{wz} *= 2.8 m/s,* v_{wx} *= V = 33.33 m/s (120 km/h),*
h_z *= 30 mm,*
f'_c *= 80 MPa,*
stiff track.

5.4.5 Discussion of results

From the point of view of track parameters, the risk of rebound increases with a stiffer track as well as with an aged concrete sleeper.

In terms of initial state conditions, a higher longitudinal wheel velocity, i.e. a higher train speed, and a lower vertical wheel position at impact (high h_z), lead to an increase risk of rebound. Additionally, a lower initial vertical wheel velocity, leads to a higher risk of rebound as the wheel travelled over three subsequent sleepers. However, this relationship is expected to change as the wheel is allowed to move longitudinally over a longer period of time.

Although not simulated, the following relationship is assumed to be valid: a lower vertical force imposed by the primary suspension on the wheel, the higher is the risk of rebound.

It is expected that the initial state conditions which impose the highest risk of rebound, i.e. high vertical wheel velocity, consequently low vertical wheel position and a low vertical primary suspension force, are to be found in conjunction with the wheel's initial sleeper impact. Since the results presented in the previous section are based on the wheel's initial impact sequence, one is tempted to believe that *the risk of wheel rebound above the sleeper's surface is limited.*

However, at this stage, no definite conclusion could be postulated in this issue. It is anticipated that three-dimensional *MBS* simulations, with implemented hysteresis loops in the wheel-sleeper contact algorithm, will give a more complete picture of this complex phenomenon.

6 Conclusions and future work

6.1 Summary of the present work

The more general analysis of past incidents and accidents has led to the identification of several critical vehicle features and parameters that are capable to influence the outcome of a derailment. However, many accident and incident reports lack information of critical data being relevant for this study. This makes it difficult to give a verdict based on observations only.

However, some tendencies can be distinguished:

- The low-reaching bogie frame design on the Swedish high-speed train *X 2000* and commuter train *X 10* is believed to be advantageous when the vehicle comes into a derailed condition. This has been observed in a number of cases.
- The French *TGV* train has showed favourable properties even at high-speed derailments, at least for track sections with no potential aggravating elements, i.e. curves and switches. Whether this is a result of the articulated train architecture or it is due to other properties of the articulated vehicles or is related to the running gear design, is not possible to determine with the scarce detailed information being available at this stage.
- Brake discs with appropriate geometrical parameters may prevent the wheelset to deviate laterally.
- Accidents involving double-deckers cars, mostly from USA, indicate that these vehicle seem to be prone to overturning.
- The sole factor with the most devastating potential for a derailed rail vehicle is track switches.

In order to perform a more systematic investigation on the influence of different vehicle properties and parameters, a multi-body simulation (*MBS*) model has been developed and employed. As a first step the conditions for derailment of *X 2000* power units have been investigated. As part of the initial simulations, the proposed computer model has successfully been validated for two Swedish derailment cases, both in curves. The model can predict the derailment of the leading wheelset towards the lower side of a curve as a result of an axle journal failure on the trailing wheelset above the high rail. In connection to this phenomenon an explanation has been proposed. The parameters that are unknown or difficult to estimate may also affect the tendency of the wheelset to derail. The influence of these parameters has been subject to a sensitivity analysis.

As a result of the simulation studies, it is found that a most important parameter for the possibility of a bogie to derail as a result of an axle journal failure is the *vertical mechanical restriction* between the wheelset and the bogie frame. This tendency is the same for both the power unit and the trailer car of *X 2000*.

The choice of wheelset guidance stiffnesses in combination with an arbitrarily located axle journal failure on an *X 2000* power unit bogie has been studied, considering three combinations of the lateral and longitudinal stiffnesses. The results show a slight

tendency that a stiffer primary suspension causes a higher predisposition for derailment through flange climbing.

Further, the influence of lateral and vertical geometry of an axle mounted brake disc in order to prevent a potentially disastrous lateral deviation of the wheelset after a flange climbing derailment has been subject to a tentative simulation study. Post-derailment analysis has been performed with an *X 2000* trailer car model running in different curves at its maximum permissible cant deficiency. For *UIC 60* rail, a minimal lateral play between the wheel and the brake disc was found to be approximately 0.130 m for a safe engagement with the rail, with no large dependency on the brake disc diameter, presupposed that the disc diameter is large enough to engage with the rail. This a tentative result assuming no rebound in the wheel-concrete sleeper impact.

In order to prepare for studies of a possible wheel rebound and also for a more general *MBS* study of wheels rolling on sleepers, a finite element (*FE)* model of a railway wheel, connected with the sprung mass through a simplified suspension model, has been developed and tentatively validated. This model shows a good agreement for one authentic derailment, in terms of the wheel indentation in the concrete sleeper for three subsequent sleepers.

Further, several *FE* simulation sets have been performed on an *X 2000* trailer car wheel model impacting three subsequent sleepers with various initial conditions as well as different track parameters. No wheel-concrete sleeper impact scenario has resulted in a wheel rebound reaching above the sleeper surface during the first three sleepers. However, no reliable conclusion can be reached at this stage regarding the tendency of a railway vehicle wheel to rebound after impact with concrete sleepers. This is due to the limited number of concrete sleepers included in the model in combination with the shortcomings imposed by the simple two-dimensional approach. However, based on the studies accomplished so far, it is the author's opinion that if a rebound does occur, a relatively limited magnitude is expected.

6.2 General conclusions

- A number of vehicle features have been identified with the potential to favourably affect the course of events associated with high-speed derailments
- Correlating authentic derailment observations with *MBS* computer simulations appears to be a feasible approach for validating the computer model. Limitations commence as a relatively small amount of incident and accident reports contain sufficient detailed data.
- Two vehicle features have been studied in more detail leading to tangible proposals of their possible implementation in vehicles
- Finite element computer models appear to complement well the *MBS* computer simulation approach to derailment studies.

6.3 Future directions of research

The ultimate goal of the present research is to reduce the consequences after derailments by studying the influence of various train properties and design parameters. This can only be achieved by allowing the running gear to roll on track structures, i.e sleepers and ballast. In this respect, the wheel-concrete sleeper contact issue has emerged as a central part, on which a great number of future results are dependent.

The following future work with the *FE* simulation model is proposed:

- Additional eligible authentic cases should be simulated and validated, preferably cases at higher train speeds and where a more exact sleeper indentation value can be acquired. However, the possibilities to perform such validation is dependent of the availability of additional data from authentic cases.
- Acquiring hysteresis data from *FE* simulation for the wheel contact forces as function of concrete material indentation, to be used in *MBS* simulations.
- Extending the wheel *FE* model, by introducing three more degrees of freedom, two rotational, i.e. yaw and pitch (wheel rotation), and one translation in the lateral direction.

Thereafter, a reliable wheel-concrete sleeper impact algorithm should be developed and transferred to the *MBS* computer code. Furthermore, the relationship between the wheel's yaw angle and its lateral force resultant due to rolling concrete indentation should be examined.

The following possible future work is proposed, once the above mentioned dependencies are implemented in the *MBS* simulation model:

- The brake disc diameter requirements should be further studied, considering the dynamic effects arising as the wheelset rolls or rebounds over the sleepers.
- The rotational effects of the brake disc when contacting the rail should be incorporated.
- Studies on the lateral and vertical geometrical parameters in order for a low-reaching bogie frame design to engage successfully with the rails.
- Estimating the order of magnitude of the lateral force that axle mounted brake discs and low-reaching bogie frames should be able to withstand.
- The lateral and vertical brake disc geometry should be assessed for a wider spectrum of bogie designs.
- The general vehicle behaviour after a derailment should be simulated and validated with appropriate authentic incidents or accidents.
- Further studies on the influence of mechanical restrictions between bogies and carbody, including gaps in the suspension as well as the yaw resistance.
- Parameter studies on the influence of couplings and other restrictions between carbodies in a train.
- Multiple parameter studies based on the concept of articulated trains and bogie design including complete simulations of coupled vehicles.

- Assessing the influence of the height of centre of gravity on general vehicle behaviour after derailments.
- Developing at least a simple model that accounts for wheel-ballast interaction.
- Studies on the effects of track switches, i.e. the course of events when a derailed wheelset or low-reaching bogie frames impacts switch structures after a derailment.
- A computer model should eventually be developed to assess axle failures inside the wheels, as up to now only failures outside the wheels have been studied by simulations.

Appendix A - Database events overview

The tables presented here is an attempt to facilitate an overview in order to find an empirically based correlation between different types of vehicles, the initial cause with its immediate sequence of events as well as the existence of potentially track aggravating elements. The complete narrative description of each event is found in Section 2.2

The lateral deviation should be regarded as an estimation only, indicated with respect to the track centre line.

The general consequence gradation has the following significance:

minor	no serious harm to any passenger or member of the staff;
luckily minor	no serious injuries on any passenger or member of the staff, but could have resulted severe consequences, i.e. parts of the train deviate laterally as to foul another track, but, by chance, no other train was scheduled at that time;
severe	injuries of various degree to passenger and/or member of the staff;
catastrophic	at least one fatality registered.

Table A-1 Axle failure on the outside of the wheels.

ID	Type of vehicles	Initial cause	Initial sequence of events	Speed (km/h)	Potentially aggravating elements	Lateral deviation (m)	General consequences
1	X 2000	failure on axle 2 left-hand on rear end power unit	wheelset 1 on rear end power unit derails right	200	right-hand curve, 1 right-hand trailing switch	<0.1	minor
2	X 2000	failure on axle 3 right-hand front end power unit	no derailment	180	S-curve	0	minor
3	X 2000	failure on axle 4 right-hand front end power unit	no derailment	140	Both left- and right-hand curves	0	minor

Table A-2 Axle failure on the inside of the wheels.

ID	Type of vehicles	Initial cause	Initial sequence of events	Speed (km/h)	Potentially aggravating elements	Lateral deviation (m)	General consequences
4	X 2000	failure on axle 1 on car 4	wheelset 1 on car 4 derails on the inside	140	left-hand curve, right-hand trailing switch, left-hand trailing switch, right-hand facing switch	<0.1	minor
5	X 2000	failure on axle 1 on front end driving trailer	right-hand wheel on wheelset 1 on front end driving trailer derails on inside	190	trailing switch facing switch curve	<0.1	minor
6	X 10	failure on axle 1 on car 2	wheelset 1 on car 2 derails	90	facing switch	0.2-0.7	minor
7	2 F40 + 19 cars	failure on axle 1 on loco 2	right-hand wheel on wheelset 1 on loco 2 derails on inside	107	trailing switch	>5	catastrophic
8	3 F40-PH+18 coaches	failure on axle 1 on loco 3	wheelset 1 on loco 3 runs on the inside of the rails	126	left-hand trailing switch	>5	severe

Table A-3 Broken rails or other track defects.

ID	Type of vehicles	Initial cause	Initial sequence of events	Speed (km/h)	Potentially aggravating elements	Lateral deviation (m)	General consequences
9	1 Rc + 13 cars	rail failure under train	rearmost 2 wheelsets in the train derail	110	unclear	<1.5	luckily minor
10	1 Rc + 13 cars +1 Rc	rail failure under train	bogie 2 on car 8 and bogie 1 on car 9 derail towards opposite track	125	unclear	<0.75	luckily minor
11	1 Rc + 7 cars	track buckle developed under train	bogie 2 on car 6 and bogie 1 and 2 on car 7 derail	110	curve	<0.8	luckily minor
12	1 Rc + 12 cars	track misalignment ahead of train due to lorry impacting viaduct	all wheelsets of loco and subsequent 6 cars derail	100	unclear	<2	luckily minor
13	TGV	rail fracture beneath the train	unclear	130	unclear	0.1-0.75	luckily minor, overturned power unit
14	TGV	unsupported track structure	rearmost 4 cars and power unit derailed with all wheelsets	294	unclear	<0.1	minor
15	IC225	outer rail failure beneath car 4	all wheelsets derail from car 4 onwards	180	curve	>5	catastrophic, overturning
16	2 F40 + 9 cars	outer rail fracture beneath car 2	all wheelsets derail from car 2 onwards	115	curve	>5	catastrophic, overturning
17	365 EMU (4 vehicles)	facing switch moving under car 3	trailer bogie on car 3 and both bogies on car 4 derail	153	1 facing switch	>5	catastrophic, overturning
18	2 P42 + 13 cars	track buckle ahead of train	all wheelsets derail from car 1 to car 12	96	no	>5	severe, overturning

(to be continued)

Table A-3 Broken rails or other track defects. (continued)

ID	Type of vehicles	Initial cause	Initial sequence of events	Speed (km/h)	Potentially aggravating elements	Lateral deviation (m)	General consequences
19	2 F40 + 16 cars	rail failure under train	all wheelsets derail up to rearmost 5 cars	80	no	>5	severe, overturning
20	2 F40 + 16 cars+ 24 Auto-rack	track buckle ahead of train	all axles derail from c 5 to 18	90	curve	>5	severe, overturning
21	2 F40 + 16 cars	track buckle developed under train	all wheelsets derail on rear-most 8 cars	120	1 trailing switch	<4	severe
22	2 F40 + 12 cars	track buckle ahead of train	all axles derail from car 2 to the rear end	112	no	<5	severe, overturning
23	4 F40 + 26 cars	11 m of unsup-ported track structure	all wheelsets derail from loco 2 to car 19	145	no	<5	luckily minor
24	1 loco + 8 Mark3 cars + 1 DVT	obstructed flangeway	wheelset 1 and 2 derail on car 5	200	no	<0.1	minor

Table A-4 Wheel defects.

ID	Type of vehicles	Initial cause	Initial sequence of events	Speed (km/h)	Potentially aggravating elements	Lateral deviation (m)	General consequences
25	IC225	broken wheel rim on wheelset 2 on rearmost car	all wheelsets derail on rearmost car	200	curve, 1 trailing switch, 1 facing switch	<0.1	minor
26	TGV	flat wheel	1 bogie derailed	270	?	?	minor
27	ICE 1	broken wheel rim on wheelset 3 on car 1	no initial derailment-	200	1 trailing switch, 1 facing switch	>0.75	catastrophic, impact
28	1 Rc + 13 cars	broken wheel rim on wheelset 3 on car 6	wheelset 3 and 4 derail on car 6	120	1 trailing switch	>0.6	catastrophic, overturning

Table A-5 Other causes.

ID	Type of vehicles	Initial cause	Initial sequence of events	Speed (km/h)	Potentially aggravating elements	Lateral deviation (m)	General consequences
29	Eurostar	transmission assembly dropping off from bogie 2 on front end power unit	bogie 2, 3, 23 in the train derail	300	unclear	<0.1	minor
30	IC225	impact with stationary car trailer, DVT front end	wheelset 1 and 2 of DVT derail	200 (car impact) 140 (switch impact)	1 trailing switch	>0.75	catastrophic, impact
31	VT610	unknown	wheelset 1 and 2 derail on front end loco	70	curve	<0.5	minor
32	HST 125 (1 loco + 8 Mark3 + 1 loco)	impact with stationary car	wheelset 1 on front end loco derails	160	1 facing switch	>0.75	catastrophic
33	1 F40 + 9 cars	improper positioned switch	all, but the rearmost 2 wheelsets, derail	120	no	>0.5	luckily minor

Appendix A - Database events overview

Appendix B - Wheel position at impact with the sleeper

The analytical equations for the two-dimensional trajectory of an imaginary point F, located at the lowest possible vertical position on the wheel, see Figure B-1, are:

$$x_F = x_{iF} + v_{wx}t + \frac{1}{2}a_{wx}t^2 \qquad \text{(B-1)}$$

$$z_F = z_{iF} + v_{wz}t + \frac{1}{2}a_{wz}t^2 \qquad \text{(B-2)}$$

where,

x_{iF}	initial longitudinal position of point F,
v_{wx}	longitudinal wheel velocity,
a_{wx}	longitudinal wheel acceleration,
z_{iF}	initial vertical position of point F
v_{wz}	initial vertical wheel velocity,
a_{wz}	vertical wheel acceleration,
t	time elapsed from the initial wheel position.

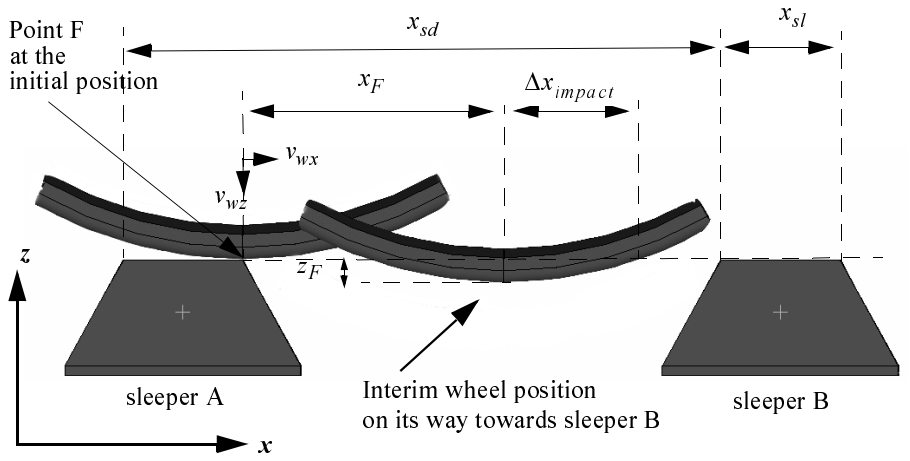

Figure B-1 Sketch over various geometrical parameters involved in the analytical calculations of the vertical wheel position at the instant of impact with sleeper B.

Introducing Equation (B-1) into Equation (B-2) and assuming a zero longitudinal wheel acceleration up to the instant of impact, leads to:

$$z_F = z_{iF} + v_{wz}\frac{x_F - x_{iF}}{v_{wx}} + \frac{1}{2}a_{wz}\left(\frac{x_F - x_{iF}}{v_{wx}}\right)^2 \qquad \text{(B-3)}$$

Furthermore, the following equation describes the relationship between the wheel's vertical position, h_z relative to the sleeper surface and the longitudinal segment Δx_{impact}:

$$\Delta x_{impact} = \sqrt{h_z\left(2\left(\frac{d}{2} + h_f\right) - h_z\right)} \qquad \text{(B-4)}$$

where

d wheel diameter,

h_f flange height.

At the instant of impact, the following equation has to be satisfied:

$$x_F + \Delta x_{impact} = x_{si} - x_{sl} \qquad \text{(B-5)}$$

where,

x_{si} sleeper spacing interval

x_{sl} longitudinal length of sleeper's upper surface.

Appendix C - Concrete material modelling details

The finite element simulations described in this thesis make use of a concrete material model called *Pseudo-Tensor* or Material Type 16 incorporated in the *LS-DYNA* code. Furthermore, this model can be used in two major modes by means of a tabulated yield stress versus pressure (mode I) or two curve model with damage and failure (mode II). The latter model was chosen with a further option of allowing the code to internally generate various material constants based on the concrete unconfined compressive strength.

The above mentioned material model option provides two yield versus pressure curves, σ_{failed} (minimum, damaged strength) and σ_{max} (maximum, undamaged strength), which limit the second invariant of the deviatoric stress σ_{yield}, where

$$\sigma_{yield} = \sigma_{failed} + \eta(\sigma_{max} - \sigma_{failed}) \tag{C-1}$$

with,

$$\sigma_{failed} = a_0 + \frac{P}{a_1 + a_2 P} \tag{C-2}$$

$$\sigma_{max} = a_{0f} + \frac{P}{a_{1f} + a_2 P} \tag{C-3}$$

where

P - pressure

η - damage scale factor

The internally generated values for the material constants are:

$a_0 = f'_c/4$, $a_1 = 1/3$, $a_2 = 1/3f'_c$, $a_{0f} = 0$, $a_{1f} = 0.385$,

where f'_c is the concrete unconfined compressive strength.

The damage scale factor η shifts the σ_{yield} curve between the failed and the maximum state. The scale factor is tabulated against a damage function λ according to recommendations [49], see Figure C-1.

The damage function is a measure of the accumulated plastic strain ε^p, and takes the form:

$$\lambda = \int_0^{\varepsilon^p} \left(1 + \frac{P}{\sigma_{cut}}\right)^{-b_1} d\varepsilon^p, \tag{C-4}$$

where b_1 is set to 1.25

and

$$\sigma_{cut} = 1 \cdot 7 \left(\frac{f'_c}{-a_0} \right)^{\frac{2}{3}} \tag{C-5}$$

The concrete relative strength increase when subjected to higher strain rates is captured by applying the curve in Figure C-2, which scales the compressive strength parameter according to the tentative recommendations of *CEB* [10] for an f'_c = 50 MPa concrete.

.

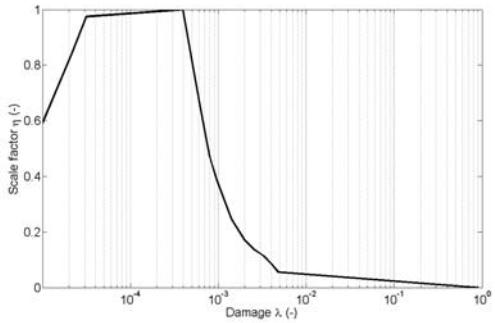

Figure C-1 ***Tabulated value pairs for the scale factor*** η ***vs. the damage function*** λ ***presented on a logarithmic scale*** [49].

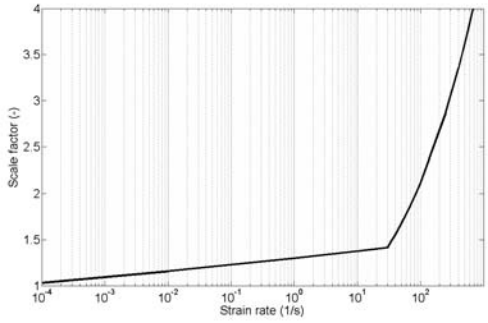

Figure C-2 ***Tabulated value pairs for the concrete compressive strength increase vs. strain rates*** [10].

Appendix D - Tentative *FE* model validation results

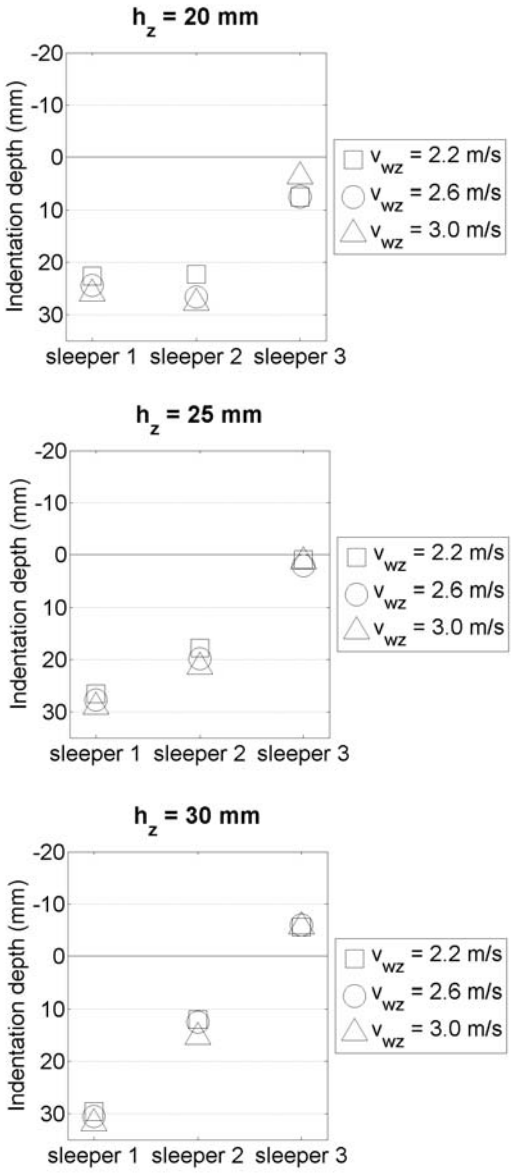

Figure D-1 Permanent concrete indentation of three subsequent sleepers for three different h_z and v_{wz} values.
f'c = 60 MPa, soft track.

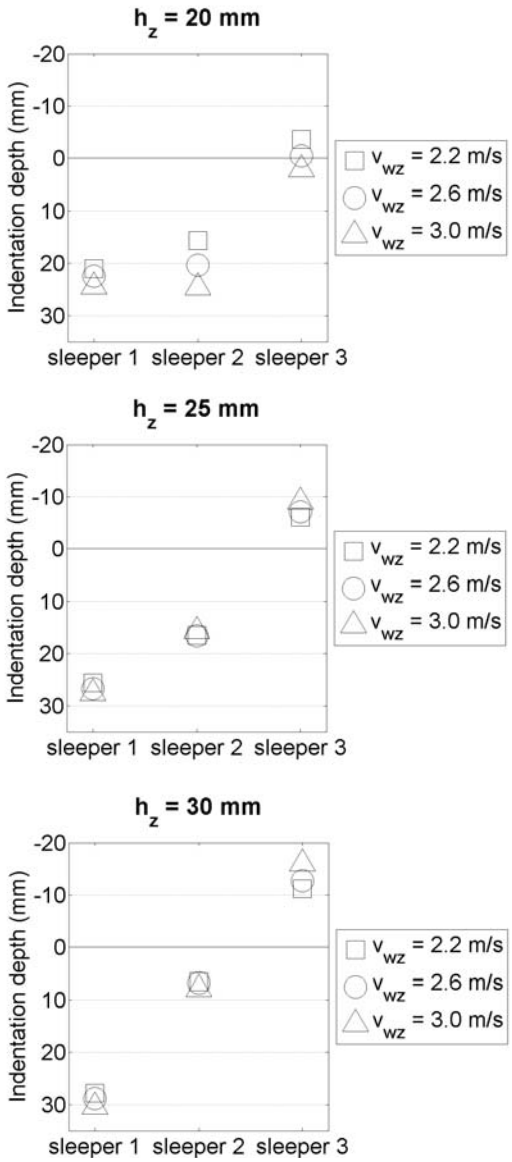

Figure D-2 Permanent concrete indentation of three subsequent sleepers for three different h_z and v_{wz} values.
f'c = 80 MPa, soft track.

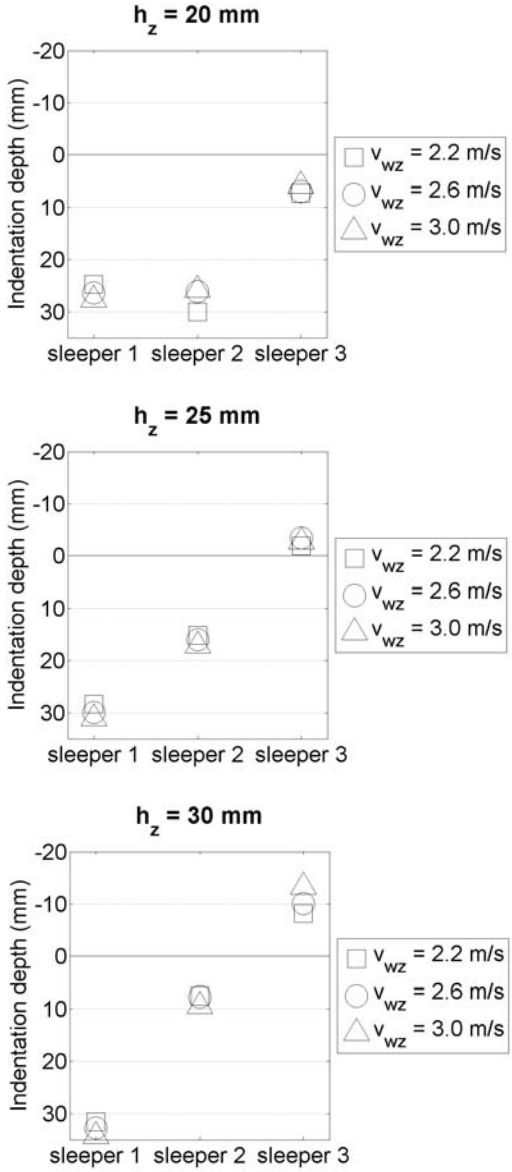

Figure D-3 Permanent concrete indentation of three subsequent sleepers for three different h_z and v_{wz} values.
f'c = 60 MPa, standard track.

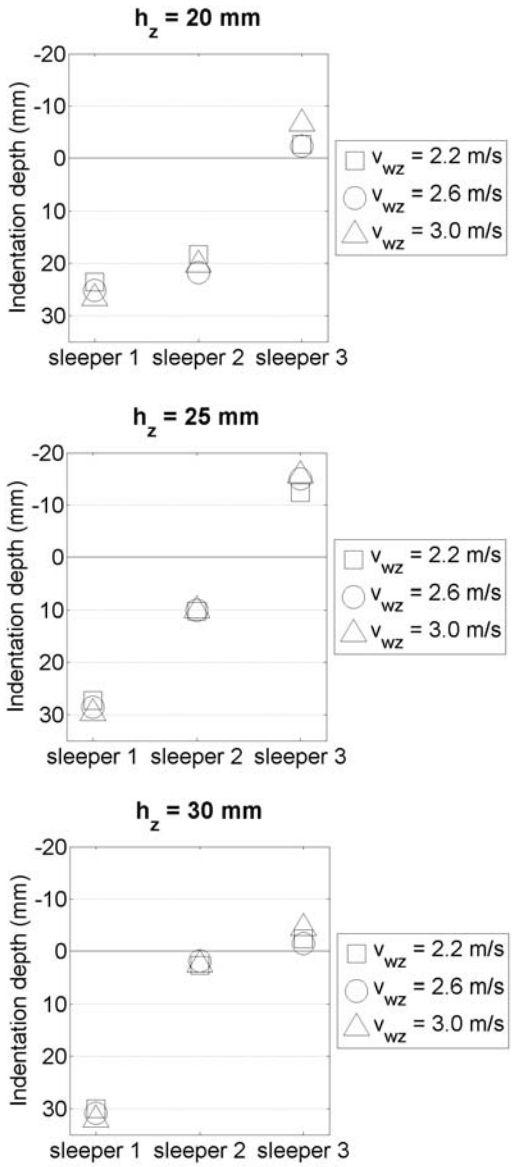

Figure D-4 Permanent concrete indentation of three subsequent sleepers for three different h_z and v_{wz} values.
f'c = 80 MPa, standard track.

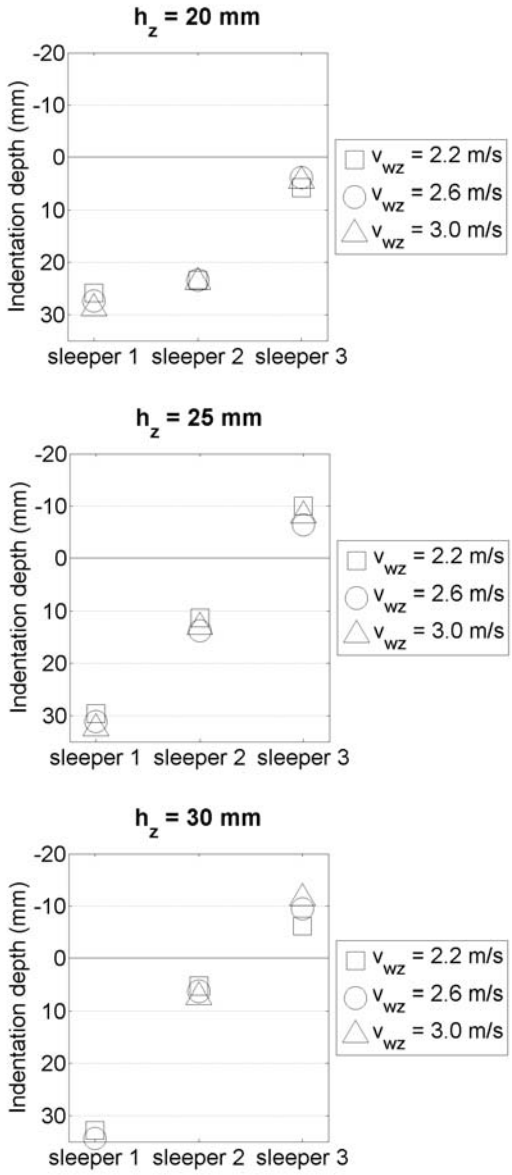

Figure D-5 Permanent concrete indentation of three subsequent sleepers for three different h_z and v_{wz} values.
f'c = 60 MPa, stiff track.

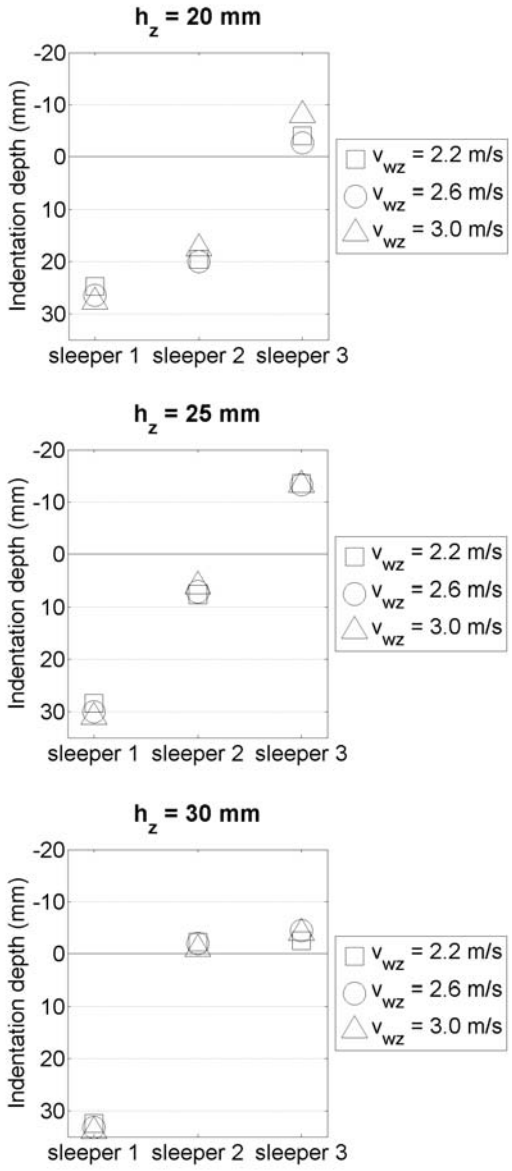

Figure D-6 Permanent concrete indentation of three subsequent sleepers for three different h_z and v_{wz} values.
f'c = 80 MPa, stiff track.

Appendix E - Wheel motion after impact

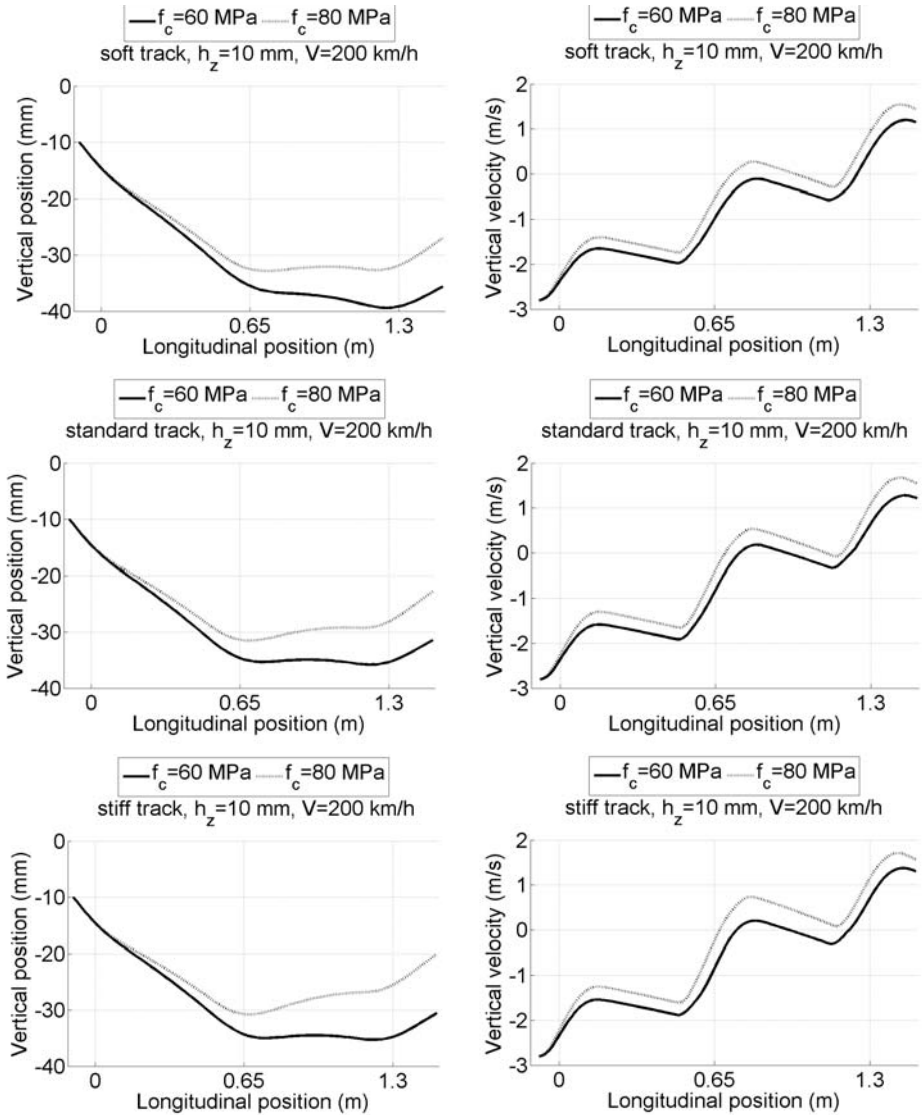

Figure E-1 ***The absolute vertical position*** *(left-hand)* ***and velocity*** *(right-hand)* ***along three subsequent sleepers*** *of the wheel's lowest point relative to the sleeper surface.*
Simulation set 1:
$V = v_{wx} = 55.56$ m/s (200km/h),
$v_{wz} = 2.8$ m/s,
$h_z = 10$ mm,
$f'_c = 60$ and 80 MPa
soft, standard and stiff track.

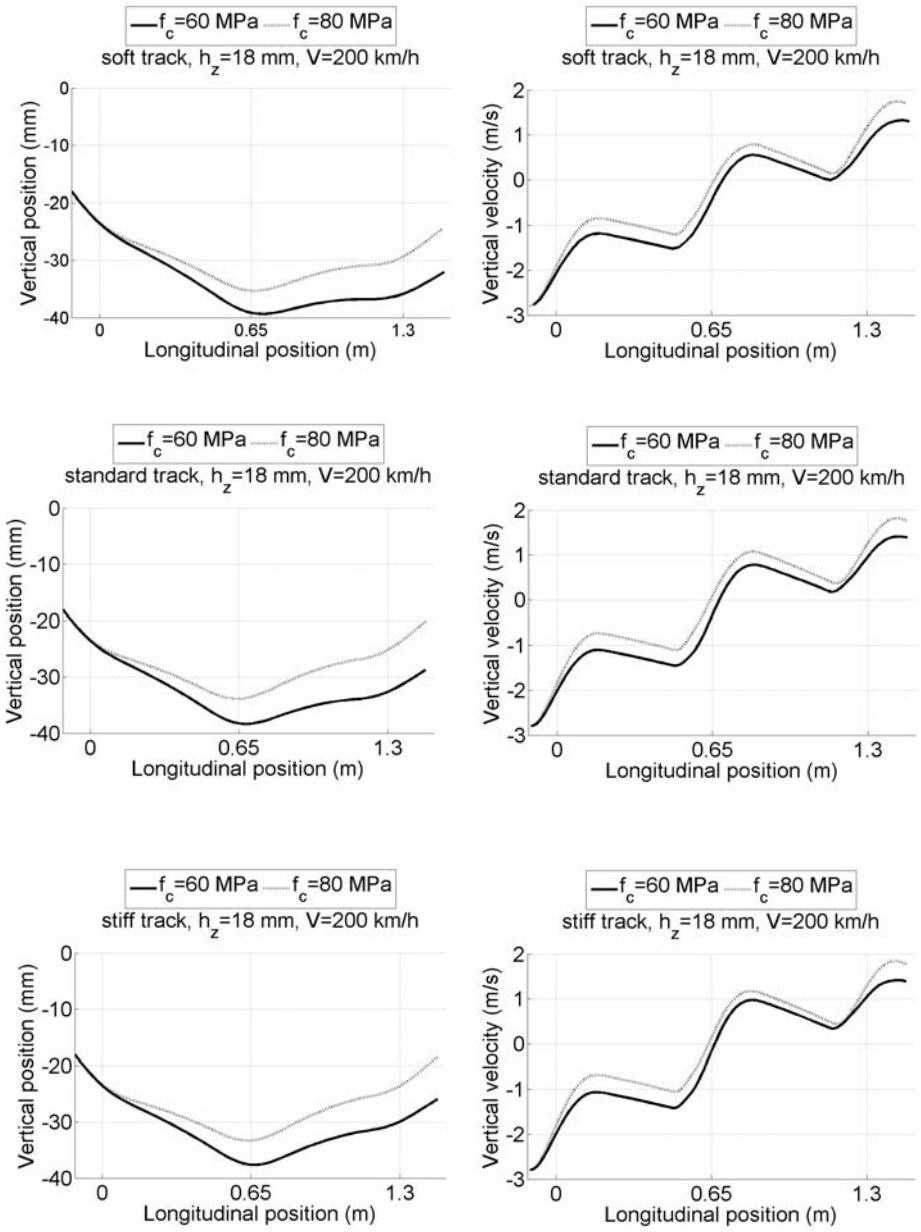

Figure E-2 ***The absolute vertical position*** *(left-hand)* ***and velocity*** *(right-hand)* ***along three subsequent sleepers*** *of the wheel's lowest point relative to the sleeper surface.*
Simulation set 1:
$V = v_{wx} = 55.56$ m/s (200km/h),
$v_{wz} = 2.8$ m/s,
$h_z = 18$ mm,
$f'_c = 60$ and 80 MPa,
soft, standard and stiff track.

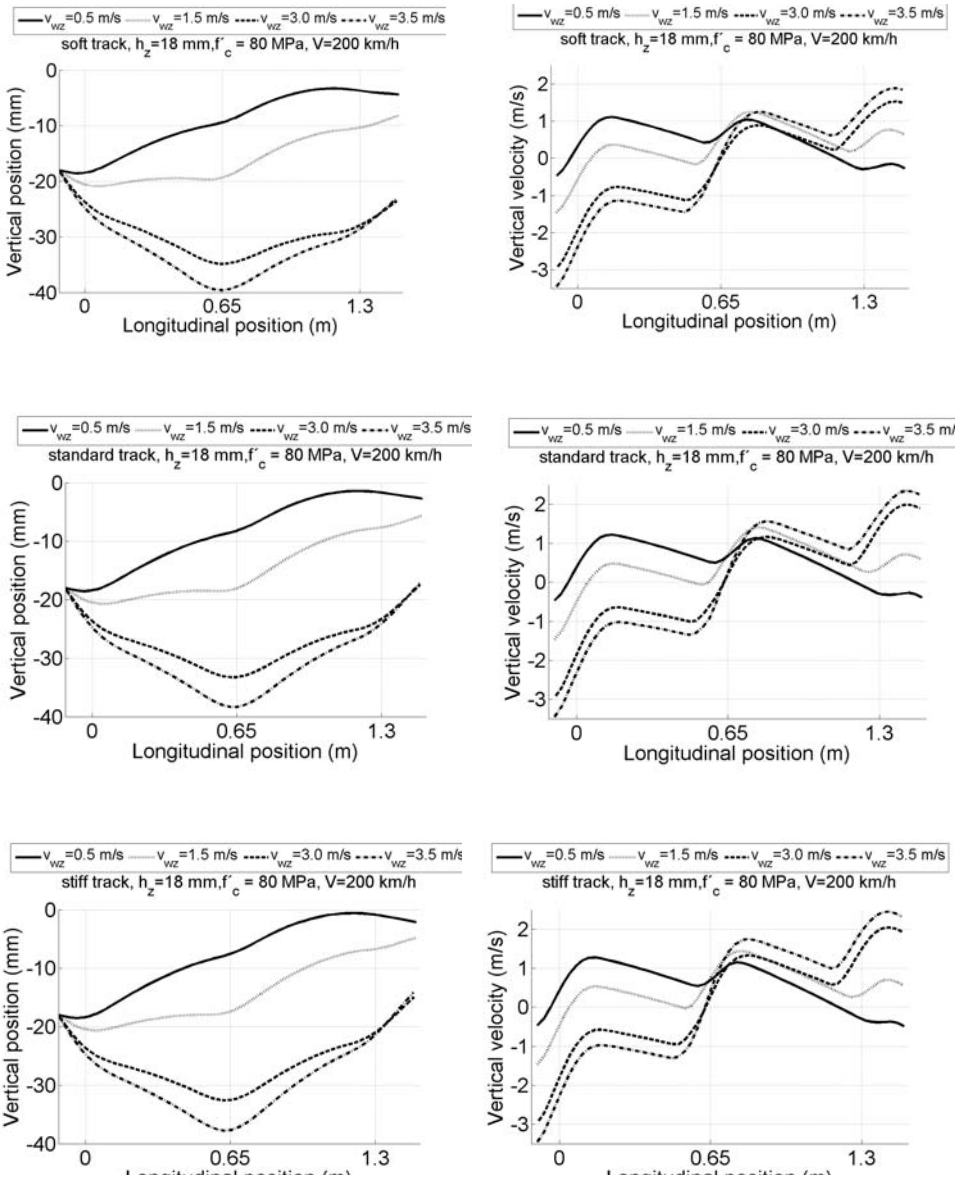

Figure E-3 ***The absolute vertical position*** *(left-hand)* ***and velocity*** *(right-hand)* ***along three subsequent sleepers*** *of the wheel's lowest point relative to the sleeper surface. Simulation set 2:*
$V = v_{wx} = 55.56$ m/s (200km/h),
v_{wz} = 0.5, 1.5, 3.0, 3.5 m/s,
h_z = 18 mm,
f'_c = 80 MPa,
soft, standard and stiff track.

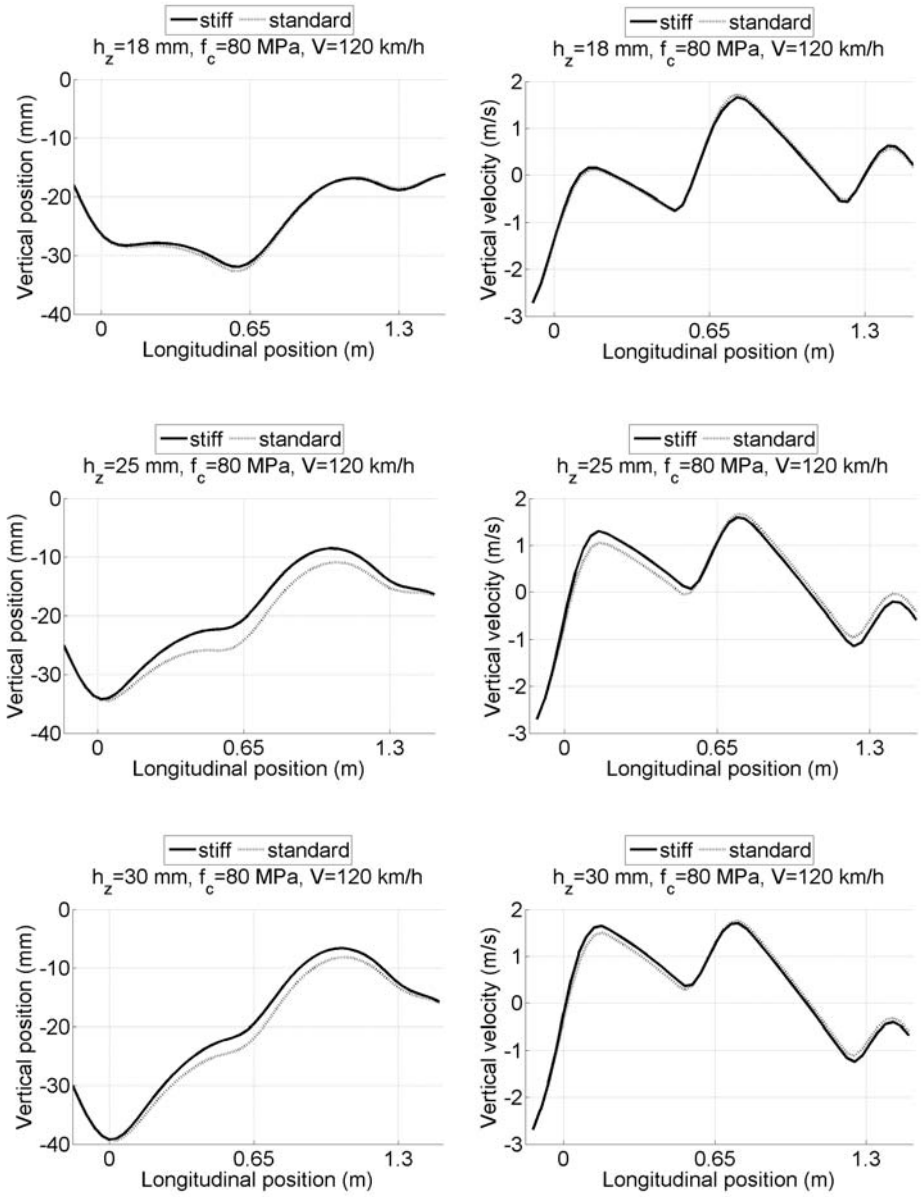

Figure E-4 ***The absolute vertical position*** *(left-hand)* ***and velocity*** *(right-hand)* ***along three subsequent sleepers*** *of the wheel's lowest point relative to the sleeper surface. Simulation set 3:*
$V = v_{wx} = 33.33$ m/s (120 km/h),
$v_{wz} = 2.8$ m/s,
$h_z = 18, 25, 30$ mm,
$f'_c = 80$ MPa,
standard and stiff track.

References

[1] ANSYS, Inc.: *Ansys Release 8.1 Documentation,*USA, 2004.

[2] Banverket (former SJ Banavdelning): *Measurments by Banverket in 1975,* Sweden, 1975.

[3] Barberon, M., Bromberger, L., Herisse, P.: *High speed train derailment* (in French: *Déraillment à grande vitesse*), La vie du rail et des transports, nr. 2426, December, 1993.

[4] Berg, M.: *A moving track model for the vehicle dynamics analysis*, Proceedings of 4th Mini Conference on Vehicle Systems Dynamics, Identification and Anomalies, Budapest, Hungary, 1994.

[5] Bernheim, A. (SNCF Département des TGV et des Voitures): *Further information regarding the safety of TGV*, private correspondence, 2002.

[6] Birk, A.M., Andersson, R.J., Coppens, A.J.: *A Computer Simulation of a Derailment Accident. Part 1 Model Basis*, Journal of Hazardous Materials, v 25 number 1-2, October, 1990.

[7] Birk, A.M., Andersson, R.J., Coppens, A.J.: *A Computer Simulation of a Derailment Accident. Part 2 Sample Simulation*, Journal of Hazardous Materials, v 25 number 1-2, October, 1990.

[8] Burton, D.E., Lettis L.A. Jr., Bryan J.B., Frary N. R.: *Physics and Numerics of the Tensor Code*, UICD-19428, Lawerence Livermore Laboratory, July, 1982.

[9] Bäckman, J.: *Railway Safety, Risks and Economics*, Ph.D. dissertation, ISBN 91-7323-019-7, Dept. of Infrastructure and Transport planning, Royal Institute of Technology, Stockholm, Sweden, 2001.

[10] CEB: *Concrete Structures under Impact and Impulsive Loading: Rate Effects*, Synthesis report, Bulletin d'Information No. 187 (Comité Euro-Internationel du Béton), Lausanne, 1988.

[11] Connolly, H. (Alstom): *The safety of the TGV, the articulated trainset*, private correspondence, 2002.

[12] Danger Ahead!: *Special Feature Eschede, Germany. ICE High Speed Train Disaster*, internet address: http://danger-ahead.railfan.net/features/eschede.htm, accessed 2004.

[13] Eisenbahn-Bundesamt: private correspondence, 2002.

[14] Eisenbahn-Bundesamt: *Unfalluntersuchung - Entgleisung des RE3521 am 25.08.2003,* not public, Germany, 2003.

[15] ETSC (European Transport Safety Council): *ETSC calls for the EU to mandate independent maritime and rail accident investigation and to set up EU accident and incident database*, Press release 25 April 2001, Belgium, 2001.

[16] Hajdin, N., Mandic, R., Miskovic, Z.: *Computer Aided Analysis of Train Impact on Structures Adjacent to the Track*, Advances in Computational Methods for Simulation, Civil-Comp Press, Edinburgh, Scotland, pp 133-137, 1996.

[17] Han, H.S., Koo J.S.: *Simulation of Train Crashes in Three Dimensions*, Vehicle Systems Dynamics, Vol. 40, No.6, pp. 435-450, 2003.

[18] Herisse, P.: *Why the TGV Derailed* (in French: *Pourquoi le TGV a déraillé*), La vie du rail et des transports, nr. 2821, November, 2001.

[19] HSE Investigation Board: *Derailment of First Great Western high speed train at Southall East on Sunday 24 November 2002*, Health and Safety Executive, UK, February, 2004.

[20] HSE Investigation Board: The track obstruction by a road vehicle and subsequent train collision at Great Heck 28 February 2001, ISBN 0 7176 2163 4, HSE Books, UK, December, 2002.

[21] HSE Investigation Board: *Train derailment at Hatfield, 17 October 2000, Second interim report*, Health and Safety Executive, UK, January, 2001.

[22] HSE Investigation Board: *Train derailment at Potter Bar 10 May 2002, A progress report by the HSE Investigation Board*, Health and Safety Executive, UK, June, 2002

[23] HSE Investigation Board: *Train derailment at Ufton level crossing, near Ufton Nervert, Berkshire, Saturday, 6 November 2004*, HSE Interim Report, Health and Safety Executive, UK, November, 2004.

[24] Kirkpatrick, S.W., Schroder, M.,Simons, J.W.: *Evaluation of Passenger Vehicle Crashworthiness*, International Journal of Crashworthiness, Vol. 6, No.1, pp 95-106, 2001.

[25] National Transportation Safety Board: Railroad Accident Brief*, Accident number: DCA-01-MR-003,* Washington, D.C., USA, March, 2002.

[26] National Transportation Safety Board: Railroad Accident Brief*, Accident number: DCA-02-MR-005,* Washington, D.C., USA, May, 2004.

[27] National Transportation Safety Board: Railroad Accident Report*, Derailment of Amtrack Auto Train P052-18 on the CSXT Railroad Near Crescent City, Florida, April 18, 2002*, Report number NTSB/RAR-03/02, National Technical Information Service, USA, August 2003.

[28] National Transportation Safety Board: Railroad Accident Report, *Derailment of Amtrack Train No. 4, Southwest Chief, on the Burlington Northern Santa Fe Railway Near Kingman,Arizona, August 9, 1997*, Report number NTSB/RAR-98/03, National Technical Information Service, USA, August 1999.

[29] National Transportation Safety Board: Railroad Accident Report, *Derailment of Amtrack Train No. 6 on the Burlington Northern Railroad, Batavia,Iowa, April 23, 1990*, Report number NTSB/RAR-91/05, National Technical Information Service, USA, December 1991.

[30] National Transportation Safety Board: Railroad Accident Report, *Derailment of Amtrack Train No. 21 (The Eagle) on the Missouri Pacific Railroad, Woodlawn, Texas, November 12, 1983*, Report number NTSB/RAR-85/01, National Technical Information Service, USA, February 1985

[31] National Transportation Safety Board: Railroad Accident Report, *Derailment of Amtrack Train No. 81, The Silver Star on the Seaboard System Railroad, Kitterell, North Carolina, March 5, 1984*, Report number NTSB/RAR-85/03, National Technical Information Service, USA, March 1985.

[32] National Transportation Safety Board: Railroad Accident Report, *Derailment of Amtrack Train No. 97 on Seaboard Coast Line Railroad Track, Lochloosa, Florida, May 26, 1981*, Report number NTSB-RAR-81-9, National Technical Information Service, USA, September 1981.

[33] National Transportation Safety Board: Railroad Accident Report, *Derailment of National Railroad Passenger Corporation, Train 7, on Burlington Northern Railroad, near Saco, Montana, August 5, 1988*, Report number NTSB-RAR-89-03, National Technical Information Service, USA, April 1989.

[34] Network Rail Management Information System: Safety event: QNE/1998/0337101, Network Rail, UK, 2003.

[35] Peilow, D.: *A High Speed Future for Britain's Railways*, 2001.

[36] Persson, I.: *Using GENSYS.0203*, ISBN 91-631-3110-2, DEsolver, Östersund, Sweden, 2003.

[37] SJ Accident Report: *Axle failure and derailment of train 2703, Rosersberg 920316*, (in Swedish: *Axelbrott och urspårning tåg 2703, Rosersberg 920316*), SJ Persontrafikdivisonen, Trafiksäkerhetsenheten, Stockholm, Sweden, 1992.

[38] SJ Accident Report: *Cst MR 86-0460/0631*, SJ Driftsektionen, Stockholm, 1986.

[39] SJ Accident Report: *Sävsjö 92-01-24 approximately at 0220; passenger train 206 derails with its last car* (in Swedish: *Sävsjö 92-01-24 ca kl 0220; resandetåg 206 urspårar med sista vagnen*), Sweden, 1992.

[40] SJ Accident Report: *Train derailment 94-07-18 on Section Varberg-Hamra* (in Swedish: *Tågurspårning 94-07-18 på Sträckan Varberg-Hamra*) Report number SÄ-94-0563/0607, September 1994, Sweden.

[41] SJ Accident Report: Train derailment Upplands-Väsby 1980-08-24 (in Swedish: Tågurspårning Upplands-Väsby 1980-08-24), SJ Stockholm trafikdistrikt, Sundbyberg, 1980.

[42] SJ Investigation Report: *Derailment at Lindekullen, 2001-02-18* (in Swedish: *Urspårning i Lindekullen, 2001-02-18*), SJ AB Trafiksäkerhet, Stockholm, 2001.

[43] SJ Investigation Report: *Investigation: Axle failure on the Mölnbo - Gnesta section 2001-09-10 on train 437* (in Swedish*: Utredningsrapport: Axelbrott på sträckan Mölnbo - Gnesta 2001-09-10 i tåg 437),* SJ AB Trafiksäkerhet, Sweden, 2001.

[44] SJ Investigation Report: *Investigation: Derailment on the Tierp - Orrskog section 2001-09-08* (in Swedish*: Utredningsrapport: Urspårning på sträckan Tierp-Orrskog 2001-09-08),* SJ AB Trafiksäkerhet, Ånge, Sweden, 2001.

[45] SJ Investigation Report: *Investigation of axle failure on vehicle class X2 at Slätte and Kumla - Hallsberg* (in Swedish: *Utredning av axelbrott på fordon litt X2 i Slätte och Kumla - Hallsberg*, SJ Stab Trafiksäkerhet, Sweden, 1999.

[46] Swedish Railway Inspectorate (in swedish: Järnvägsinspektionen): *Derailment on section Lästringe - Tystberga, 1997-07-06* (in swedish: *Urspårning på sträckan Lästringe - Tystberga, 1997-07-06*), Report number J 97-876/56, Borlänge, Sweden, 1998.

[47] TGV Web: *TGV Accidents*, Internet address: http://www.railfaneurope.net/tgv/tgvindex.html, accessed 2002.

[48] Transportation Safety Board of Canada: *03 September 1997 - Derailment VIA Rail Canada Inc. Passenger Train No. 2 Mile 7.5, CN Wainwright Subdivision Near Biggar, Saskatchewan,* Report number R97H0009, Canada, 1998.

[49] Whirley R.G., Hallquist O.: *DYNA3D: A Nonlinear Explicit Three-Dimensional Finite Element Code for Solid and Structural Mechanics,* User Manual, Report UCRL-MA-107254, LLNL, Livermore, CA, USA, 1991.

[50] Wood S.L.: *Evaluation of the long-term properties of concrete*, ACI Materials Journal, 88 No. 8 pp 630-43, 1991.

[51] Yang, T.H. et al.: *A Study Continuation of Derailment Behaviour, Final Report*, Pullman-Standard Research Project No. 39-1833, RPI-AAR Railroad Tank Car Safety Research and Test Project, Report RA-08-1-12, February, 1972.

[52] Yang, T.H., Manos W.P., Johnstone, B.: *Dynamic Analysis of Train Derailments*. AMEA Winter Annual Meeting, New York, N.Y. Nov. 26-30, 1972.

References

Symbols and Abbreviations

Symbol	Significance	Units
a_{wz}	vertical wheel acceleration	m/s^2
a_y	lateral track plane acceleration	m/s^2
b_r	rail width	m
$b_{w\text{-}bd}$	lateral gap between wheel and brake disc	m
d	wheel diameter	m
D	track cant	m
f'_c	concrete unconfined compressive strength	N/m^2
F_{cn}	normal component of the force exerted on wheel during sleeper contact	N
F_{cx}	longitudinal component of the force exerted on wheel during sleeper contact	N
F_{cz}	vertical component of the force exerted on wheel during sleeper contact	N
f_y	brake disc lateral margin parameter	m
f_z	brake disc vertical margin parameter	m
h_f	wheel flange height	m
h_r	vertical distance from top of the rail to sleeper upper surface	m
$h_{w\text{-}bd}$	vertical distance brake disc to rail head (radius difference between wheel and brake disc)	m
h_z	vertical wheel position at the instant of impact with the sleeper	m
m_{cb}	equivalent mass acting on the primary suspension above each wheel	kg
m_{wheel}	wheel mass	kg
P	pressure	N/m^2
R	track curve radius	m
r_{bd}	brake disc radius	m
r_w	nominal wheel radius	m

$t,\ \Delta t$	time, elapsed time	s
V	train speed	m/s
$v_{bd\text{-}y}$	lateral brake disc velocity	m/s
$v_{bd\text{-}z}$	vertical brake disc velocity	m/s
v_{wx}	longitudinal wheel velocity	m/s
$v_{wz},\ \Delta v_{wz}$	vertical wheel velocity	m/s
x_{iF}	initial longitudinal position of point F (the lowest point on the wheel)	m
x_F	longitudinal position of point F	m
x_{si}	sleeper spacing interval	m
x_{sl}	longitudinal length (width) of sleeper's upper surface	m
z_F	vertical position of point F	m
z_{iF}	initial vertical position of point F	m
β	angle between longitudinal and normal force component exerted on wheel during sleeper contact	degree, °
ε^p	plastic strain	(-)
η	damage scale factor in concrete	(-)
λ	damage function in concrete	(-)
σ_{cut}	tensile strength in concrete	N/m^2
σ_{failed}	minimum, damaged strength of concrete	N/m^2
σ_{max}	maximum, undamaged strength of concrete	N/m^2

Abbreviations

ATC	Automatic Train Control
CEB	Comité Euro-Internationel du Béton
DVT	Driving Van Trailer
EU	European Union
FE	Finite Element
HSE	Health and Safety Executive
HST	High Speed Train

KHST	Korean High-Speed Train
KTH	Kungliga Tekniska Högskolan (Royal Institute of Technology)
MBS	Multy-Body Systems
MHC	Material Handling Car
NTSB	National Transportation Safety Board
ORE	Office for Research and Experiments (former, of UIC)
SJ	Formerly Statens Järnvägar (Swedish State Railways)
SL	Storstockholms Lokaltrafik (Stockholm Transport)
SNCF	Société Nationale des Chemins de Fer
TGV	Train à Grande Vitesse
UIC	Union Internationale des Chemins de fer